P- 344416

24/6/97 KM

AGARD-AR-321

AGARD-AR-321

AGARD

## ADVISORY GROUP FOR AEROSPACE RESEARCH & DEVELOPMENT

7 RUE ANCELLE, 92200 NEUILLY-SUR-SEINE, FRANCE

AGARD ADVISORY REPORT 321

Sonic Nozzles for Mass Flow Measurement and Reference Nozzles for Thrust Verification

(les Tuyères soniques pour le contrôle du débit massique et les tuyères de référence pour la vérification de la poussée)

Report of the Fluid Dynamics Panel Working Group 19.
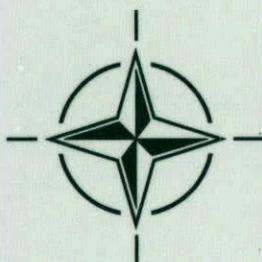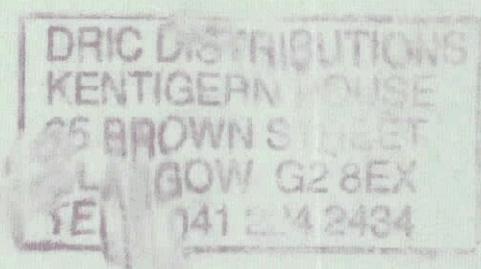
NORTH ATLANTIC TREATY ORGANIZATION

Published June 1997

Distribution and Availability on Back Cover

AGARD-AR-321

AGARD

**ADVISORY GROUP FOR AEROSPACE RESEARCH & DEVELOPMENT**

7 RUE ANCELLE, 92200 NEUILLY-SUR-SEINE, FRANCE

AGARD ADVISORY REPORT 321

Sonic Nozzles for Mass Flow Measurement and Reference Nozzles for Thrust Verification

(les Tuyères soniques pour le contrôle du débit massique et les tuyères de référence pour la vérification de la poussée)

Report of the Fluid Dynamics Panel Working Group 19.
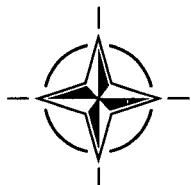
North Atlantic Treaty Organization
Organisation du Traité de l'Atlantique Nord

The Mission of AGARD

According to its Charter, the mission of AGARD is to bring together the leading personalities of the NATO nations in the fields of science and technology relating to aerospace for the following purposes:

— Recommending effective ways for the member nations to use their research and development capabilities for the common benefit of the NATO community;

— Providing scientific and technical advice and assistance to the Military Committee in the field of aerospace research and development (with particular regard to its military application);

— Continuously stimulating advances in the aerospace sciences relevant to strengthening the common defence posture;

— Improving the co-operation among member nations in aerospace research and development;

— Exchange of scientific and technical information;

— Providing assistance to member nations for the purpose of increasing their scientific and technical potential;

— Rendering scientific and technical assistance, as requested, to other NATO bodies and to member nations in connection with research and development problems in the aerospace field.

The highest authority within AGARD is the National Delegates Board consisting of officially appointed senior representatives from each member nation. The mission of AGARD is carried out through the Panels which are composed of experts appointed by the National Delegates, the Consultant and Exchange Programme and the Aerospace Applications Studies Programme. The results of AGARD work are reported to the member nations and the NATO Authorities through the AGARD series of publications of which this is one.

Participation in AGARD activities is by invitation only and is normally limited to citizens of the NATO nations.

Sonic Nozzles for Mass Flow Measurement and Reference Nozzles for Thrust Verification

(AGARD AR-321)

Executive Summary

Accurate measurement of massflow and thrust is essential to the success of windtunnel tests supporting engine-airframe aerodynamic integration studies. Among other benefits, optimising engine integration results into reductions of the cruise drag of an aircraft by at least several percent. Hence, mastering this technique at an early stage of a project allows, within a given set of specification (e.g. the range), to save on the mass of the aircraft and consequently on its cost - more generally it contributes to reducing technical/economical risk.

Refinement of experimental techniques contributing to cruise drag prediction, and possibilities offered by small scale engine simulators are today somewhat limited by the accuracy of massflow and thrust measurements on reference nozzles, which have to be used at various stages of the experiments. Indeed, determining thrust-drag balance with an accuracy better than one percent often requires subtracting large quantities which need to be known individually within a few thousandths. This is today still difficult to do, even in the simple case of reference nozzles. Moreover, within cooperative programmes, systematic interfacility bias resulting from slight differences in test methodology can raise complex issues for the partners.

For these reasons, and although the topic is far from being new, the Fluid Dynamics Panel decided in 1993 to create a Working Group (WG 19) to report on the state-of-the-art and make practical recommendations.

Progress has been made in the physical understanding of some flow phenomena and a consensus has been reached on how to proceed, while keeping in mind usual wind tunnel constraints and cost-effectiveness. As regards practical results, it can be said that measuring gaseous mass flows within $\pm 0.1\%$ or better is still very difficult. For most tests, however, with reasonable care, bias and random (repeatability) errors can be kept within $\pm 0.1\%$ each. For thrust measurements, these values must typically be doubled.

X. Bouis,
Chair, WG 19
January 1997

Mesures de débit par cols soniques et vérification de la poussée par tuyères étalon

(AGARD AR-321)

Synthèse

La mesure précise des débits et des poussées contribue de manière essentielle au succès des études en soufflerie de l'intégration aérodynamique cellule-propulsion. Optimiser cette intégration permet par exemple de réduire de plusieurs pour-cent la traînée aérodynamique d'un aéronef en croisière. La maîtrise de telles techniques au cours des premières étapes d'un projet permet, à spécifications données (ex : le rayon d'action) de réduire la masse de l'avion et par conséquent son coût ; plus généralement, cette maîtrise contribue à la minimisation du risque technico-économique.

L'affinement des techniques expérimentales concourant à la prévision de la traînée en croisière, et les possibilités offertes par les simulateurs de moteurs à échelle réduite butent aujourd'hui sur la précision des mesures de débit et de poussée sur les tuyères étalon qui interviennent à divers stades des expériences. En effet, la détermination d'un bilan poussée-traînée avec une précision supérieure au pour-cent passe en pratique par la soustraction de grandeurs importantes dont chacune doit être connue à quelques millièmes près. Ceci est encore difficile aujourd'hui, même pour le cas de simples tuyères étalon. De plus, dans les programmes menés en coopération, les écarts systématiques entre installations d'essais résultant de petites différences de méthodologie ne vont pas sans poser des problèmes aux partenaires.

Pour ces raisons, et bien que le sujet ne date pas d'hier, la Commission de Dynamique des Fluides a décidé en 1993 de demander à un Groupe de Travail (WG 19) de faire le point sur l'état de l'art dans ce domaine et d'établir des recommandations pratiques.

Des progrès ont été accomplis sur la compréhension physique des phénomènes et un consensus a été obtenu sur les procédures à suivre compte-tenu des contraintes habituelles des souffleries et du souci d'un bon rapport coût/efficacité. En pratique, on peut dire que mesurer des débits gazeux à mieux que $\pm 0,1\%$ demeure très difficile. Pour la plupart des essais cependant, des précautions raisonnables permettent de contenir l'erreur systématique et l'erreur aléatoire (répétabilité) chacune dans la limite de $\pm 0,1\%$. En ce qui concerne la mesure de la poussée, il faut approximativement doubler les valeurs ci-dessus.

X. Bouis,
Président du WG 19
Janvier 1997

Contents

Recent Publications of
the Fluid Dynamics Panel

AGARDOGRAPHS (AG)

Turbulent Boundary Layers in Subsonic and Supersonic Flow
AGARD AG-335, July 1996

Computational Aerodynamics Based on the Euler Equations
AGARD AG-325, September 1994

Scale Effects on Aircraft and Weapon Aerodynamics
AGARD AG-323 (E), July 1994

Design and Testing of High-Performance Parachutes
AGARD AG-319, November 1991

Experimental Techniques in the Field of Low Density Aerodynamics
AGARD AG-318 (E), April 1991

Techniques Expérimentales Liées à l'Aérodynamique à Basse Densité
AGARD AG-318 (FR), April 1990

A Survey of Measurements and Measuring Techniques in Rapidly Distorted Compressible Turbulent Boundary Layers
AGARD AG-315, May 1989

Reynolds Number Effects in Transonic Flows
AGARD AG-303, December 1988

REPORTS (R)

Advances in Cryogenic Wind Tunnel Technology
AGARD R-812, Special Course Notes, January 1997

Aerothermodynamics and Propulsion Integration for Hypersonic Vehicles
AGARD R-813, Special Course Notes, October 1996

Parallel Computing in CFD
AGARD R-807, Special Course Notes, October 1995

Optimum Design Methods for Aerodynamics
AGARD R-803, Special Course Notes, November 1994

Missile Aerodynamics
AGARD R-804, Special Course Notes, May 1994

Progress in Transition Modelling
AGARD R-793, Special Course Notes, April 1994

Shock-Wave/Boundary-Layer Interactions in Supersonic and Hypersonic Flows
AGARD R-792, Special Course Notes, August 1993

Unstructured Grid Methods for Advection Dominated Flows
AGARD R-787, Special Course Notes, May 1992

Skin Friction Drag Reduction
AGARD R-786, Special Course Notes, March 1992

Engineering Methods in Aerodynamic Analysis and Design of Aircraft
AGARD R-783, Special Course Notes, January 1992

ADVISORY REPORTS (AR)

Cooperative Programme on Dynamic Wind Tunnel Experiments for Manoeuvering Aircraft
AGARD AR-305, Report of WG-16, October 1996

Hypersonic Experimental and Computational Capability, Improvement and Validation
AGARD AR-319, Vol. I, Report of WG-18, May 1996

Aerodynamics of 3-D Aircraft Afterbodies
AGARD AR-318, Report of WG-17, September 1995

A Selection of Experimental Test Cases for the Validation of CFD Codes
AGARD AR-303, Vols. I and II, Report of WG-14, August 1994

Quality Assessment for Wind Tunnel Testing
AGARD AR-304, Report of WG-15, July 1994

Air Intakes of High Speed Vehicles
AGARD AR-270, Report of WG-13, September 1991

Appraisal of the Suitability of Turbulence Models in Flow Calculations
AGARD AR-291, Technical Status Review, July 1991

Rotary-Balance Testing for Aircraft Dynamics
AGARD AR-265, Report of WG11, December 1990

Calculation of 3D Separated Turbulent Flows in Boundary Layer Limit
AGARD AR-255, Report of WG10, May 1990

Adaptive Wind Tunnel Walls: Technology and Applications
AGARD AR-269, Report of WG12, April 1990

CONFERENCE PROCEEDINGS (CP)

The Characterization & Modification of Wakes from Lifting Vehicles in Fluids
AGARD CP-584, November 1996

Progress and Challenges in CFD Methods and Algorithms
AGARD CP-578, April 1996

Aerodynamics of Store Integration and Separation
AGARD CP-570, February 1996

Aerodynamics and Aeroacoustics of Rotorcraft
AGARD CP-552, August 1995

Application of Direct and Large Eddy Simulation to Transition and Turbulence
AGARD CP-551, December 1994

Wall Interference, Support Interference, and Flow Field Measurements
AGARD CP-535, July 1994

Computational and Experimental Assessment of Jets in Cross Flow
AGARD CP-534, November 1993

High-Lift System Aerodynamics
AGARD CP-515, September 1993

Theoretical and Experimental Methods in Hypersonic Flows
AGARD CP-514, April 1993

Aerodynamic Engine/Airframe Integration for High Performance Aircraft and Missiles
AGARD CP-498, September 1992

Effects of Adverse Weather on Aerodynamics
AGARD CP-496, December 1991

Manoeuvering Aerodynamics
AGARD CP-497, November 1991

Vortex Flow Aerodynamics
AGARD CP-494, July 1991

Missile Aerodynamics
AGARD CP-493, October 1990

Aerodynamics of Combat Aircraft Controls and of Ground Effects
AGARD CP-465, April 1990

Computational Methods for Aerodynamic Design (Inverse) and Optimization
AGARD CP-463, March 1990

Applications of Mesh Generation to Complex 3-D Configurations
AGARD CP-464, March 1990

Fluid Dynamics of Three-Dimensional Turbulent Shear Flows and Transition
AGARD CP-438, April 1989

Validation of Computational Fluid Dynamics
AGARD CP-437, December 1988

Aerodynamic Data Accuracy and Quality: Requirements and Capabilities in Wind Tunnel Testing
AGARD CP-429, July 1988

Aerodynamics of Hypersonic Lifting Vehicles
AGARD CP-428, November 1987

Aerodynamic and Related Hydrodynamic Studies Using Water Facilities
AGARD CP-413, June 1987

1. INTRODUCTION

1.1 Background, objectives, scope of work

For drag measurement of aircraft models in wind tunnels, a precision of 1 "drag count",
$\Delta C_D = \pm 1.10^{-4}$, which represents about 0.3 % of the total drag at cruise conditions, is today required, and can actually be obtained, at least in repeatability [1], [2].

AGARD Advisory Report 184 [3] presents the wind tunnel flow quality and data accuracy requirements which are related to that precision.

On models equipped with engine simulators, and used to study engine installation drag, if the global forces on the model are measured with an accuracy of 0.3%, the homogeneous accuracy to be insured on the evaluation of the engine simulator thrust is also 0.3%.

The thrust of an engine simulator is derived from a preliminary measurement of the exhaust flow thrust on a static test bench.

At high subsonic cruise Mach number, a ratio of 1.4 between the exhaust speed of a fan flow to the flight speed is representative, so that an error of 0.3 % on the net thrust is equivalent to an error of 0.3% x (1.4 - 1)/1.4 = 0,086 % on the exhaust flow gross thrust, which is only measured at static. In fact, taking also into account the thrust of the core flow of a turbofan exhaust configuration, it is the near value of 0.1% which can be retained as an objective for thrust measurement on a static test bench.

Consistently, the same precision of 0.1% should also be aimed at on any static test bench for turbofan exhaust models.

Since thrust is generally expressed as a ratio of thrust to mass flow, the precision of 0.1 % equally applies to mass flow measurement.

Mass flow is usually measured by the way of a sonic throat, and thrust test benches are often checked by testing a reference nozzle.

The accuracies of these measurements are assessed by theoretical calculations and/or by calibration process.

As different sonic throat profiles, different flow calculation methods, and different calibration techniques are used among the various NATO countries, a working group was initiated by the Fluid Dynamic Panel of AGARD to present the state of the art, and to compare different possibilities and attainable precisions.

It is the subject of this report, which includes the next chapters :

2 - Basic calibration
       2.1 - Mass-time calibration of massflowmeters
       2.2 - Calibration of massflowmeters by using transfer-standard nozzles
       2.3 - Nozzle thrust measuring benches
       2.4 - General precautions for all tests
3 - Flow analysis
       3.1 - Cylindrical throat nozzles : the ASME Long Radius Nozzle
       3.2 - Toroidal throat nozzles
       3.3 - Real gas effects
       3.4 - Viscous effects on thrust
       3.5 - Practical formulæ to calculate mass flow rate and thrust

2

4 - Examples of experimental results
      4.1- Boeing's experience on ASME and "cubic" nozzles
      4.2- 3" "cubic" nozzle test results of different calibration tanks
      4.3- Discussion
5 - Conclusions

1.2 General remarks

1- Reference should be made, before starting the presentation, to the existing international standards on mass flow measurements (ISO-4006, ISO-5167, ISO-5168, ISO-9300), and the several excellent review papers ([4], [23], [25]), some of them being nearly 30 years old.

2- It should be stressed that the goal of mass flow and thrust measurements with an accuracy of ±0.1% is a serious challenge and that careful application of ISO standards is necessary but far from being sufficient to get it. ISO generally refers to errors in the range of 0.5% to 2%.

3- A repeatability of the order of 0.1% to 0.2% is however currently achieved in some wind tunnels which can offer with considerable precautions a level of drag measurement repeatability close to 1 drag count. This indicates that if systematic errors are properly eliminated, the above serious challenge is not a dream.

4- Above-mentioned articles should already be known by the reader of this AGARD document. They are indeed the starting point for the following discussions and most of their analysis, recommendations and conclusions are still valid today.

5- The case of cryogenic wind tunnels is not adressed in the report although engine/jet simulation is planned in some of these facilities, e.g. ETW and KKK. It poses some additional problems which could not be fully identified within the scope of this working group.

1.3 Contributors, group members and meetings

To complete the assignment, a number of highly qualified specialists were nominated by the national delegates of AGARD. Representing both panel and non-panel members, industry, government agencies and universities these individuals were :

R. Decuypere	ERM	Belgium
W.E. Carscallen	NRCA	Canada
J.P. Bècle	ONERA	France
X. Bouis	ONERA	France
J. Leynaert	ONERA	France
W. Baumert	DLR	Germany
G.E.A Meier	DLR	Germany
E. Barbantini	Alenia	Italy
G.H. Hegen	NLR	Netherlands
J.F. Slauerhoff	NLR	Netherlands
H. Norstrud	Univ. Trondheim	Norway
J. Reid	NEL	United Kingdom
R. Sale	ARA	United Kingdom
C. Stewart	NEL	United Kingdom
E. Fromm	Boeing (retired)	United States

In addition N. Kubberud, Norway attended several meetings of the group and B. Masure FDP Member, France who could not join the group at its beginning took part in the review of the document

and brought important contributions to chapter 3.

On formation the group was chaired by J. Leynaert. After Mr. Leynaert's retirement mid-1993 X.Bouis assumed his role.

Four meetings were arranged to co-ordinate the work of the group :

26-27 april 1993   Winchester, U.K
11-12 october 1993   Modane, France
24-25 march 1994   Göttingen, Germany
12-13 september 1994   Trondheim, Norway

1.4 Acknowledgments

The chairman of the Working Group is pleased to acknowledge the support of the agencies involved and of the management of different institutions and companies which have allowed their members to participate in this activity.

We also thank the host countries for the local arrangements of the meetings.

Special thanks should be addressed to JP. Bècle who, besides his appreciated technical contribution, took care of most of the coordination and editing of the document.

Finally we express our thanks to our panel executive, Dr. J. Molloy and the FDP secretaries AM. Rivaut and D. Pelat for their help and patience as we accomplished our tasks.

4

2. BASIC CALIBRATION

Basic calibration for a massflowmeter means that direct measurements of mass and time are used to determine the mass flow rate. A number of facilities over the world are able to provide such calibrations, mostly for the natural gas industries, but very few with air as fluid and giving the required accuracy. The working group could only find two such facilities, one at the Colorado Engineering Experiment Station Inc., CEESI, in the USA and the other at the National Engineering Laboratory, NEL, in the UK. Both are briefly described hereafter. The mass flow ranges of these facilities are limited and it is impossible to calibrate each massflowmeter in such a facility. So transfer standard nozzles, once a basic calibration has been performed, are used as references. Although simple combinations of nozzles in series and/or in parallel do give proper answers if repeatability only is looked at, the target of 0.1% in absolute accuracy can only be reached if a sophisticated methodology is applied, like that of Boeing described in 2.2.

2.1 Mass-time calibration of massflowmeters

2.1.1 CEESI gravimetric calibration facility

This facility currently seems to have the most accurate system to calibrate venturis or nozzles with air. It is presented in line diagram form in figure 6.
The principle is to discharge air from a tank over a measured time interval at constant conditions through the venturi or nozzle under test. The tank is accurately weighed after filling, and again after air has been discharged to determine the mass of air used during the time interval. Details are presented in ref.[8].
Mass flow is limited to 0.113 kg/s.
Mass flow accuracy is thought by Boeing engineers to be in the order of 0.05%, hence compatible with the 0.1% goal.

2.1.2 NEL facility

Although seemingly less accurate than CEESI facility, NEL gravimetric system is presented hereafter in order to show some details of the procedure which should be followed.

2.1.2.1 Test rig and instrumentation

The primary gravimetric gas flow standard which is used for the calibration tests is shown in line diagram form in fig.8.

Air is supplied at a pressure of 210 bar by two reciprocating compressors which have a combined free air delivery of some 0.06 m^3/s. After leaving the compressors the air passes through a purification plant in which oil, water vapour and solid particles are removed. The purification plant is designed to provide air with a dew-point not higher than -40°C and an oil content not exceeding five parts per million. A particle filter removes all solid matters with size ratings greater than 5 μm.

This purified air is used to charge the air storage vessel and the control loop and in the tests reported here the air storage vessel is charged at pressures up to 76 bar with the control loop being charged at pressures up to 65 bar. During each test run, air from the control loop passes through the pressure control system "B" via valve L1, which is used to start and stop the flow, to the nozzle under test. The air flowing from the loop is replaced by air from the air storage vessel which flows into the loop through pressure control system "A". Both of these pressure control systems utilise dome-loaded valves which are set to give selected downstream pressures.

After passing through the nozzle under test the air enters the diverter unit. In the diverter unit two 50 mm ball valves are located as shown in fig.8. When the diverter unit is operated one valve closes and the other opens so that the air flow can be directed either through the disconnecting fixture to the spherical weighing vessel or through the test and bypass lines to atmosphere. The weighing vessel disconnect fixture consists of valves and a scaling system so arranged that the charged weighing vessel can be completely disengaged from the system before being weighed.

The weighing vessel is a hollow steel sphere 1.5 m in diameter. It is capable of withstanding pressures up to 300 bar at temperatures in the range -20 to +50°C. To weigh the vessel and its contents a sensitive platform scale is used. The scale is back-balanced to allow for the tare weight of the spherical vessel. The weights are read on a steelyard indicator and the sensitivity of the system is such that changes of mass of 10 g can be detected in diverted masses of typically 40 to 60 kg.

The instrumentation used during the tests is as follows :

Nozzle under test
The probe containing the nozzle upstream pressure and temperature sensors is designed to measure the stagnation values of these parameters. The following accuracies are required to meet the 0.1% goal in mass flow measurement (see also chapter 2.4):
        - upstream pressure (P0): accuracy better than ±0.02 per cent of reading.
        - upstream temperature (T0): accuracy better than ±0.25°C.

Unweighed volume
Pressure : Wallace and Tiernan precision pressure gauge of range 0-35 bar or Barnet test gauge of range 0-80 bar. Accuracy : ±0.3 per cent of reading.

Temperature : Rosemount platinum resistance thermometer with ASL type F25 measurement system. Accuracy : ±0.25°C.

Weighbridge : Avery type 4206 ABA of range 0-500 kg.
Accuracy : ±0.02 kg of reading.

Barometric pressure : Model 145, Texas Instruments Ltd, precision pressure gauge with type 1 capsule of range 0-1080 mbar abs. installed. Accuracy : ±0.05 per cent of reading.

Ambient temperature : Mercury-in-glass thermometer. Accuracy : ±1°C.

2.1.2.2 Test procedure

The weighing vessel is lowered from the disconnect fixture onto the weighbridge and its "empty" (i.e. with the air inside at ambient pressure) weight measured. This reading is recorded and the temperature of the air surrounding the weighing vessel is also noted. The vessel is then raised into its operating position in the disconnect fixture, the securing lock engaged, valves H1 and H2 opened and vent valve H3 closed.

Valve L1 is opened very gradually to initiate flow through the nozzle under test, valves D1, L2, L3, B1, B2, C1, C2, C3 and C4 already having been opened.

The pressure upstream of the nozzle under test is then set by adjusting the regulating valves of pressure control system "B". When conditions have stabilised the diverter mechanism is actuated switching the flow into the weighing vessel and starting the timer. At the instant of diversion the pressure and temperature of the air in the unweighed volume are recorded. During the diversion period the pressure and temperature upstream of the nozzle under test are noted at regular intervals.

6

When the pressure in the weighing vessel reaches approximately 80 per cent of the nozzle upstream pressure (or 40 bar, whichever is the lower) the diverter is again operated and at the moment of operation the pressure and temperature of the air in the unweighed volume recorded. Valves L1, H1 and H2 are closed, valve H3 is opened, the lock is disengaged and the vessel then lowered on to the weighbridge to obtain its weight after the test. This weight, the diversion time and the temperature of the air surrounding the vessel are noted. During the test run the barometric pressure is also recorded.

The vessel is raised once again into the disconnect fixture, the lock is engaged, valves H1 and H2 are opened and then valve H3 is opened to exhaust the air from the vessel in preparation for the next test point.

The above procedure is repeated for each test point carried out.

2.1.2.3 Test results

The reference mass flowrate through the nozzle under test is obtained from the gravimetric system and is given by m/t i.e. the ratio of the mass (m) introduced in the vessel to the duration (t) of the diversion period.
Minor corrections are made (e.g. atmospheric buoyancy etc...) to get m with the best precision from the weighing machine.
Nozzles results are given with references to the nozzle Reynolds number. NEL states that the overall accuracy of the process is 0.25%, and will very soon be improved to reach 0.15% or better.

2.2 Calibration of massflowmeters by using transfer-standard nozzles

2.2.1 Types of airflow transfer standards.

Most wind tunnel facilities use sonic venturis to measure air mass flow. The geometry of the venturi is usually close to that of the Smith-Matz circular arc venturi described in ref.4. This geometry has the advantage of a very thin boundary layer, so that the transition process between the laminar and turbulent flow regimes introduces a minimum of uncertainty in the discharge coefficient. However, based on theoretical predictions (ref. 5 & 6), errors of 0.3 % or greater in discharge coefficient should be expected. Careful analysis of the flow can reduce this uncertainty (see chapter 3). Nevertheless, calibrations traceable to primary standards are required if much greater accuracy is to be achieved.

Primary standards are designed to provide the high accuracy required for calibration of transfer standards. As seen above, their mass flow range is not large enough to calibrate directly most of the flowmeters used in wind tunnel tests and the methods are too time consuming and expensive for the routine calibration of flowmeters. Therefore, any facility requiring such accuracy and traceability must provide and have calibrated a transfer standard suitable for calibration of the flowmeters that are normally used for testing. Calibration of the transfer standard must include the adequate accuracy and traceability of pressure and temperature instrumentation, which must also be used when calibrating flow meters at the user facility. Failure to do so will result in airflow measurements which have lost the accuracy and traceability to the primary standard.

The transfer standard must be designed to meet the needs of the user facility, as well as the capabilities and limitations of the primary standards laboratory. The transfer standard can be a single critical venturi, a multiple critical venturi (MCV) with binary sized venturis such as fig.9, or a multiple critical venturi with uniform sized venturis such as fig. 1. Each of these transfer standards must include an effective upstream flow distributor so that flow distortions cannot affect the airflow measurements. Significant deviations from the Smith-Matz venturi configuration, such as shown in fig.2, perform equally as well as evidenced in the data of reference 7.

2.2.2 Recommendations for calibration of working venturis.

Calibration of a working venturi with a transfer standard can be accomplished with a minimum loss of accuracy using the following procedures :

2.2.2.1

Steady state conditions must be achieved at each test condition for both the transfer standard and the working venturi before data are recorded. Temperatures will take much longer time than pressures to stabilize due to the Joule - Thomson temperature effects caused by the pressure drop of source pressure control as well as the pressure drop between the two sonic devices. For instance, a 50 bar pressure drop between the two choked nozzles can result in a 10 degrees decrease of temperature. Therefore many minutes can be necessary to stabilize temperatures at the beginning of a test sequence or run. Heat exchangers upstream of each sonic device could eliminate this problem, and improve data accuracy.

2.2.2.2

Pressure measurements for both the transfer standard and the working venturi can be measured with an accuracy of $\pm$ 0.01 % to $\pm$ 0.02 % at all conditions. A method which can achieve this accuracy utilizes dead weight testers, small range differential transducers, and solenoid valves as shown in figure 10. Transducer zero can be recorded at each pressure level by switching the solenoid valves so that both sides of the transducer are exposed to the dead weight tester, then switching the measuring side to read the small pressure differences from the dead weight testers to the transfer standard or the working venturi for the data record.

2.2.2.3

Temperatures for both the standard and the working venturi must be verified to an accuracy of $\pm$ 0.1°C or better at ambient temperature, as described under the section on instrumentation calibration and checks (§2.4.1).

2.2.3 Boeing transfer standard methodology

Reference 7 describes the Boeing airflow transfer standard with accuracy of 0.05 % or better (figure 1). This standard is traceable to the Colorado Engineering Experiment Station, Inc., (CEESI) Gravimetric Mass-Time System (ref.8), which is directly traceable to the U.S.National Bureau of Standards.

The mass-time system is limited to a maximum flow rate of 0.113 kg/s (0.25 lbm/sec). Therefore, the transfer standard contains 162 identical venturis (fig 2), each calibrated over the range from 0.0182 to 0.113 kg/s (0.04 to 0.25 lbm/sec), permitting the transfer standard to provide calibrations from 0.0182 to 18 kg/s (0.04 to 40 lbm/sec). This transfer standard has the added advantage that the venturis operate only in the laminar flow regime, so that when used to calibrate a working venturi, the uncertainty encountered during transition of the working venturi can be accurately measured. The CEESI calibration of the Boeing transfer standard is described in ref.9.

Essential to the development and calibration of the Boeing transfer standard was the venturi screening facility (fig.3). This facility consisted of two venturi stations in series, totally submerged in a circulating water bath maintained at 26.6 °C (80 ° F). This was to ensure that the plumbing, the venturis, and the air passing through the system were all at the same temperature. The upstream venturi was a common reference venturi with a nominal throat diameter of 0,0067 m (0.263 in.) and the downstream venturi station permitted each of the 163 venturis to be installed in turn. The design throat diameter was 0.00793 m (0.313 in.) for each of the 163 venturis.

Testing at Boeing with the venturi screening facility verified a high level of repeatability (fig.4), and the ability to accurately measure differences between the 163 venturis. Because the venturis were manufactured to be as identical as possible, it was not surprising that they had virtually identical Reynolds Number characteristics, and repeatable but different levels of discharge coefficient. These differences were found to be caused by the inability to accurately measure the venturi throat diameter (area). Therefore, the throat areas were adjusted to reflect effective area rather than measured area,

8

which resulted in a common Cd vs Rd curve for all 163 venturis (fig 5). This process is explained in detail in ref.7. This ability to accurately measure the venturi differences, eliminated the need to calibrate all 163 venturis by gravimetry. Such a calibration would have taken an estimated 4 years.

The calibrations at CEESI were done with the Boeing venturi screening facility installed directly downstream of the CEESI mass-time system (fig.6). Fourteen venturis were selected for calibration starting with S/N 1 and ending with S/N 160, with the selections somewhat uniformly spaced to cover the entire manufacturing sequence. S/N 1 venturi was calibrated at the beginning and end of the calibrations, and twice more between the other venturi calibrations. Of course, the common reference venturi was calibrated 17 times, since it was in series with each of the other venturis. Using the effective throat areas for each venturi which were evaluated earlier at Boeing, the CEESI gravimetric calibrations verified the common Cd vs Rd characteristic as well as the absolute levels of Cd (fig.7) for all 163 venturis.

An uncertainty analysis considering all elements of the calibration setup is presented in ref.7. This analysis estimates the uncertainty of discharge coefficient to be $\pm$ 0.07 % for an individual venturi, and $\pm$ 0.05 % for 2 or more venturis in parallel.

S/N 1 venturi has been preserved as a permanent control venturi for future calibration work. It is not used as part of the transfer standard. Should any of the other 162 venturis become damaged or deteriorated, the venturi screening facility could be reactivated using S/N 1 venturi to verify the integrity of the common reference venturi, which in turn could evaluate the Cd vs Rd characteristic and effective throat area for replacement venturis.

2.3 Nozzle thrust measuring benches.

Thrust measuring benches are required to enable the thrust and discharge characteristics of nozzle systems to be determined in isolation. A number of facilities exist world-wide to either support nozzle system design and/or for calibration of nacelle exhaust nozzle configurations for use in wind tunnel testing.

The basic requirements for thrust benches are common to most applications. A means is required whereby the thrust of the individual nozzles (primary and fan) can be derived from the measured overall thrust of the system and related to known upstream conditions. The nozzle system must be placed in a quiescent exhaust environment but under conditions that match the required model external pressures. The test technique necessitates careful bookkeeping of all the mass flows and forces involved in the system if the required accuracies are to be achieved.

In general the thrust bench will comprise a live (metric) model support frame, capable of measuring as a minimum the force along the nozzle thrust axis, surrounded by plenum shells and a means to provide the required inlet and/or exhaust pressure environments. Careful attention has to be given during facility design to minimise the tare loads generated on the live frame by the transfer of air across the force balance system as well as to minimise the pressure area terms acting on it.

Sonic venturis are typically used to measure the air mass flows entering into and exiting from the system: these require high precision and ideally should be traceable to recognised standards.

Procedures are required to routinely check correct operation of all the facility instrumentation (force, pressure and temperature) and to ensure that consistent calibration practices are followed.

Nozzles with 'known' characteristics (thrust and discharge) should be used on a regular basis to provide overall facility calibrations and to ensure continued satisfactory operation.

For Turbo-Powered-Simulator tests dryness for primary and secondary flows must be strictly controlled in order to avoid any ice formation. For all tests air should be dry enough to make sure that no risk of local condensation exists at slightly supersonic speeds in the nozzles.

Different types of thrust benches routinely used at ONERA, DLR, ARA , NLR and Boeing are described in appendix A to E.

2.4 General precautions for all tests

2.4.1 Instrumentation calibration and recommended checks for all tests

Nothing can be left to chance if the goal of 0.1% accuracy of thrust measurement is to be achieved or nearly achieved. The only item that is not calibrated or checked in the test set-up will probably be the one that does not work as advertised. There is nothing so wasteful as running a test with undiscovered and uncorrected errors or malfunctions. Calibrations and checks should be done prior to every test, and repeated at intervals during a test to develop confidence in the reliability and stability of the data. The intervals can be : every shift ; every day ; or anytime a malfunction is suspected.

Pressure transducers :
Must be isolated from acoustic noise, vibration, thermal input.
Must be calibrated with a traceable standard-dead weight tester.
Must exhibit small hysteresis characteristics.
Curve fit of data must be within ± 0.02%. (1)
Check calib's each shift must repeat within ± 0.02%. (1)

Force Measurement Systems :
Precision, traceable weights used for all loads.
All components of the balance must be calibrated.
Horizontal forces use a cable and pulley or knives for loading.
Axial force pulley must be at least 12" dia. low friction.
Curve fit of axial force data must be within ±0.02%. (1)
Check calib's each shift, axial force must repeat within ± 0.02% . (1)
Other 5 components can be less accurate.

Temperature Sensors :
When placed in a suitable heat sink with a traceable standard thermometer, should agree with the standard within ± 0.1°C or better after stabilization. (2) or (3)

Traceable Pressure Standards : Dead weight testers.
Make sure Metrology Lab. certifications meet your needs.
Do not accept certifications at face value.
Understand Metrology Lab. methods of data analysis.

(1) ± 0.02% of data values in the upper 80% of range.

(2) For removable sensors, an aluminium block makes an excellent heat sink, with holes to insert sensors and a standard thermometer. When placed on a styrofoam block away from draughts and heat sources, it will stabilize to room temperature in 15 to 20 minutes.

(3) For sensors permanently mounted in a blowing nacelle or Turbo-Powered-Simulator, plug the inlet/exhaust with soft cloths, carefully insert two or more standard thermometers past/through the cloths so the sensing bulbs are in contact with structure near the sensors. Wrap the entire nacelle with a blanket so the only source of thermal input is through the strut. Protect from draughts and heat sources. Allow to stabilize.

2.4.2 Determination of Tare Loads

2.4.2.1 General

For tests on powered models (isolated or installed) compressed air is often used as power source. The compressed air has to be supplied to the powered model through an air duct which has to pass the balance system with only minor interaction. In the calibration of the (internal or external) balance system, only dead weight effects and elasticity effects of the inoperative (decompressed) air duct have been taken into account implicitly. When compressed air and possibly heated air flows through the air duct towards the model in the test section, the duct may exert residual forces and moments on the balance structure, that will be interpreted by the balance system as forces and moments in the Balance Centre BC. Three separate effects in the air duct can be distinguished, although they occur simultaneously when compressed air is supplied to the powered model :

2.4.2.1.1 Pressure

The pressure inside the air duct deforms the structure in such a way, that an extra force may act on the balance system. This effect depends on the magnitude of the pressure inside the duct. A part of this pressure effect is also due to the weight of the compressed air. The type of uncoupling bellows and the overall layout of the rig can considerably reduce any of these effects.

2.4.2.1.2 Temperature

When the air duct is heated, the duct expands and consequently an extra force may act on the balance system. This effect depends mainly on the temperature difference between air duct and balance structure.

2.4.2.1.3 Momentum tare

In order to avoid any momentum effect of the air at the entrance of the metric part of the balance, the momentum of the air coming from the earth-fixed ducts and entering the ducts of the metric part of the balance must be strictly perpendicular to the axis of the nozzle.
The non fulfilment of this conditions, e.g. if the velocity disk in the air duct is possibly skew, gives rise to a momentum effect. This effect depending on both pressure and velocity levels at the entrance of the metric part of the balance must be carefully evaluated.

The air duct pressure and temperature effects on the balance system can easily be determined statically. Proper evaluation of the momentum tare loads is on the other hand more cumbersome but can be accomplished with reference nozzles. Two different methods (nozzles) will be discussed beneath. An alternative, using standard nozzles, is presented in ref. [28].

2.4.2.2 Zero-thrust body

Evaluation of momentum tare can be accomplished with a zero - thrust - body, as shown in fig.11. This is a simple device, but it must be accurately constructed so that the nozzle centrelines are coincident with each other, and perpendicular to the main body centreline. The bolt pattern at each end of the main body should be identical, so that the body can be reversed end - to - end, or rotated about its centreline in 90 ° increments. A thick, subsonic, perforated plate is needed at the entrance to the tube supporting each nozzle to align and distribute the flow. A series of pairs of nozzles is required so that 4 or 5 sizes can be used to evaluate each size airbridge. The nozzles should be sonic at all conditions, which keeps the air duct at a constant velocity whatever be the pressure level, for each nozzle size. A pressure and temperature measurement is required at the end of the body as shown.

Once the nozzle pairs have been calibrated by a sonic venturi, the nozzles can be used to measure the mass-flow rate for momentum tare evaluation, using the pressure and temperature in the zero-thrust body.

Each of the nozzle pairs may not be identical in size, and as a result, may not cancel or produce zero thrust. Therefore, it is recommended that when the nozzles are oriented in the plane of balance side force, that both side force and yaw moment loads are ignored. Similarly, when the nozzles are oriented in the plane of normal force (vertical plane), that both normal force and pitching moment loads are ignored.

For each powered test installation, a pressure and temperature measurement must be installed at the discharge end of the air duct system to relate to the pressure and momentum tare equations. These equations are shown in figure 11. Total mass flow for the air duct can be obtained from the sonic venturi/venturis used for the test.

2.4.2.3 Blown nozzle in the wind tunnel

An evaluation of momentum tare in the wind tunnel can also be accomplished with a blown nozzle. The blown nozzle should deliver thrust along the nozzle centreline. The blown nozzle can be used either in an isolated or installed test set-up. The principle is explained below for an isolated blown nozzle which is mounted to a strut (air duct) for air supply and connection to the external balance system.
The strut-nozzle interface should be designed in such a way that the nozzle can be mounted to the strut in "up-wind" and "down-wind" blowing direction. In this way the thrust exerts the external balance during one test in positive and during the other test in negative direction.
The isolated blown nozzle should be tested at wind-off conditions to determine the internal thrust and mass flows. The exhaust flow however can entrain flow completely around the tunnel circuit leading to external aerodynamic forces on the metric parts (strut, nozzle, etc.). This can be suppressed as follows :

a) Main jet flow in tunnel direction (down - wind blowing, see fig.12 A).
The tunnel test section is closed by a barrier ahead of the test section, surplus air should be vented to the environment at the settling chamber.

b) Main jet flow in opposite tunnel direction (up - wind blowing, see fig.12 B).
The tunnel test section is closed by a barrier behind the test section, surplus air should vented to the environment at the diffusor section (not shown in fig.12 B).

A second non - metric barrier might be required just upstream of the nozzle exit, to confine secondary recirculation flow downstream of this barrier and separate from the metric parts.

The blown nozzle should be supplied with pressure and temperature rakes. During the test compressed air is supplied to the nozzle up to the operational levels of pressure and flow. The mass flow can be obtained from the sonic venturi mounted in the drive air supply line. The balance readings should have been properly corrected for the static pressure and temperature effects (as described above) and for the measured strut deflections (change of engine centre N with respect to balance centre BC and rotation of nozzle axis respectively), which are introduced by forces, moments, temperature effects etc.

The blown nozzle should be calibrated in down-wind and up-wind direction and the derived components of the engine velocity coefficient vector are determined as a function of nozzle pressure ratio NPR.
The momentum tare loads are derived from:

1) The differences in the magnitude of the velocity vector components between both test set - ups (in this way the force and moment in Z - direction is not derived).

12

2) The magnitudes of the velocity vector components, with exception of X- direction. Theoretically all these thrust components should be zero.

One should be aware that only sensible momentum tare loads are derived when they are larger than might be expected from the balance accuracy and nozzle misalignment errors.

Some explanations concerning this technique of momentum tare evaluation with down-wind and up-wind blowing nozzles are given in figure 13.

3. FLOW ANALYSIS

There are several good reasons for paying attention to the detailed behaviour of the flow in the two types of nozzles which are currently in use for mass flow and thrust measurements in aerodynamic facilities.

    <u>a</u>- it may be difficult to justify the time and expense that Boeing expended in developing its Transfer Standard tools and methodology. However, the same repeatability and consistency of mass flow measurement can be achieved by calibrating each working venturi in series with a theoretically defined Standard venturi even though absolute accuracy may be slightly in error. Cross checking data with other facilities can determine if a systematic error remains in the absolute level of mass flow. This implies that accuracy of theoretical predictions is much better than the above quoted 0.3 %.

    <u>b</u>- assumptions of how toroidal throat nozzles do work, i.e. which boundary layer thickness should be accounted for at the throat, were slightly different in the different establishments, generating <u>differences</u> in the order of 0.2% on calculated discharge coefficients.

    <u>c</u>- most members of the group had had bad experiences in using cylindrical throat nozzles (ASME LRN) as references and they could not state precisely why; see for example fig. 32, 33, 34. Hence the Working Group decided that it was worth asking specialists to proceed with a few calculations and physical discussions in order to clarify above items (b) and (c) and to make a clear statement on what can be achieved with (a).

3.1 Cylindrical throat nozzles: the ASME Long Radius Nozzle

3.1.1 General considerations on ASME Long Radius Nozzle

The ASME Long Radius Nozzle (ASME LRN) is composed of a convergent inlet section described by a quarter ellipse, and a circular cylinder throat section. The connecting plane between the two sections is at their point of tangency. There are two designations for the ASME LRN based on internal geometric shape. The geometric shape is defined by the ratio of the nozzle throat diameter (d) to the upstream internal pipe diameter (D). This ratio is denoted as "β", where $\beta = d/D$. Typically β falls within the range of $0.2 \le \beta \le 0.8$. When $\beta \ge 0.45$ the nozzle is referred to as a "high β" nozzle and when $\beta \le 0,5$ it is referred to as a "low β" nozzle. The range between 0.45 and 0.50 is common to both types of nozzles. The relationships between β and the various geometric parameters describing the convergent inlet section, the cylindrical throat section and the internal pipe and throat diameter are shown in figure 14. From a practitioners perspective the "high β" nozzle minimizes flow restriction within the piping system while the use of a "low β" nozzle causes a greater flow restriction for a given mass flow and thus a correspondingly higher pressure differential which yields greater accuracy.

The ASME Long Radius Nozzle was designed for and is traditionally operated with subsonic flow in the nozzle throat. However, the nozzle can also be operated in a critical or choked flow condition, in which case the massflow rate of a given fluid through a given nozzle can in principle be easily calculated from simple one-dimensional theory as it is only a function of upstream total temperature and pressure. This theoretical massflow rate however is always different from the actual one due to :

    1- real gas effects;
    2- growth and development of the boundary layer within the nozzle;
    3- sonic line curvature.

The coefficient of discharge (C_D) is defined as the ratio of the actual to the theoretical massflow rate and is expected to account for all discrepancies between theory and the actual flow conditions. Examples of discrepancies are well documented by B.T. Arnberg [14].

Very few references pertaining to the coefficients of discharge and the operation of ASME LRN at high subsonic and critical or choked flow conditions are available in the open literature. Those that are available indicate that the uncertainty in the values of C_D was significant when the nozzle operates

14

with high subsonic or critical throat flow. This uncertainty was primarily attributed [17, 18, 19, 20] to boundary layer transition which occurred at throat Reynolds numbers between 0.6E6 to 2E6. The transition was promoted by the local adverse pressure gradient generated by the discontinuity in the wall-radius of curvature at the juncture of the elliptical inlet section and the cylindrical throat section. The sensitivity of this boundary layer transition to boundary layer development in the converging inlet section was discussed by Reimer [15] who found that the effects of machining and polishing could increase the C_D by 0.0025 for a given nozzle. Smith and Matz [17] found for critical flow the uncertainty in C_D resulting from transition was further exacerbated by the presence of a local supersonic flow zone at the juncture of the elliptical inlet section and the cylindrical throat section. This supersonic flow region was likely accompanied by downstream lambda shocks. All the above flow phenomena affect the level of uncertainty in C_D due to sensitiveness of boundary layer and flow development within the nozzle. The magnitude of this uncertainty was of the order of $\pm 0.3\%$ (95% confidence band) over the transition range. Uncertainty was reduced to $\pm 0.15\%$ downstream of the transition zone.

In order to further understand the physics of compressible air flow through a low ß value ASME LRN, a 2-D axisymetric CFD study was undertaken by Kubberud of CFD norway. Both Euler and viscous Navier-Stokes codes were employed. The Euler code (1515 grid points) was run for two nozzle geometries, first an ASME LRN and second, a modified ASME LRN that is with a divergent exit section mated to the downstream end of the cylindrical portion of the nozzle. The grids for the two geometries are shown in fig.15.
The Navier-Stokes code (6161 grid points, Baldwin Lomax turbulence model, Sutherland's viscosity formula, Red=8 10^6) was run using the second geometry.

Upstream boundary conditions were as follows: total pressure : 45 bar; total temperature: 293K.
Figures 16a and 16b (Euler code) and 16c (Navier-Stokes code) show computed iso-Mach number lines superimposed on the nozzle outlines. For the two Euler calculations, the location of the sonic line was found to be independent of nozzle exit geometry as is shown fig.16a and 16b. Figure 16c shows the effect of viscosity (growth of the wall boundary layer) on the location of the sonic line which has moved approximatively one-half a nozzle diameter downstream from the location shown in fig.16a and 16b. A reduction of 0.8% in the discharge coefficient Cd results from the growth of the boundary layer. The table hereafter shows the results.

Flow condition	C_D	
Isentropic (one dimensional)	1.0	
Non viscous, Euler (Axisymetric)	0.99916	) sonic line curvature effect only
Viscous, Navier-Stokes, Red= 8 10^6 (Axisymetric)	0.99088	)) boundary layer and sonic line) curvature effects

These effects also exist in other nozzles such as short radius nozzles discussed below. The point is that they are about twice stronger with the ASME LRN.

Accurate determination of C_D for a critical flow nozzle is only one of the many parameters required to calculate the mass flow, see Arnberg [14]. The uncertainty in C_D of the ASME LRN exceeds the desired uncertainty of 0.1% in the measurement of the mass flow rate required by AGARD Working Group 19. The experimental data cited in the literature [15 to 21] typically lie 0.7% below the ASME curve and the strong experimental evidence of boundary layer transition is neither shown nor replicated by the ASME curve.

This uncertainty makes the ASME Long Radius Nozzle unsuitable for use as a sonic nozzle for mass flow measurement and thrust calibration. The ASME Long Radius Nozzle was not designed for operation with high subsonic or critical flow conditions within the nozzle throat. The fact that its ability to measure mass flow rate with minimal uncertainty is unsatisfactory reflects not on the nozzle design but on the inappropriate operating condition of the nozzle.

3.2 Toroidal throat nozzle

3.2.1 Short radius nozzles: descriptions and references

In wind tunnels or other facilities where accurate mass flow measurements are required, mass flows are usually measured through sonic venturis with short radius nozzle. This geometry has the advantage of a well known curvature effect and of a very thin boundary layer.

Smith-Matz recommends a circular arc nozzle (fig. 17), (ref.4); the ratio of the arc radius to the throat diameter is 1.8175. ONERA uses similar circular arc nozzle with a ratio of 2 (Appendix F). For the Boeing transfer standard nozzle, Stevens (ref.7), uses a continuous curvature entrance shape with such parameters that in the throat region, the curve shape approximates the Smith-Matz circular arc contour (fig.17).

The centrifugal forces created by the turning of the flow in the contraction section produces a non one dimensional flow and then, a non uniform pressure and velocity distribution at the throat. This effect can be accurately predicted for circular arc nozzles (ref. 23 and 25).

The area reduction due to the boundary layer can be also accurately calculated, but the nature of the boundary layer (laminar or turbulent) can produce differences of 0.2 to 0.3%. The nature and thickness of the boundary layer at the throat are subject to a discussion beneath.

3.2.2 Examples of discharge coefficient calculations (calorically perfect gaz, $\gamma = 1.4$)

Various numerical flow analysis have been undertaken on the ONERA short radius nozzle described in appendix F, by CFD norway at Trondheim and by the Aerodynamic Division at ONERA.
Four cases of calculations can be reported and summarized as follows:

CASE	Throat diameter (mm)	Stagnation pressure (bar)	Reynolds number Red
1	10	25	$3.8\ 10^6$
2	10	45	$6.8\ 10^6$
3	20	25	$7.6\ 10^6$
4	20	45	$14\ 10^6$

The Reynolds number Red is calculated with the throat diameter and the throat flow conditions (critical flow):

$$Re\,d = \frac{a_c \cdot d \cdot \rho_c}{\mu_c}$$ - A stagnation temperature of 293 K was held constant in all cases.

3.2.2.1 CFD norway results

The associated numerical grid for non-viscous and viscous calculations, i.e. the grid used for solving the axisymetric Euler and Navier-Stokes equations respectively, are shown in figure 18. The discharge coefficient C_D has been evaluated with the results tabulated in the following:

Flow conditions	Discharge coefficient C_D Case 1	Discharge coefficient C_D Case 2	Discharge coefficient C_D Case 3	Discharge coefficient C_D Case 4
Isentropic 1-dim	1.0	1.0	1.0	1.0
Non viscous	0.99889	0.99888	0.9983	0.9984
Viscous, laminar	0.99685	0.99733	0.9973	-
Viscous turbulent	0.99330	0.99358	0.99472	0.99509
Viscous relaminarized	0.99330	0.99359	-	-

Case 3 was calculated for both laminar and turbulent flow (Stock-Haase turbulence model), and the

16

results are presented figure 19. As it can be seen, a laminar separation bubble is visible in the first part of the nozzle. However, the influence on the sonic line at the throat is negligible and the turbulent flow case is regarded as the most realistic one (Red = 7.6 10^6).

3.2.2.2 ONERA results

The same calculations have been performed independently by ONERA. The results are the following:

Flow conditions	Discharge coefficient C_D Case 1	Discharge coefficient C_D Case 2	Discharge coefficient C_D Case 3	Discharge coefficient C_D Case 4
Isentropic 1-dim	1.0	1.0	1.0	1.0
Non viscous	0.9991	0.9991	0.99902	0.99902
Viscous turbulent	0.99428	0.99477	0.99471	0.99515

When making the same physical assumptions, calculations should give very close results. In the "simple" non-viscous case, differences can however attain 0.06% and in the viscous case they can slightly exceed 0.1% which is already too much!

3.2.2.3 Comparison with previous results

It is worth asking whether these sophisticated codes bring much improvement comparing with analytical calculations made long ago by Masure in 1968 (ref.23) and Green in 1971 (ref.25). Results according to Masure (turbulent case) and Green ((laminar case) are shown hereafter, compared with the above results. They have been derived respectively from ref.23 and 25.
Nota: Masure's charts extracted from ref.30 and reproduced figure 17bis, allow to predict quickly short nozzle flow and thrust coefficient. These charts will be used for the so called « practical formulae » of chapter 3.5. Warning! Reynolds number mentioned on these charts is calculated with the half throat diameter h=d/2, and upstream stagnation conditions:

$$Re_{0,h} = \frac{a_0 \cdot h \cdot \rho_0}{\mu_0}$$

One finds: Red ≈ 1,34 $Re_{0,h}$

Non viscous

Case	1	2	3	4	
CFD norway	0.9989	0.9989	0.99833	0.99833	Sonic line
ONERA	0.9991	0.9991	0.99902	0.99902	curvature effect
Masure	0.99857	0.99857	0.99857	0.99857	only
Green	0.99844	0.99844	0.99844	0.99844	

Viscous (turbulent)

Red	3.8 10^6	6.8 10^6	7.6 10^6	14 10^6	
Isentropic 1-dim	1	1	1	1	Boundary layer
CFD norway	0.9933	0.99359	0.99472	0.99509	and sonic line
ONERA	0.99428	0.99477	0.99471	0.99515	curvature
Masure	0.99475	0.99510	0.99516	0.99548	effects

Green's results are not given because they are calculated using laminar boundary layer at the throat. One can see that all these results can deviate by up to 0.0007 for the sonic line curvature effect and by more than 0.001 for the viscous (turbulent) case.

Nevertheless, assuming that this 0.1% difference between calculations will be eliminated some day, it was decided to discuss the more important topic of the boundary layer behaviour in order to understand why it could have been considered laminar by one author and turbulent by another, the result being an uncertainty of 0.2% to 0.3% on the predicted discharge coefficient.

3.2.2.4 Boundary layer discussion

It is important for both theoretical predictions and experimental work to know the nature of the boundary layer i.e. laminar or turbulent in the nozzles:
- mass-flow computations may change by about 0.2% if a wrong assumption is made in theoretical models,
- selection of types of nozzles, machining and handling precautions, avoidance of transitional situations are directly affected by actual or assumed boundary layer conditions.
Such a discussion is not new. The topic has been adressed in the 30's and more in depth by Hall in 1959 (ref.27). However, since reputable scientists like Masure and Green have been led on this matter to what at first glance was appearing as contradicting assumptions, the working group had initially some difficulties to understand how different approaches could result in what seemed to be a reasonably good and consistent set of data. It was unfortunately impossible to find an unquestionable experimental description of the boundary layer behaviour for the considered family of sonic nozzles through a large enough Reynolds number range, however :
- well below 10^6 R.L.Steven's direct calibration with mass-time standards shows trends versus Reynolds number inferring that throat boundary layers are laminar;
- well above 10^6 numerous specialists following Masure have made with some good reasons the assumption that the throat boundary layer is turbulent.
Suspecting that both might be right at least at their end of the Reynolds number range and being aware of recent progress in the field of laminar flow control, a few calculations of typical nozzle flows using up to date models have been performed by boundary layer specialists at CFD norway and at ONERA-CERT.
Difficulties start with the nature of the incoming flow. In most cases the contraction ratio is large and the flow is fairly slow but turbulent. There is generally no clear stagnation line at the nozzle intake from which a boundary layer could start laminar. If therefore a nozzle throat is partly or fully laminar this can only result from some form of relaminarization under a strong positive velocity gradient.
In order to discuss this problem, the criteria for relaminarization due to Launder and Jones (ref.26) has been adopted, and applied to case 1 (Red = 3.8 10^6) and case 2 (Red = 6.8 10^6):

$$\frac{v}{u^2} \frac{du}{dx} > 2.5 \; to \; 5.10^{-6} \quad \Rightarrow \text{laminar flow}$$

$$\frac{v}{u^2} \frac{du}{dx} \leq 2.5 \; to \; 5.10^{-6} \quad \Rightarrow \text{turbulent flow}$$

- for throat Reynolds numbers $\mathrm{Re}\,d = \dfrac{a_c \cdot d \cdot \rho_c}{\mu_c}$ well below 10^6, $\dfrac{v}{u^2}\dfrac{du}{dx}$ stays above 2.5 10^{-6} or even

5.10^{-6} from early in the contraction down to the close neighbourhood of the sonic line. If, besides, the surface is smooth there is little doubt that the flow will be laminar for a wide range of upstream conditions.

- for high Reynolds numbers, say well above 10.10^6, the term $\dfrac{v}{u^2}\dfrac{du}{dx}$ does not reach such high

values as before and even if the boundary layer is not already turbulent upstream, at the nozzle intake, it will trip shortly and stay turbulent till the exit.
- in between, the situation is less simple : assuming as above that the boundary layer is initially

turbulent (no stagnation point !) the question is whether $\dfrac{v}{u^2}\dfrac{du}{dx}$ will reach 2.5 10^{-6} or 5.10^{-6} and stay

above such values long enough and close enough to the throat in order to get laminar-like throat conditions.

18

Figure 20 collects the various boundary layer thickness parameters calculated by CFD norway, whereas figure 21 depicts the value of the Launder and Jones parameter along the nozzle axis. As figure 21 indicates, a relaminarization of the boundary layer is expected for both cases and this is again visible in figure 22.

Cousteix and Aupoix at ONERA-CERT have observed that very soon after $\dfrac{v}{u^2}\dfrac{du}{dx}$ ceases being high enough, there is a quick transition back to turbulent conditions. Based on such data, computations have been made for case 1 (Red = 3.8 10^6) (fig.23), showing again that the boundary layer becomes laminar but trips back to turbulent far enough from the throat to get at the sonic line a boundary layer thickness nearly equal to what it would have been if the flow had never been laminar (fig.24).

What may happen between say 0.5 10^6 and about 3.5 10^6 is more difficult to predict and may be seriously depending on details of the upstream conditions. Especially whether it may be considered that some form of stagnation line exists is certainly important.

Basic experiments should be made at these Reynolds number with various upstream geometries and flows, i.e. having or not zero velocity (stagnation line) at the upstream "lips" of the nozzle. It will be desirable to go beyond "single" back to back comparisons with a reference nozzle and to include any possible means of boundary layer observation. This would help to answer important practical questions on the design of the flowmeters and help to make sure that flow rate measurements do add properly when several low Reynolds nozzles are installed in parallel.

A thorough understanding of these phenomena would also greatly simplify test operation, increase confidence and, as a result, reduce the overall cost of these tedious calibration processes.

3.3 Real gas effects

Early in the activity of the Working Group, it appeared that real gas effects were not always understood in the same way by the various specialists and that tables and formulae used to predict these important effects should be compared.

In order to avoid any misunderstanding the equations allowing to perform such predictions and comparisons are reported hereafter.

3.3.1 Notations (these notations apply to §§ 3.3 through 3.5)

a	:	Celerity of sound (m/s)
A	:	Area (m^2)
B(T)	:	Virial coefficient
C(T)	:	Virial coefficient
C*	:	Critical flow factor introduced by Johnson (see equation (7))
C_i^*	:	critical flow factor for a calorically perfect gas $= \left[\gamma(2/\gamma+1)^{\gamma+1/\gamma-1}\right]^{1/2}$
		For $\gamma = 1.4$, $C_i^* = 0.6847314$
C_{D_δ}	:	Correction factor for the mass flow rate through a choked nozzle due to viscous effect
C_{D_K}	:	Correction factor for the mass flow rate through a choked nozzle due to the curvature of the sonic surface
C_{D_V}	:	Correction factor for the mass flow rate through a choked nozzle due to real gas effect (virial effect) : $C_{D_V} = Q$ real gas / $Q_{\gamma=1.4}$ for a given couple p_o, T_o
C_{T_V}	:	Correction factor for thrust per mass flow unit due to real gas effect (virial effect) : $C_{T_V} = \dfrac{(F_V/Q)\,\text{real air}}{(F_V/Q)\,\gamma = 1.4}$ for a given couple p_o, T_o - see eq. (18)
D(T)	:	Virial coefficient

d	:	Diameter of the nozzle throat ($= 2\,h$) (m)
F	:	Thrust (N)
Fv	:	Thrust in vacuum (or absolute thrust) (N)
h	:	Enthalpy. Also radius of the throat of a nozzle . A_c being the geometrical area of the throat : $A_c = \pi\,h^2$
K_{TA}	:	Absolute thrust coefficient : $K_{TA} = \dfrac{F_V}{Q\sqrt{RT_o}\,/\,C_i^*}$
M	:	Mach number
M_E	:	Mach number in the exit plane of a contoured nozzle (ideal)
M'_E	:	Mach number in the "inviscid" part of the flow at the exit plane of a contoured nozzle (see eq. (25 bis))
M''_E	:	Mach number defined by eq. (28 bis). No physical meaning
$\mathscr{M}$	:	Mass of one mole of air (kg) : $= 28.965 \times 10^{-3}$ kg
p	:	pressure (N/m^2)
Q	:	Mass-flow rate (kg/s)
$\mathfrak{R}$	:	Universal constant of gas : $= 8.31409$ Joule/(mole . K)
R	:	$\dfrac{\mathfrak{R}}{\mathscr{M}} = \dfrac{8,31409}{28,965 \times 10^{-3}} = 287,04\,(m/s)^2 \cdot (K)^{-1}$; also radius of curvature of the throat of a nozzle (m)
R e	:	Reynolds number
$Re_{o,h}$	:	Reynolds number defined with stagnation conditions and half diameter of the throat : $Re_{o,h} = \dfrac{\rho_o\,a_o\,h}{\mu_o}$
Re_d	:	Reynolds number defined with critical conditions and diameter d of the throat : $Re_d = \dfrac{\rho_c\,a_c\,d}{\mu_c}$ N.B. : $Re_d = 1.34\ Re_{o,h}$ for 288 K stagnation temperature
s	:	Entropy
T	:	Temperature in K (Kelvin), °C (Celsius), °R (Rankine) N.B. : T (°R) = 9/5 T (K)
V	:	Velocity (m/s)
Z	:	Compressibility factor. For a perfect gas : $Z \equiv 1$

Grecian notations

γ	:	Ratio of specific heats ($\gamma = C_p/C_v$). For a biatomic calorically perfect gas : $\gamma = 1.4$
Δ	:	Thickness of a boundary layer
$\delta^{(1)}$	:	Displacement thickness of a boundary layer
$\delta^{(2)}$	:	Momentum thickness of a boundary layer
μ	:	Viscosity coefficient (Poiseuille). Sutherland's law : $\mu = \mu_o \dfrac{T_o + C}{T + C}\left(\dfrac{T}{T_o}\right)^{3/2}$ with T(K) ; $T_o = 288$ K ; C = 110,4 K $\mu_o = 1,789 \times 10^{-5}$ Poiseuille
ρ	:	Density (kg/m^3)
$\overline{\omega}\,(M)$	:	Defined by $\overline{\omega}\,(M) = \left(1 + \dfrac{\gamma-1}{2}M^2\right)^{-\gamma/\gamma-1}$
$\Sigma\,(M)$	:	Defined by $\Sigma\,(M) = (2/\gamma+1)^{\frac{\gamma+1}{2(\gamma-1)}} \cdot \dfrac{1}{M} \cdot \left(1 + \dfrac{\gamma-1}{2}M^2\right)^{\frac{\gamma+1}{2(\gamma-1)}}$
$\varnothing\,(M)$	:	Defined by $\varnothing\,(M) = \overline{\omega}\,(M)\,\Sigma\,(M)\left(1 + \gamma M^2\right)$

20

Indices

o   :   Stagnation conditions

c   :   Generally means critical conditions (M = 1). But A_c is the geometrical area of the throat of a nozzle ($A_c = \pi\, h^2$)

E   :   In the exit plane of a nozzle

v   :   In vacuum

3.3.2 Real gas effects on mass flow rate

Frequently it happens that the stagnation pressures used in the flowmeters reach relatively high levels (10 to 50 bars). In these conditions, and at moderate stagnation temperature levels (between 0 to 50°C), air does not behave any longer as a calorically perfect gas, neither as a perfect gas. Then its equation of state takes the form :

$$p = Z\,(T, \rho)\,\rho\,RT$$

where Z (equal to one for a perfect gas) is the compressibility factor known and tabulated by means of the virial coefficients :

$$Z = 1 + B(T)\,\rho + C\,(T)\,\rho^2 + D\,(T)\,\rho^3 + \dots ,$$

B(T), C(T), D(T) being the virial coefficients.

The entropy-enthalpy diagram resulting from this state equation allows to calculate isentropic expansions for various stagnation conditions. More precisely :

- p_o and T_o being a <u>given</u> couple of stagnation pressure and temperature, it is possible to determine the critical values (M = 1) of the density (ρ_c) and of the celerity of sound (a_c) resulting from an isentropic expansion. The corresponding mass-flow rate for a sonic throat of geometrical area A_c is therefore, for a <u>one-dimensional flow</u> :

$$Q\,_{\text{real gas}} = \rho_c \cdot a_c \cdot A_c \tag{1}$$

- for the same couple p_o, T_o of stagnation pressure and temperature, it is possible on the other hand to calculate a fictitious mass-flow rate assuming that air behaves as a calorically perfect gas (Z = 1 ; γ = 1.4) all along the isentropic expansion from (p_o, T_o) to M = 1.

This fictitious mass-flow rates called $Q_{\gamma=1.4}$ for a sonic throat of same geometrical area A_c as previously, reads, again for a one dimensional flow :

$$Q_{\gamma=1.4} = \rho_{c\gamma=1.4} \cdot a_{c\gamma=1.4} \cdot A_c$$

Or

$$Q_{\gamma=1.4} = \left(\frac{\rho_c}{\rho_o}\right)_{\gamma=1.4} \left(\frac{a_c}{a_o}\right)_{\gamma=1.4} \frac{p_o}{T_o} \sqrt{\gamma\,R\,T_o}\; A_c \qquad \text{(all terms derived from } p_o, T_o \text{ through } \gamma=1.4 \text{ perfect gas equations)}$$

$$Q_{\gamma=1.4} = \left\{ \gamma \left(\frac{2}{\gamma+1}\right)^{\frac{\gamma+1}{\gamma-1}} \right\}^{1/2} \frac{p_o\,A_c}{\sqrt{R\,T_o}}$$

$$Q_{\gamma=1,4} = C_i^* \frac{p_o A_c}{\sqrt{R T_o}} \tag{2}$$

$$\text{with } C_i^* = \left\{ \gamma \left(\frac{2}{\gamma+1} \right)^{\frac{\gamma+1}{\gamma-1}} \right\}^{1/2} \tag{3}$$

$$\text{for } \gamma = 1,4, \ C_i^* = 0,6847314 \tag{4}$$

It is then possible to define a coefficient C_{D_V} (V for Virial effect) which is the ratio of the real mass-flow rate Q real gas given by (1) to the fictitious mass-flow rate $Q_{\gamma=1,4}$ given by (2)

$$C_{D_V} = \frac{Q \text{ real gas}}{Q_{\gamma=1,4}} \tag{5} \quad \text{(same } p_o, \ T_o)$$

The values of $[C_{D_V} - 1] \times 10^3$ as a function of p_o and T_o have been calculated by Masure and are given in fig. 17 bis-c extracted from [30] and in figure 25. It should be noticed that the correction appears to be, at constant T_o, a linear function of p_o. Then, we can use, for the domain of stagnation temperature and pressure considered here, the practical following formula :

$$C_{D_V} = 1 + 0,035 \frac{p_o \text{ (atm)}}{T_{o (K)} - 210} \tag{6}$$

It is worth noting that Masure's calculations are based on the Thermodynamics tables of Michels, Wassenaar, Wolkers [24].

Many other authors made similar calculations. For instance Johnson [11], combining analytical developments and use of Thermodynamic tables of Hilsenrath, Joseph and al [22], gives the values of a "critical flow factor" C^* defined as below :

$$Q \text{ real gas} = \rho_c \cdot a_c \cdot A_c = C^* \cdot \frac{p_o A_c}{\sqrt{R T_o}} \tag{7}$$

Therefore, (2) and (7) give :

$$C_{D_V} = \frac{C^*}{C_i^*} \tag{8}$$

$$\text{with } C_i^* = 0,68473 \text{ (see (4))}$$

Table I gives some values of C_{D_V} as obtained by Masure (formula (6)) and Johnson (formula (8)) for p_o = 10, 20, 30, 40 atm and T_o = 480°R (266.7 K) ; 500°R (277.8 K) ; 540°R (300 K) ; 580°R (322.2 K).

This table leads to the three following remarks :

a) The real gas effect on mass flow rate is far from negligible. For instance for p_o = 40 atm and T_o = 266.7 K, the correction due to real gas effect is about 25×10^{-3}.
b) The actual mass-flow rate is always higher than the mass-flow rate calculated, were the air a calorically perfect gas (Z = 1 ; γ = 1.4).
c) Values given by Masure and Johnson are very near each other but different : the difference between them never exceeds 0.6×10^{-3} on table I. The ratio of these two values is presented on the figure 26 for a larger range of pressure : $0 \leq p_o \leq 60$ bar. On this figure, the gap is slightly smaller than 1.10^{-3}. Since Masure and Johnson made what is indeed the <u>same</u> calculation in two

22

different ways but starting from two different sources of thermodynamic data, reducing the gap would need to recheck thermodynamic tables !

Remark : the pressure range for formula (6) is : 0 atm to about 50 atm. For higher pressures $(50 \leq p_o \leq 100$ atm), it is recommended to use Johnson's values of the critical flow factor C^* given in [11] and to apply equation (8).

Conclusions

If high accuracy is needed when measuring mass flow rate with sonic Venturis, real gas effect (virial effect) must be taken into account.

The actual mass flow rate is :

$$Q_{\text{real gas}} = C_{D_V} \cdot C_i^* \cdot \frac{p_o A_c}{\sqrt{R T_o}} \qquad (9)$$

Were air a calorically perfect gas with $\gamma = 1.4$, then C_{D_V} is equal to one. The difference $C_{D_V} - 1$ can be substantial.

Refining real gas corrections (C_{D_V}) beyond 1.10^{-3} would require to check thermodynamic tables.

Table I

Real gas effect (virial effect) on mass flow rate for a sonic Venturi

T_o (°R)	T_o (K)	p_o (atm) 10		20		30		40	
480	266.7	(J)	$1 + 6.1 \times 10^{-3}$	(J)	$1 + 11.9 \times 10^{-3}$	(J)	$1 + 17.9 \times 10^{-3}$	(J)	$1 + 24.1 . 10^{-3}$
		(M)	$1 + 6.2 \times 10^{-3}$	(M)	$1 + 12.3 \times 10^{-3}$	(M)	$1 + 18.5 \times 10^{-3}$	(M)	$1 + 24.7 \times 10^{-3}$
500	277.8	(J)	$1 + 5.4 \times 10^{-3}$	(J)	$1 + 10.5 \times 10^{-3}$	(J)	$1 + 15.6 \times 10^{-3}$	(J)	$1 + 20.8 \times 10^{-3}$
		(M)	$1 + 5.2 \times 10^{-3}$	(M)	$1 + 10.3 \times 10^{-3}$	(M)	$1 + 15.5 . 10^{-3}$	(M)	$1 + 20.7 \times 10^{-3}$
540	300	(J)	$1 + 4.0 \times 10^{-3}$	(J)	$1 + 8.0 \times 10^{-3}$	(J)	$1 + 11.9 \times 10^{-3}$	(J)	$1 + 15.7 \times 10^{-3}$
		(M)	$1 + 3.9 \times 10^{-3}$	(M)	$1 + 7.8 \times 10^{-3}$	(M)	$1 + 11.7 \times 10^{-3}$	(M)	$1 + 15.6 \times 10^{-3}$
580	322.2	(J)	$1 + 3.0 \times 10^{-3}$	(J)	$1 + 6.1 \times 10^{-3}$	(J)	$1 + 9.0 \times 10^{-3}$	(J)	$1 + 11.9 \times 10^{-3}$
		(M)	$1 + 3.1 \times 10^{-3}$	(M)	$1 + 6.2 \times 10^{-3}$	(M)	$1 + 9.4 \times 10^{-3}$	(M)	$1 + 12.5 \times 10^{-3}$

Coefficient $C_{D_V} = \dfrac{Q_{\text{real gas}}}{Q_{\gamma=1,4}}$ for a sonic venturi as given by Johnson (J) and Masure (M)

Remark : Johnson's C_{D_V} values have been deduced from data given in table II of reference [11] using equation (8) of the present report.

Masure's C_{D_V} values have been deduced from equation (6) of the present report.

3.3.3 Real gas effects on thrust
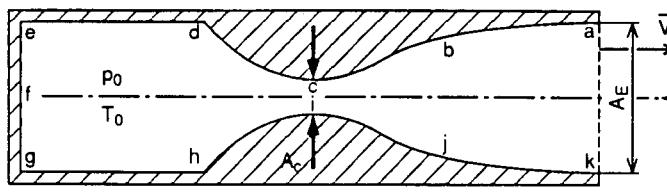
For a subsonic-supersonic nozzle, the thrust in vacuum $\overrightarrow{F_v}$ (also called absolute thrust) can be calculated using momentum equation :

$$\overrightarrow{F_v} = \left[\left(p_E + \rho_E\, V_E^2\right) A_E\right] \overrightarrow{x}$$

where $\overrightarrow{x}$ is a unitary horizontal vector oriented upstream.

The quantity $\left(p_E + \rho_E\, V_E^2\right) A_E\, \overrightarrow{x}$ is equal to the integral of pressure on the <u>internal</u> surface a b c d e f g h i j k of the nozzle.

We now calculate F_v assuming <u>one-dimensional</u> isentropic flow for both cases :

1) air is assumed to be a perfect gas (compressibility factor equal to one : Z = 1) with constant specific heats (γ = 1.4).

2) air is considered as a real gas (Z $\neq$ 1).

1 Case 1 : <u>air is assumed to be a calorically perfect gas (Z = 1 ; γ = 1.4)</u>

$$F_v = \left(p_E + \rho_E\, V_E^2\right) A_E$$

$$= p_E \left(1 + \gamma M_E^2\right) A_E \qquad (10)$$

$$= \frac{p_E}{p_0} \frac{A_E}{A_c}\left(1 + \gamma M_E^2\right) p_0\, A_c$$

(E means : in the exit plane A_E, M_E : Mach number in A_E, A_c : sonic throat area, P_0 : stagnation pressure of the upstream flow).

On the other side, in the frame of the same assumption, the mass-flow rate is :

$$Q = C_i^* \frac{p_0}{\sqrt{RT_0}} A_C \qquad \text{with } C_i^* = \left\{\gamma\left(\frac{2}{\gamma+1}\right)^{\frac{\gamma+1}{\gamma-1}}\right\}^{1/2} \qquad (11)$$

$$\text{for } \gamma = 1.4 : C_i^* = 0{,}6847314$$
$$T_0 : \text{stagnation temperature of the upstream flow (K)}$$

Combining (10) and (11) gives :

$$F_v = \left(\frac{p_E}{p_0}\right)\left(\frac{A_E}{A_C}\right)\left(1 + \gamma M_E^2\right)\frac{Q\sqrt{RT_0}}{C_i^*}$$

Or

$$\frac{F_v}{Q\sqrt{RT_0}/C_i^*} = \frac{p_E}{p_0} \cdot \frac{A_E}{A_C} \cdot \left(1 + \gamma M_E^2\right) \qquad (12)$$

24

In order to recall that the ratio $\dfrac{F_v}{Q \sqrt{RT_o} / C_i^*}$ is equal to the right-hand side of (12) only if air

is assumed to be a calorically perfect gas, we use hereafter the abbreviation $\gamma = 1.4$:

$$\frac{F_{v(\gamma=1,4)}}{Q_{(\gamma=1,4)} \sqrt{RT_o} / C_i^*} = \frac{p_E}{p_o} \cdot \frac{A_E}{A_c} \cdot \left(1 + \gamma M_E^2\right) \tag{13}$$

Remarks :

- $\dfrac{p_E}{p_o} = \left(1 + \dfrac{\gamma - 1}{2} M_E^2\right)^{-\gamma/\gamma-1}$

- $\dfrac{A_E}{A_c} = \left(\dfrac{2}{\gamma + 1}\right)^{\frac{\gamma+1}{2(\gamma-1)}} \cdot \dfrac{1}{M_E} \cdot \left(1 + \dfrac{\gamma - 1}{2} M_E^2\right)^{\frac{\gamma+1}{2(\gamma-1)}}$

R = defined in 3.3.1 as the ratio of the universal constant of gases to the molar mass of air.

2 Case 2 : air is considered as real gas (Z ≠ 1)

F_v being now the thrust in vacuum in real gas conditions, we have :

$$\begin{aligned} F_v &= \left(p_E + \rho_E V_E^2\right) A_E \\ &= p_E A_E + \left(\rho_E V_E A_E\right) V_E \end{aligned} \quad \begin{array}{l}\text{(all quantities consistent with} \\ \text{isentropic real gas expansion)}\end{array} \tag{14}$$

Starting from given values of the stagnation pressure p_o and stagnation temperature T_o, it is possible, using either thermodynamic tables of air or alytical formulas taking into account the virial effect for air, to calculate isentropic expansions of the gas. For a particular value of the pressure, called critical pressure p_c, the velocity of the flow is equal to the celerity of sound : $V = a_c =$ and the corresponding value of the density is p_c If A_c is the area of the throat (assumed sonic), the mass-flow rate is :

Q real air $= \rho_c \cdot a_c \cdot A_c$

For any other pressure p_E below p_c, the values of the velocity of the flow, of the celerity of sound and of the density, for the same isentropic expansion, will be called V_E, a_E, ρ_E.

To calculate the area A_E occupied by the flow in this new state, we use the continuity equation :

$\rho_E \cdot V_E \cdot A_E = \rho_c \, a_c \, A_c = Q$ real air

This gives :

$$A_E = \frac{Q \text{ real air}}{\rho_E \cdot V_E} \tag{15}$$

Therefore, (14) becomes :

$$F_{v_{\text{real air}}} = p_E \cdot \frac{Q \text{ real air}}{\rho_E \cdot V_E} + Q \text{ real air} \cdot V_E \tag{16}$$

We now introduce, in the same way as for case 1, the ratio :

$$\frac{F_{V_{real\ air}}}{Q\ real\ air\ \sqrt{RT_0}\ /\ C_i^*}.$$

Using (16) we find :

$$\frac{F_{V_{real\ air}}}{Q_{real\ air}\ \sqrt{RT_0}\ /\ C_i^*} = \frac{\dfrac{P_E}{\rho_E\ V_E} + V_E}{\sqrt{RT_0}\ /\ C_i^*} \qquad (17)$$

It is now interesting to compare the two ratios as given by equations (13) and (17) for the same nozzle defined by A_E/A_c, each of these two ratios being in fact, besides the coefficient $\sqrt{RT_0}/C_i^*$, the unitary thrust (that is to say the thrust per mass flow unit) for each of the two cases 1 and 2 .

We introduce consequently a coefficient C_{T_V} (T for thrust, V for virial) defined by :

$$C_{T_V} = \frac{F_{V_{real\ air}}/Q_{real\ air}}{F_{V_{(\gamma=1,4)}}/Q_{(\gamma=1,4)}} \qquad (18)$$

Masure [30], carrying out calculations using thermodynamic tables of reference [24] in the domain $0 < p_o < 40$ atm, $0°C < To < 75°C$ and for different values of A_E/A_c ($A_E/A_c = 1$; 1.7 ; 3 ; ∞ (ultimate expansion)), found that, for a given nozzle and a given stagnation temperature To, the coefficient C_{T_V} is a function practically linear of the stagnation pressure p_o (like for the mass flow rates). The effect of pressure may therefore be outlined by putting it in the form indicated in fig. 17 bis-d, where the results of the calculations are presented for various A_E/A_c.

Let us recall that the statements made here for the thrust are only valid within a domain of stagnation pressure identical to that considered for mass flow rates.

Let us consider an example : $p_o = 40$ atm ; $T_o = 0°C$; $A_E/A_c = 3$

$$C_{T_V} = \frac{F_{V_{real\ air}}/Q_{real\ air}}{F_{V_{(\gamma=1,4)}}/Q_{(\gamma=1,4)}} = 1 - 24.4 \times 10^{-3}$$

Such a correction is far from negligible.

Johnson [11] carried out similar calculations which can be compared to Masure's as it has been done for thrust in above 3.3.2.

Such a comparison will be carried out for sonic nozzle only because, Johnson did not carry out his isentropic expansions beyond critical flow (M = 1)

For a sonic nozzle, equation (17) reads :

$$\frac{F_{V_{real\ air}}}{Q_{real\ air}\ \sqrt{RT_0}/C_i^*} = \frac{\dfrac{p_c}{\rho_c \cdot a_c} + a_c}{\sqrt{RT_0}/C_i^*} \qquad (19)$$

Using $\quad Q_{real\ air} = \rho_c \cdot a_c \cdot A_c = C_{D_V}\ C_i^* \dfrac{p_o A_c}{\sqrt{RT_0}},$

26

equation (19) becomes :

$$\frac{F_{v_{real\ air}}}{Q_{real\ air}\sqrt{RT_o}/C_i^*} = \frac{p_c/p_o}{C_{Dv}} + C_i^* \frac{a_c}{\sqrt{RT_o}} \qquad (20)$$

Johnson's results [11] can now be used to calculate the right-hand side of (20). Choosing values for the stagnation pressure p_o and stagnation temperature T_o, one finds in [11]:

α) the value of p_c/p_o (see table II(c) : Critical pressure ratio)

β) the value of $C_{Dv} = \dfrac{\text{critical flow factor}}{C_i^*}$ (see table II (a) : critical flow factor)

γ) the value of a_c : a_c is equal to the nozzle-throat velocity because $M = 1$. In table II(b), Johnson gives the values of the ratio of nozzle-throat velocity to the speed of sound at 1 atmosphere and 491.688°R (1087.42 ft/sec). Remark : 1087.42 ft/sec = 331.4456 m/s.

With these values and with C_i^* given by (4) and R given following 3.3.1 by

$$R = \frac{8.31409}{28.965 \times 10^{-3}} = 287.04 \ (m/s)^2 \ (K)^{-1},$$

the ratio $\dfrac{F_{v_{real\ air}}}{Q_{real\ air}\sqrt{RT_o}/C_i^*}$ can be determined thanks to (20).

The value of the same ratio for $\gamma = 1.4$ is given by (13) in which one has to assume that the nozzle is sonic ($M_E = 1$) :

$$\frac{F_{v_{(\gamma=1.4)}}}{Q_{\gamma=1.4}\sqrt{RT_o}/C_i^*} = \left(\frac{p_c}{p_0}\right)_{\gamma=1.4} \cdot 1.(\gamma+1) = 1.26788$$

Finally, we obtain $C_{Tv} = \dfrac{F_{v_{real\ air}}/Q_{real\ air}}{F_{v_{\gamma=1.4}}/Q_{\gamma=1.4}} = \dfrac{F_{v_{real\ air}}/\left(Q_{real\ air} \times \sqrt{RT_o}/C_i^*\right)}{1.26788} \qquad (21)$

Johnson's C_{Tv} values as given by (21) have been calculated for $p_o = 10 ; 20 ; 30 ; 40 ; 50$ atm and To = 480°R (266.7 K) ; 500°R (277 K) ; 540°R (300K) ; 580°R (322.2K) ; 620°R (344.4K).

Results are presented on figure 27. It appears clearly that C_{Tv} is almost a linear function of p_o for a given T_o, confirming Masure's conclusion.

The comparison between Johnson's results and Masure's results concerning sonic nozzle is presented on table II and figure 28.

Figures 27 and 28, and table II lead to the following remarks :

a) The real gas effect on the coefficient C_{T_V} is far from negligible for a <u>sonic nozzle</u>. For instance for $p_o = 50$ atm and $T_o = 266.7$ K, the correction due to real gas effect is about - 24×10^{-3}.

b) The actual unitary thrust (thrust per unit of mass flow rate) is always lower than the unitary thrust calculated, were air a calorically perfect gas ($Z = 1$; $\gamma = 1.4$).

c) Values given by Masure and Johnson are very near each other : the difference between them seldom exceeds 1.10^{-3} (see table II and figure 28).

For a <u>supersonic nozzle</u>, figure 17 bis.d shows that : the higher A_E/A_C, the higher the real gas effect on thrust.

Table II

Real gas effect (virial effect) on thrust for a sonic nozzle

T_o (°R)	T_o(K) / p_o (atm)	10	20	30	40	50
480	266.7	(J) $1 - 4.9 \times 10^{-3}$ (M) $1 - 4.7 \times 10^{-3}$	(J) $1 - 9.8 \times 10^{-3}$ (M) $1 - 9.5 \times 10^{-3}$	(J) $1 - 14.4 \times 10^{-3}$ (M) $1 - 14.2 \times 10^{-3}$	(J) $1 - 19.1 \times 10^{-3}$ (M) $1 - 18.9 \times 10^{-3}$	(J) $1 - 23.4 \times 10^{-3}$ (M) $1 - 23.6 \times 10^{-3}$
500	277.8	(J) $1 - 4.3 \times 10^{-3}$ (M) $1 - 4.2 \times 10^{-3}$	(J) $1 - 8.3 \times 10^{-3}$ (M) $1 - 8.4 \times 10^{-3}$	(J) $1 - 12.2 \times 10^{-3}$ (M) $1 - 12.6 \times 10^{-3}$	(J) $1 - 16.0 \times 10^{-3}$ (M) $1 - 16.8 \times 10^{-3}$	(J) $1 - 19.7 \times 10^{-3}$ (M) $1 - 21.0 \times 10^{-3}$
540	300	(J) $1 - 3.0 \times 10^{-3}$ (M) $1 - 3.0 \times 10^{-3}$	(J) $1 - 5.9 \times 10^{-3}$ (M) $1 - 6.1 \times 10^{-3}$	(J) $1 - 8.7 \times 10^{-3}$ (M) $1 - 9.1 \times 10^{-3}$	(J) $1 - 11.4 \times 10^{-3}$ (M) $1 - 12.2 \times 10^{-3}$	(J) $1 - 13.8 \times 10^{-3}$ (M) $1 - 15.2 \times 10^{-3}$
580	322.2	(J) $1 - 2.1 \times 10^{-3}$ (M) $1 - 2.1 \times 10^{-3}$	(J) $1 - 4.1 \times 10^{-3}$ (M) $1 - 4.2 \times 10^{-3}$	(J) $1 - 6.0 \times 10^{-3}$ (M) $1 - 6.2 \times 10^{-3}$	(J) $1 - 7.8 \times 10^{-3}$ (M) $1 - 8.3 \times 10^{-3}$	(J) $1 - 9.6 \times 10^{-3}$ (M) $1 - 10.4 \times 10^{-3}$
620	344.4	(J) $1 - 1.3 \times 10^{-3}$ (M) $1 - 1.3 \times 10^{-3}$	(J) $1 - 2.7 \times 10^{-3}$ (M) $1 - 2.5 \times 10^{-3}$	(J) $1 - 4.0 \times 10^{-3}$ (M) $1 - 3.8 \times 10^{-3}$	(J) $1 - 5.2 \times 10^{-3}$ (M) $1 - 5.1 \times 10^{-3}$	(J) $1 - 6.2 \times 10^{-3}$ (M) $1 - 6.3 \times 10^{-3}$

Coefficient $C_{T_V} = \dfrac{F_{\text{real gas}} / Q_{\text{real gas}}}{F_{V_{\gamma=1.4}} / Q_{\gamma=1.4}}$ for a sonic nozzle as given by Johnson (J) and Masure (M)

<u>Remark</u> : Johnson's C_{T_V} values have been deduced from data given in table II of reference [11] using equations (20) and (21) of the present report.

Masure's C_{T_V} values are deduced from figure 17 bis-d.

3.4 Viscous effects on thrust

3.4.1 Preliminary remarks

Addressing the general issue of viscous effects on thrust would obviously be far more complicated than doing it as above for mass flow rates. Indeed, amongst others, the following difficulties would be met :

- boundary layer effects of all kinds,
- shock boundary layer interaction
- computation of the supersonic free flow in presence of a boundary layer
- separation etc...

Nevertheless, it seemed useful, within the scope of this report to present some relatively simple calculations which provide in most practical cases a reasonably good approximation of thrust coefficients. This should allow operators of thrust measuring rigs to do some first cross-checking with their force measurements. The simplifying physical assumptions are the following :

- thin boundary layers at the throat and in the exit plane
- no separation in the nozzle,
- no dramatic effect of the boundary layer in the nozzles on the isentropic expansion of the supersonic free flow : the boundary layer changes slightly the « shape » of the contoured nozzle, hence changing the exit Mach number but the free flow at the exit plane remains reasonably uniform.

Calculation presented hereunder are made under these assumptions, following [31] :

3.4.2 Non viscous thrust reference

To estimate viscous effects on thrust we assume in this § 3.4 that air is a calorically perfect gas $(Z = 1 ; \gamma = 1.4)$.
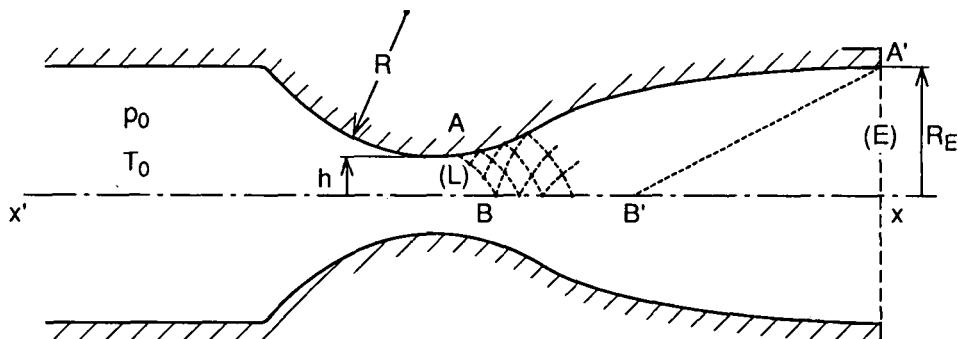
Let us consider an axisymmetric contoured subsonic-supersonic nozzle. The shape of this nozzle has been calculated in such a way that the flow in the exit plane (E) of the nozzle is supersonic, uniform and parallel to the axis x'x of the nozzle, the viscous effects being ignored for the moment. In the vicinity of the throat, the contour is assumed to be circular (radius of curvature R). The ratio R/h, h being the radius of the throat, is assumed to be in the order of what it uses to be on typical such nozzles i.e. about 4.

F_v being the thrust in vacuum, A_c the area of the geometrical throat $(A_c = \pi h^2)$, ρ_E, p_E, M_E the density, pressure and Mach number in (E) respectively, p_o and T_o the stagnation pressure and temperature, we have (see (10)) :

$$F_v = \frac{p_E}{p_o} \cdot \frac{A_E}{A_C} \cdot \left(1 + \gamma M_E^2\right) \cdot p_o A_C \qquad \text{with } A_E = \pi R_E^2 \qquad (10)$$

Due to non uniformity of the flow in the plane of the geometrical throat, the area of the (fictitious) critical throat is not A_C but $C_{D_K} A_C$ where C_{D_K} is the coefficient taking into account the curvature of the sonic surface ($C_{D_K} < 1$). The mass flow rate is therefore :
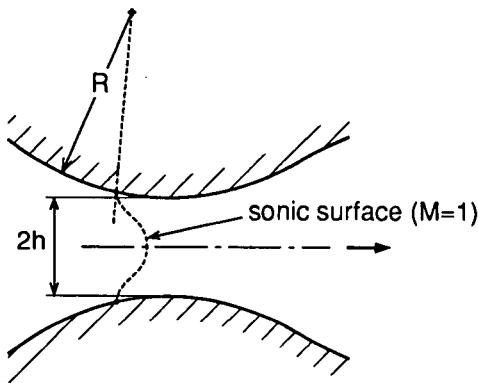
$$Q = C_{D_K} Q\binom{\text{one dimensional}}{\text{flow}} = C_{D_K} \cdot C_i^* \frac{p_o A_C}{\sqrt{RT_o}} \qquad (22)$$

We define now an absolute (i.e. in vacuum) thrust coefficient K_{TA} as :

$$K_{TA} = \frac{F_v}{Q\sqrt{RT_o}/C_i^*} \qquad (23)$$

(22) shows that :

$$K_{TA} = \frac{F_v}{p_o C_{D_K} A_C}$$

and (10) shows that :

$$K_{TA} = \frac{p_E}{p_o} \cdot \frac{A_E}{A_C C_{D_K}} \left(1 + \gamma M_E^2\right) \qquad (24)$$

Now : $p_E/p_o = \overline{\omega}(M_E)$ with $\overline{\omega}(M) = \left(1 + \frac{\gamma-1}{2} M^2\right)^{-\gamma/\gamma-1}$

$A_E/A_C \, C_{D_K} = \Sigma(M_E)$ (24 bis) with $\Sigma(M) = \left\{\frac{2}{\gamma+1}\right\}^{(\gamma+1)/2(\gamma-1)} \cdot \frac{1}{M} \cdot \left(1 + \frac{\gamma-1}{2}M^2\right)^{(\gamma+1)/2(\gamma-1)}$

so, $K_{TA} = \phi(M_E)$ with $\phi(M)) = \overline{\omega}(M) \Sigma(M)(1 + \gamma M^2)$ (25)
(inviscid flow ; γ = cte)

For instance, for $\gamma = 1.4$ and $M_E = 2$, $K_{TA} = 1,42342$

30

3.4.3 A simplified method to estimate viscous effects

Along the wall of the nozzle a boundary layer appears, the effect of which is to reduce the mass flow rate, for given p_o, To, and to modify the mean Mach number in the exit plane (E). The thrust coefficient defined by (23) will therefore be somewhat different from that given by (25).
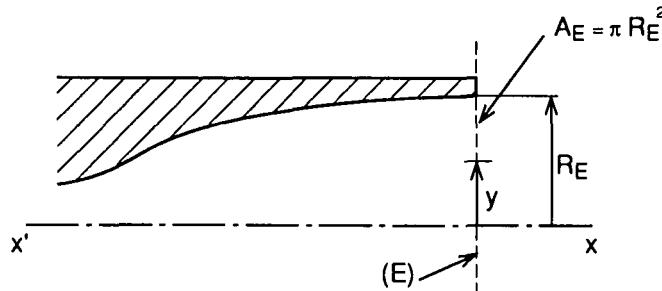
F_v' being the new thrust in vacuum, the momentum equation permits to write :

$$F_v' = \int_0^{R_E} \left(p + \rho V^2\right) 2\pi y\, dy$$

Let M_E' be defined by $\Sigma\left(M_E'\right) = \dfrac{A_E - 2\pi R_E\, \delta_E^{(1)}}{A_C\, C_{D_K} \cdot C_{D_\delta}}$ (25 bis)

where C_{D_δ} is the coefficient of mass flow rate reduction due to the boundary layer at the throat of the nozzle and where $\delta_E^{(1)}$ is the displacement thickness of the boundary layer in the exit plane (E).

$F_v' = p_E'\, A_E + \int_0^{R_e} \rho V^2 \cdot 2\pi y\, dy$, the pressure p_E' , assumed uniform in the exit plane (E), being connected to the upstream stagnation pressure p_o through :

$$p_E'/p_o = \overline{\omega}\left(M_E'\right) \quad \left(\text{we recall that } \overline{\omega}(M) = \left(1 + \frac{\gamma-1}{2}\, M^2\right)^{-\gamma/\gamma-1}\right)$$

Let ρ_E' and V_E' be the values of density and velocity of the flow in the exit plane (E), <u>outside of the boundary layer</u> : these values are connected to the upstream stagnation conditions through the above mentioned Mach number M_E'.

The new mass flow rate Q', now equal to $C_{D_\delta}\left(C_{D_K} \cdot C_i^* \dfrac{p_o A_c}{\sqrt{RT_o}}\right)$ is also given by :

$$Q' = \rho_E'\, V_E'\, \pi\left(R_E - \delta_E^{(1)}\right)^2 \tag{26}$$

Moreover, taking into account the definition of the momentum thickness $\delta_E^{(2)}$ in the exit plane (E), that is :

$$\int_{R-\Delta}^{R} \rho V \left(V_E' - V \right) 2\pi y dy = \rho_E' V_E' \, 2\pi R_E \, \delta_E^{(2)} . V_E' \quad,$$

it is easy to demonstrate the following relation :

$$F_v' = p_E' . A_E + Q' V_E' - 2\pi R_E \, \delta_E^{(2)} \, \rho_E' \, V_E'^{\,2} \tag{27}$$

Let us show now that, following [32], the relation (27) can be simplified. Consider a fictitious nozzle fed with a <u>non viscous gas</u> of same stagnation pressure and temperature p_o, T_o, as the real one, having the same exit area A_E and the same mass flow rate Q' as the real one.

Since, by hypothesis, p_o, T_o, Q' are the same in the two nozzles, the critical area $A_{c,f}$ of the fictitious nozzle is given by :

$$A_{c,f} = A_c . C_{D_K} . C_{D_\delta}$$

Let F_v'' be the thrust in vacuum of this fictitious nozzle fed with air considered as a <u>non viscous gas</u> :

$$F_v'' = p_E'' A_E + Q' V_E'' \tag{28}$$

with $\qquad p_E''/p_o = \overline{\omega}\left(M_E''\right) \quad$ and $\quad \Sigma\left(M_E''\right) = \dfrac{A_E}{A_{c,f}} = \dfrac{A_E}{A_c . C_{D_K} . C_{D_\delta}} \qquad$ (28 bis)

From (27) and (28) :

$$F_v' - F_v'' = p_E' A_E + Q' V_E' - 2\pi R_E \, \delta_E^{(2)} \rho_E' V_E'^{\,2} - \left(p_E'' A_E + Q' V_E'' \right) \tag{29}$$

As $\quad Q' = \rho_E'' V_E'' A_E$, (29) reads :

$$F_v' - F_v'' = A_E \left[\left(p_E' - p_E'' \right) + \rho_E'' V_E'' \left(V_E' - V_E'' \right) \right] - 2\pi R_E \, \delta_E^{(2)} \, \rho_E' \, V_E'^{\,2} \tag{30}$$

But p_E' and p_E'' can be considered as the values of the pressure in two neighbouring states during an isentropic expansion from the stagnation pressure p_o, these two neighbouring states being defined by the Mach numbers M_E' and M_E'', near each other. It is exactly the same for the two velocities V_E' and V_E''.

We may therefore write : $\begin{cases} p_E' - p_E'' = dp_E \\ V_E' - V_E'' = dV_E \end{cases}$

On the other hand, h being the enthalpy and s the entropy, we have :

$$dh = Tds + dp/\rho \qquad \text{(thermodynamics)}$$

$$dh + VdV = 0 \qquad \text{(first law of thermodynamics)}$$

and, as ds = 0, $\qquad \rho \, VdV + dp = 0$

Consequently : $\qquad p_E' - p_E'' + \rho_E'' V_E'' \left(V_E' - V_E'' \right) = 0 \quad$ and (30) reads :

$$F_v' - F_v'' = - 2\pi R_E . \delta_E^{(2)} . \rho_E' . V_E'^{\,2}$$

32

Or, with an error of second order :

$$F'_v = F''_v - 2 \pi R_E . \delta_E^{(2)} . \rho''_E . V''^2_E \tag{31}$$

Dividing the left-hand side of (31) by $Q'\sqrt{RT_o}/C_i^*$ and the right-hand side of the same equation by $C_{D_\delta} C_{D_K} p_o A_c$, one obtains :

$$K_{TA} = \varnothing(M''_E) - \gamma\bar{\omega}(M''_E) \Sigma(M''_E) M''^2_E . \frac{2\delta_E^{(2)}}{R_E} \tag{32}$$

$$\left\{ \begin{array}{c} \text{actual nozzle} \\ \text{viscous flow} \\ \gamma = 1.4 \end{array} \right\}$$

We recall that $\phi(M) = \bar{\omega} \Sigma(1 + \gamma M^2)$ (see (25)) and that the Mach number M''_E is the (supersonic) solution of $\Sigma(M''_E) = A_E/(A_c.C_{D_K}.C_{D_\delta})$. This Mach number has no physical meaning. One sees that, to apply (32), it is necessary to know the displacement thickness $\delta_c^{(1)}$ at the throat of the nozzle $\left(\text{because } C_{D_\delta} = 1 - \frac{2\delta_c^{(1)}}{h} \right)$ and the momentum thickness $\delta_E^{(2)}$ in the exit plane (E).

Use of (32) will be presented later (see § 3.5).

Another writing of equation (32)

It is possible to give another formulation of equation (32) in which not only $\delta_E^{(2)}$ but also $\delta_C^{(1)}$ appear explicitly.

We first remember that the Mach numbers M_E and M''_E, which are near each other, are the supersonic solutions of the following equations :

$$\Sigma(M_E) = \frac{A_E}{A_C.C_{D_K}} \tag{see 24(bis)}$$

$$\Sigma(M''_E) = \frac{A_E}{A_C.C_{D_K}.C_{D_\delta}} \tag{see 28(bis)}$$

Then, neglecting second order terms :

$$\phi(M''_E) = \phi(M_E) + \frac{d\phi}{d\Sigma}(M_E)\left[\Sigma(M''_E) - \Sigma(M_E) \right]$$

As $\phi(M)$, $\Sigma(M)$, $\bar{\omega}(M)$ verify $\dfrac{d\phi}{d\Sigma} = \bar{\omega}$, it is easy to obtain after some straight-forward but lengthy calculations :

$$K_{TA} \left\{ \begin{array}{c} \text{viscous flow} \\ \gamma = 1,4 \end{array} \right\} = \phi(M_E)\left\{ 1 + \frac{2\delta_c^{(1)}/h}{1+\gamma M_E^2} - \frac{\gamma M_E^2}{1+\gamma M_E^2} . 2 \delta_E^{(2)}/R_E \right\}$$

Or :

$$K_{TA} \left|\begin{array}{l} \text{viscous flow} \\ \gamma = 1,4 \end{array}\right. = K_{TA} \left|\begin{array}{l} \text{non viscous flow} \\ \gamma = 1,4 \end{array}\right. \cdot \left\{ 1 + \frac{2\delta_c^{(1)}/h}{1+\gamma M_E^2} - \frac{\gamma M_E^2}{1+\gamma M_E^2} \cdot 2\,\delta_E^{(2)}/R_E \right\} \qquad (32\text{ bis})$$

3.5 Practical formulae to calculate mass flow rate and thrust

3.5.1 Introduction

In §§ 3.3 and 3.4 several formulae have been proposed to calculate mass flow rates and thrust coefficients. It is proposed now to show how such formulae can be used practically. This will allow to give examples of the relative magnitude of the various correction factors.

3.5.2 Practical formulae to calculate mass flow rate in a sonic Venturi
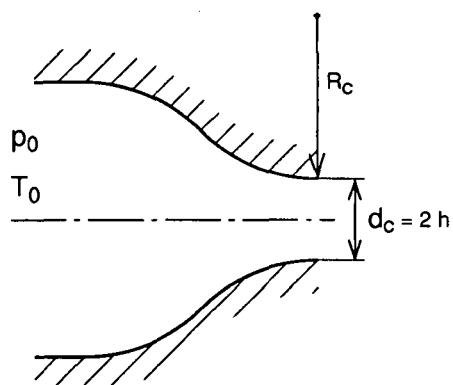
The actual mass flow rate is :

$$Q = C_{D_V} \cdot C_{D_\delta} \cdot C_{D_K}\, C_i^* \,\frac{p_0 A_c}{\sqrt{RT_0}} \qquad (33)$$

with :

p_0 : stagnation pressure of the upstream flow (N/m²)

T_0 : stagnation temperature (K)

$R = 287.04\ (\text{m/s})^2\ (\text{K})^{-1}$

A_C : Area of the geometrical throat (πh^2) (m²) assumed choked

$C_i^* = 0.6847314$

C_{D_K} : coefficient due to the curvature of the sonic surface

C_{D_δ} : coefficient due to boundary layer effect

$$\left(C_{D_\delta} = 1 - 2\frac{\delta_c^{(1)}}{h} \right)$$

C_{D_V} : coefficient due to real gas effect.

As an example, let us assume that the sonic Venturi is the ONERA short radius nozzle $R_c/d_c = 2$ (see appendix F) with $d_c = 20$ mm, $p_0 = 45$ bar, $T_0 = 288$ K. We have now to determine C_{D_K}, C_{d_δ}, C_{D_V}.

α) C_{D_K} For $d_c/R_c = 0.5$, figure 17 bis-a gives :

$$C_{D_K} = 0.99857 \qquad (34)$$

34

β) C_{D_δ} For $d_c/R_c = 0.5$, assuming a turbulent boundary layer at the throat and following simple boundary layer calculations used in ref [23] and in 3.2.2.3, figure 17bis-b gives :

$$(1 - C_{D_\delta}) \, Re_{0,h}^{1/6} = 0.0454 \tag{35}$$

$$\text{with } Re_{0,h} = \frac{\rho_o \, a_o \, h}{\mu_o} = 10{,}45 \times 10^6$$

$$\Rightarrow \quad C_{D_\delta} = 0.99693$$

γ) C_{D_V} For $p_o = 45$ bar (that is for $p_o = 44.41$ atm) and $T_o = 288$ K, figure 17bis-c gives the value of $(C_{D_V} - 1) \times 10^3$ after interpolation. It is easier to use the formula :

$$C_{D_V} = 1 + 0{,}035 \, \frac{p_o \, (\text{atm})}{T_o \, (\text{K}) - 210} \qquad (\text{see } (6))$$

we obtain :

$$C_{D_V} = 1 + 19.93 \times 10^{-3} = 1.01993$$

Summary :

$$\boxed{\begin{array}{l} C_{D_K} = 0.99857 = 1 - 1.43 \times 10^{-3} \\[2mm] C_{D_\delta} = 0.99693 = 1 - 3.07 \times 10^{-3} \\[2mm] C_{D_V} = 1.01993 = 1 + 19.93 \times 10^{-3} \end{array}}$$

The actual mass flow rate is therefore, from (33) :

$$Q = (1.01993)\,(0.99693)\,(0.99857)\,(0.6847314)\,45 \times 10^5 \cdot \frac{\pi \left(2.10^{-2}\right)^2 / 4}{\sqrt{287.04 \times 288}} = 3.4184 \text{ kg/s}$$

3.5.3 Practical formulae to calculate thrust coefficient K_{TA}.

Another nozzle will be considered for this example.

Let us recall that $K_{TA} = \dfrac{F_v}{Q\sqrt{RT_o}/C_i^*}$

We will calculate K_{TA} for the ONERA $M_E = 2$ supersonic nozzle. Let us recall that   The throat diameter is
$d_c = 61.64$ mm and the diameter in the exit plane (E) is : $2\,R_E = 80{,}0154$ mm.
The shape of this axisymetric nozzle has been calculated as it is explained at the beginning of § 3.4. In particular the radius of curvature of the nozzle in the vicinity of the throat is $R = 123.28$ mm, that is 2 times the throat diameter.

α) <u>Hypothesis n° 1</u> : Inviscid flow and air is a calorically perfect gas (Z= 1 ; γ = 1,4)

Equation (25) gives : $K_{TA} = \emptyset(M_E)$ with $M_E = 2$

Hence :

$$\boxed{\begin{array}{l} K_{TA} = 1.42342 \\ \text{(inviscid flow)} \\ (\gamma = 1.4 \quad) \end{array}}$$ (37)

β) <u>Hypothesis n° 2</u> : Viscous flow (turbulent boundary layer) and air is a calorically perfect gas (Z = 1 ; γ = 1.4)

To apply (32 bis), we must calculate $\delta_c^{(1)}$ and $\delta_E^{(2)}$ (or measure).

Let us assume $p_o = 8$ atm ; $T_o = 288$ K

$$\text{Then} \begin{cases} Re_{o,h} = 5.7 \times 10^6 \\ (1 - C_{D_\delta}) Re_{o,h}^{1/6} = 0.0454 \quad \text{(fig 17 bis-b)} \end{cases}$$ (38)

From (38) : $C_{D_\delta} = 0.9966$ and $\delta_c^{(1)}/h = 1.7 \times 10^{-3}$

In the exit plane, the value of $\delta_E^{(2)}$ can be obtained through two ways : computation (e.g.) integration of the integral equation of Von Karman) or direct measurement in the exit plane with a Pitot rake.

According to [33], the results are :

Integration of integral equation of Von Karman : $\dfrac{\delta_E^{(1)}}{h} = \dfrac{14.2}{1000}$; $\dfrac{\delta_E^{(2)}}{h} = \dfrac{4.74}{1000}$; $\dfrac{\delta_E^{(1)}}{\delta_E^{(2)}} = 3$

Direct measurement : $\dfrac{\delta_E^{(1)}}{h} = \dfrac{18.8}{1000}$; $\dfrac{\delta_E^{(2)}}{h} = \dfrac{5.1}{1000}$; $\dfrac{\delta_E^{(1)}}{\delta_E^{(2)}} = 3.7$

Let us retain the first value for $\dfrac{\delta_E^{(2)}}{h}$:

$$\dfrac{\delta_E^{(2)}}{h} = \dfrac{4.74}{1000} \Rightarrow \dfrac{\delta_E^{(2)}}{R_E} = \dfrac{\delta_E^{(2)}}{h} \times \dfrac{h}{R_E} = \dfrac{4.74}{1000} \times \dfrac{61.64}{80.01} = \dfrac{3,65}{1000}$$

Then, using (32 bis) :

$$\boxed{\begin{array}{l} K_{TA} = 1.41534 \\ \text{(viscous flow)} \\ \gamma = 1.4 \\ p_o = 8 \text{ atm} \\ T_o = 288 \text{ K} \end{array}}$$ (39)

36

Let us assume now that, the temperature T_o being unchanged ($T_o = 288K$), the pressure p_o is: $p_o = 48$ atm. (i.e. six times the former pressure)

$$Re_{o,h} = (5.7 \times 10^6) \times 6 = 34.2 \times 10^6$$

$$(38) \Rightarrow \left(1 - C_{D\delta}\right)Re_{0,h}^{1/6} = 0.0454 \Rightarrow C_{D\delta} = 1 - 2.50 \times 10^{-3} = 0.9975 \Rightarrow \delta_c^{(1)}/h = 1.25 \times 10^{-3}$$

$$\frac{\delta_E^{(2)}}{R_E} = \frac{2.71}{1000}$$

Then, using (32 bis) :

K_{TA} $\begin{pmatrix} \text{viscous flow} \\ \gamma = 1.4 \\ p_o = 48 \text{ atm} \\ T_o = 288 \text{ K} \end{pmatrix}$ = 1.41741

$\qquad\qquad\qquad\qquad\qquad\qquad\qquad\qquad\qquad\qquad\qquad\qquad\qquad\qquad$ (40)

γ) <u>Hypothesis n° 3</u> : Viscous flow (turbulent boundary layer) and air is no longer a perfect gas ($Z \neq 1$)

For $A/A_c = 1.7$ and $To = 288$ K ($\cong 15°C$), fig 17 bis.d gives :

$$\left(\frac{K_{TA\text{real air}}}{K_{TA\gamma=1.4}} - 1\right) \times \frac{10^4}{p_o[\text{atm}]} = -4.35$$

If $p_o = 8$ bar ($= 7.90$ atm), $\dfrac{K_{TA\text{real air}}}{K_{TA\gamma=1.4}} = 1 - 3.44 \times 10^{-3} = 0.99656$

If $p_o = 48$ bar ($= 47.37$ atm), $\dfrac{K_{TA\text{real air}}}{K_{TA\gamma=1.4}} = 1 - 20.61 \times 10^{-3} = 0.97939$

Using the values given by (39) and (40), one obtains :

K_{TA} $\begin{pmatrix} \text{real air} \\ \text{viscous flow} \\ p_o = 8 \text{ atm} \\ T_o = 288 \text{ K} \end{pmatrix}$ = 1.41534 x 0.99656 = 1.41047
K_{TA} $\begin{pmatrix} \text{real air} \\ \text{viscous flow} \\ p_o = 48 \text{ atm} \\ T_o = 288 \text{ K} \end{pmatrix}$ = 1.41741 x 0.97939 = 1.38820

$\qquad\qquad\qquad\qquad\qquad\qquad\qquad\qquad\qquad\qquad\qquad\qquad\qquad\qquad$ (41)

$\qquad\qquad\qquad\qquad\qquad\qquad\qquad\qquad\qquad\qquad\qquad\qquad\qquad\qquad$ (42)

Summary : Values of K_{TA} obtained in α, β, γ are summarized beneath

α inviscid flow
    perfect gas   ->   1.42342
    $(Z = 1 ; \gamma = 1.4)$

β viscous flow $p_o = 8$ atm   ->   1.41534
   perfect gas
   · $(Z = 1 ; \gamma = 1.4)$
   $T_o = 288$ K $p_o = 48$ atm   ->   1.41741

γ viscous flow $p_o = 8$ atm   ->   1.41047
   real gas
   $(Z \neq 1)$
   $T_o = 288$ K $p_o = 48$ atm   ->   1.38820

This example shows that, when measuring the thrust coefficient of a nozzle with a bench, attempts to cross-check experimental data with theoretical predictions must take into account both viscous effects and real gas effects in order to have any meaning.

38

4. EXAMPLES OF EXPERIMENTAL RESULTS

4.1 Boeing's experience on ASME and "cubic" nozzles

The ASME nozzle (fig.14) has long been used as a standard thrust nozzle in many wind tunnel and propulsion laboratory facilities. As accuracy of mass flow and thrust measurements has improved, discrepancies have been noted in the performance of the ASME nozzles when compared to long accepted characteristics. Reference 10 was one of the early publications to define the source of the ASME nozzle problems.

A new nozzle, called "cubic nozzle" was designed in 1978 by Boeing Propulsion Laboratory to have improved characteristics as the result of a thinner boundary layer and no cylindrical throat. The "cubic" nozzle was fabricated in 2", 3" and 4" diameters. Geometry of the cubic nozzle is shown fig.29.

Data for the "cubic" nozzles were measured repeatedly over a 7 year period in both the Boeing Thrust Stand and the Boeing Flight Simulation Chamber (FSC). The repeatability bands for the three "cubic" nozzles from both facilities are shown in figures 30 & 31. These data were obtained when mass flow accuracy was approximately 0.10 to 0.15%, traceable to the CEESI 300 cubic foot Volumetric Primary Standard (ref. 8). In addition, instrumentation tolerances were left in the data which increased the repeatability bands. It should be noted that the Velocity Coefficient (C_V, noted CVN in figures 30 and 31) for all three nozzle sizes is essentially the same, although Reynolds Number should increase C_V for the 4" nozzle by 0.1% above the 2" nozzle. This increment can easily be buried within the data repeatability. The discharge coefficients (C_D, noted CDN in figures 30 and 31) are just as measured.

ASME nozzle data repeatability bands run back-to-back with the "cubic" nozzles, show wider bands of repeatability, (fig. 32, 33 & 34) than the "cubic" nozzles. Both C_V and C_D show trends opposite to normal Reynolds Number effects.

Due to the questionable performance of the ASME nozzles, both the Boeing Wind Tunnel Facilities and the Boeing Propulsion Laboratories now use the "cubic" nozzles to verify thrust facility performance.

4.2 3" Cubic nozzle test results of different calibration tanks

4.2.1 Model

The DNW 3" cubic nozzle is a blown nozzle which delivers thrust along the model centre line. It is a convergent nozzle with 3" exit (throat) diameter. Its geometry is described by a polynomial of the third degree conformal to the 3" design used by Boeing (see fig.29) :

$$Y = 0.046648.X^3 + 1,5 \text{ (inch)}$$

The duct radius upstream of the nozzle contraction is $R_b = 3.5"$, the nozzle throat radius $R_k = 1.5"$ and the nozzle length $X_{max} = 3.5"$.

DNW owns two 3" cubic nozzles, identified as port and starboard "engine". A model drawing is given in figure 35. The compressed air is injected laterally into a settling chamber and passes successively a throttle plate and "retimet" mufflers. The throttle plate orifice area is 741 mm^2 leading to a pressure drop over the plate of about 10 bar at a Nozzle Pressure Ratio NPR=1.89 .

The nozzle instrumentation consists of :

- 1 rake consisting of 5 total pressure probes, the pressure of the centre probe is mostly used to set datapoint pressure ratio conditions. The probes are positioned in such a way that an area weighting procedure results by taking the arithmetic mean of the readings.

- 1 rake consisting of 3 total temperature probes :
 . 2 Copper/Constantan thermocouples,
 . 1 temperature resistive sensor Pt 100

4.2.2 Results

Test results on different 3" cubic blown nozzles (all conformal to the 3" design used by Boeing) are provided by the facilities (calibration tanks). The test data are given in the form of nozzle discharge and velocity coefficients (C_D and C_V) as a function of Nozzle Pressure Ratio (NPR). The following data are available :

1) NLR Engine Calibration Facility : DNW starboard nozzle
                                      DNW port nozzle

2) ONERA S4B   DNW starboard nozzle (two different venturis for mass flow
                                     measurement)

3) ARA Mach Simulation Tank 1   ARA blown nozzle

4) Boeing Thrust stand 1   Boeing blown nozzle

In figures 36 and 37 the C_D and C_V curves of the DNW "starboard nozzle" are presented. Per facility (ONERA and NLR) mean lines of the test data are shown. Balance errors have dominating effects in the C_V accuracies. Therefore error bars have been included in fig.37, based on 0.05% of the maximum axial range of the concerning balance systems (ONERA S4B : 3.0N and NLR ECF: 1.5N) The anticipated errors become relatively large at low NPR values (low thrust) because both calibration tanks are designed for much higher loads. This explains the differences in C_V at low NPR.

The test data of all nozzles (C_D and C_V) are presented in figure 38 and 39 respectively. Shown are the mean lines of the test data of each facility and the outer lines (maximum and minimum) of all the provided test data. The same comments as made above can be made with respect to the C_V curves.

4.3 Discussion

4.3.1 Mass flow

Boeing's results on the cubic nozzle (fig.30 & 31) show that over a long period of time, it is possible to report mass flow measurements on choked nozzles within $\Delta C_D = \pm 0.1\%$.

The absolute result should be very close to what is shown here because of the precaution taken to derive the measurements from those of the gravimetic facility (systematic error within 0.07%)

This is to be compared with comparisons made on the same DNW 3" nozzle with three different calibration tanks. Although these tanks were not calibrated in the same sophisticated way as Boeing's, and were using, either predicted values (ONERA) or calibrated sonic venturis (ARA, NEL) for their flowmeters, they provide consistent results. These results differ by about 0.015% and are higher than those of Boeing (obtained on a physically different nozzle) by only 0.08%.

When looking at all data collected on such nozzles, the width of the uncertainty band is about ±0.2% for choked cases, i.e. about twice the objective.

4.3.2 Thrust

Boeing's data, (as well as other data not reproduced here), fig.30 to 34, shows a good long term repeatability within $\Delta C_V = \pm 0.2\%$. More interesting is to look at what happens when comparisons are made between calibration tanks.

40

The uncertainty band for choked conditions is about ±0.3% overall and ±0.17% if using the same physical nozzle.

To summarize, one could say that the state of the art for mass flow measurement in wind tunnel models is not far from the 0.1% objective for absolute accuracy. Better understanding of nozzle flow conditions would help in making this difficult goal more economically achievable.
However, there is a factor 2 to 3 to gain in absolute accuracy on thrust. Since some wind tunnels can repeat tests with motorized models with a drag repeatability of 1 count (0.0001), it is likely that this can be achieved especially if all precautions are taken as proposed in above 2.3 and 2.4.

5. CONCLUSIONS

- To be consistent with the 1 drag count (or 0.3%) accuracy required by wind tunnel users, mass flow and thrust of engine simulators must be determined within ±0.1%.

- Survey of today's state of the art indicates that both goals could be achieved (for mass flow) or approached (for thrust) through reasonable improvements of existing methods.

- Calibration by gravimetry provides the required accuracy at least at CEESI but limitations in mass flow range make it long and complex to transfer the results to the larger flowmeters normally used in wind tunnels.

- Nevertheless, Boeing has developed a reliable methodology for such a transfer.

- Toroidal throat nozzles (short radius) must be preferred to cylindrical throat (ASME) nozzle for sonic nozzle flow measurement.

- Several facilities seem today reasonably satisfied with the use of calculated mass flow for such nozzles, these being partly validated through back to back calibrations at different Reynolds numbers and interfacility comparisons.

- Nevertheless progress should be made in the understanding of the boundary layer conditions in sonic nozzles. Little has been done on this topic since 1970. Modern CFD is not giving much more reliable results yet. Some careful, basic experiments would be useful. Such progress would allow to better design and use sonic nozzle flowmeters and possibly to avoid gravimetric calibrations and their expensive transfer.

- Real gas effects are properly accounted for with rules established in the 70's. Going further would require to check thermodynamics tables.

- Cubic nozzles are recommended as thrust reference nozzles rather than ASME type nozzles. Some authors consider that subsonic-supersonic nozzles giving a uniform flow in the exit plane could be even better candidates for thrust calibration.

- Various thrust benches have been presented, together with experimental data and interfacility comparisons.

6. REFERENCES

1. AGARD CP n°429 - Aerodynamic data accuracy and quality: requirements and capabilities in wind tunnel testing - Session III: drag accuracy achievements (1987)

2. J.Leynaert, Recent developments in wind tunnel testing techniques at ONERA - ICEFM 1991
ONERA TP 1991-135

3. AGARD AR n°184 - Wind tunnel flow quality and data accuracy requirements, Nov. 1982.

4. Smith Robert E. Jr and Matz, Roy J."A Theoretical Method of Determining Discharge Coefficients for Venturis Operating at Critical Flow Conditions" , Journal of Basic Engineering, Pages 434 - 446, Transactions of the ASME, Dec. 1962.

5. Stratford, B. S., "The Calculation of the Discharge Coefficient of Profiled Choked Nozzles and the Optimum Profile for Absolute Air Flow Measurement", Journal of the Royal Aeronautical Society, Vol. 68, pages 237 - 245, April 1964.

6. Arnberg, B. T., Britton, C. L. and Seidl, W. F. " Discharge Coefficient Correlations for Circular - Arc Venturi Flowmeters at Critical (Sonic) Flow", Journal of Fluids Engineering, pages 111 - 123, June 1974.

7. Stevens, Robert L., "Development and Calibration of the Boeing 18 kg/s (40 lbm/sec) Airflow Calibration Transfer Standard", International Symposium on Fluid Flow Measurement Washington D.C., U.S.A., Nov. 16 - 19, 1986.

8. Arnberg, B. T., and Britton, C. L., "Two Primary Methods of Proving Gas Flow Meters", Paper No. 3 - 8 - 216, Symposium on Flow, Pittsburgh, Pa., May 10 - 14, 1971.

9. Seidl, Walter F., "Primary Calibration of the Boeing 18 Kg/s (40 lbm/sec) Airflow Calibration Transfer Standard", International Symposium on Fluid Flow Measurement, Washington D.C., U.S.A., Nov. 16 - 19, 1986.

10. Smith, Robert E. Jr., and Matz, Roy J., "Performance Characteristics of an 8 Inch Diameter ASME Nozzle Operating at Compressible and Incompressible Conditions", Presented at 93rd Winter Annual Meeting, Nov. 26 - 30, 1972, ASME.

11. Johnson, Robert C. "Real - Gas Effects in Critical - Flow - Through Nozzles and Tabulated Thermodynamic Properties", NASA Technical Note NASA TN D - 2565, Jan. 1965.

12. Fromm, E. H., "The Boeing Flight Simulation Chamber for Static Calibrations of Engine Simulators", 45th Meeting of The Supersonic Tunnel Association, April 1976.

13. Fluid Meters, Their Theory and Application, Sixth Edition, 1971, ASME

14. Arnberg, B.T., Review of Critical Flowmeters for Gas Flow Measurements, ASME, Journal of Basic Engineering, December 1962, pp 447-460.

15. Reimer, R.M., Determination of ASME Nozzle Flow Coefficients by Thrust Measurement, ASME, Journal of Basic Engineering, December 1965, pp 1058-1062.

16. Benedict, R.P., Most Probable Discharge Coefficients for ASME Flow Nozzles, ASME, Journal of Basic Engineering, December 1966, pp 734-744.

17. Smith, R.E. and Matz, R.J., Performance Characteristics of an 8-In-Diameter ASME Nozzle Operating at Compressible and Incompressible Conditions, ASME, Journal of Fluids Engineering, December 1973, pp 542-550.

18. Olson, A.T., Nozzle Discharge Coefficients - Compressible Flow, ASME, Journal of Fluid Engineering, 73-WA/FE-7

19. Szaniszlo, A.J., Experimental and Analytical Sonic Nozzle Discharge
Coefficients for Reynolds numbers up to $8*10^6$, NASA Technical Memorandum NASA TM X-71595,1974.

20. Szaniszlo, A.J., Experimental and Analytical Sonic Nozzle Discharge
Coefficients for Reynolds numbers up to $8*10^6$, ASME, Journal of Engineering for power, 74-WA/FM-8.

21. Holdhusen, J.S., Some Recent Boundary Layer Measurements in a 5.5 Inch ASME Nozzle, 20th Meeting of the
AIAA Turbine Engine Testing Working Group, June 22, 1978, Minneapolis, Minnesota, USA.

22. Hilsenrath, Joseph, et al.
Tables of Thermodynamic and transport Properties of Air, Argon, Carbon Dioxide, Carbon
Monoxide, Hydrogen, Nitrogen, Oxygen, and Steam.
Pergamon Press, 1960. New York.

23. B.Masure
Etude de la precision des mesures de débits gazeux par la méthode du col sonique.
Association Technique Maritime et Aeronautique session 1968, ONERA T.P. 572 (1968).

24. Michels, A. Wassenaar, T. and Wolkers, G. J.
Thermodynamical Properties of Air for Temperatures between +75°C and - 170° C and
Pressures up to 1200 Atmospheres.
Applied scientific Research, The Hague, Section A. Vol. 5 (1955) pp 121 - 136

25. John E.Green
A design of sonic nozzle for the precise measurement of mass flow
Z.Flugwiss.19 (1971), Heft 3

26. W.P.Jones and B.E.Launder
The prediction of relaminarization with a two-equation model of turbulence
Int.Journal of Heat and Mass Transfer, Vol.15, 1972, pp.301-314

27. G.W.Hall
Application of boundary layer theory to explain sonic nozzle and venturi flow peculiarities
Proceedings of the institution of mechanical engineers, Vol.173, number 36, 1959

28. B.Masure
Banc de dynalpie au point fixe de Modane. Etude de l'effet sur les performances mesurées d'une variation des conditions
d'alimentation de l'air comprimé à l'entrée de la balance.
Note Technique ONERA 28/414 GAY (Juin.1972).

29. G.Fasso, M.Plétin, P.Broussaud
Installation pour l'étude de tuyères de réacteurs à plusieurs flux.
Note Technique ONERA n° 160 (1970).

30. B.Masure
Virial and viscosity effects on the measurement of mass flow rates by means of a sonic throat - Virial effect on nozzle
thrust.
Communication présentée à la 28ème réunion de la "Supersonic Tunnel Association" -
Denver - 30 & 31 Octobre 1967
ONERA T.P. 528 (1967) et aussi : Brève information dans: "Recherche Aérospatiale n°120 (sept.oct.1967)

31. B.Masure
Problèmes de mesure sur maquette de la poussée d'un arrière-corps d'avion supersonique. Tuyères de référence. ONERA.
T.P. N° 978 (1971) et :
Communication présentée à la réunion AGARD sur les Entrées et Sorties de Propulseurs Aérospatiaux. Sandefjord
(Norvège), 13 - 17 septembre 1971.

32. P.Carrière
Tuyères propulsives - AGARD lectures series on supersonic turbomachinery.
Varenne (Italie), 15 - 20 mai 1967.

33. B.Masure
Private communication based on ONERA NT n° 8/2772 GA, April 1968 (unpublished).

List of figures

Figure 1- Transfer Standard

Figure 2- Continuous Curvature Venturi Configuration
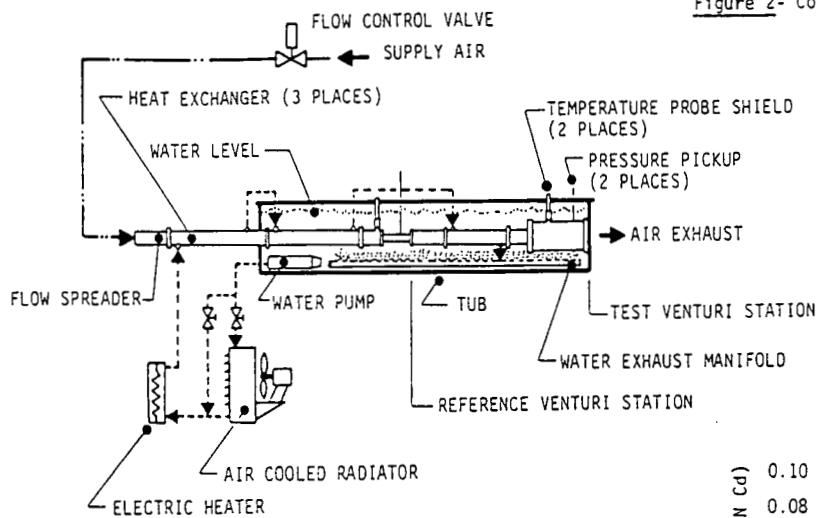
Figure 3- Venturi Screening Facility
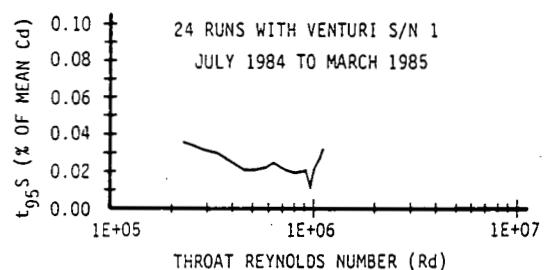
Figure 4- Repeatability of Venturi Screening Facility

46

NOTE: SYSTEM IS SUBMERGED IN A WATER BATH FROM SOLENOID VALVES TO
HEAT EXCHANGER EXIT
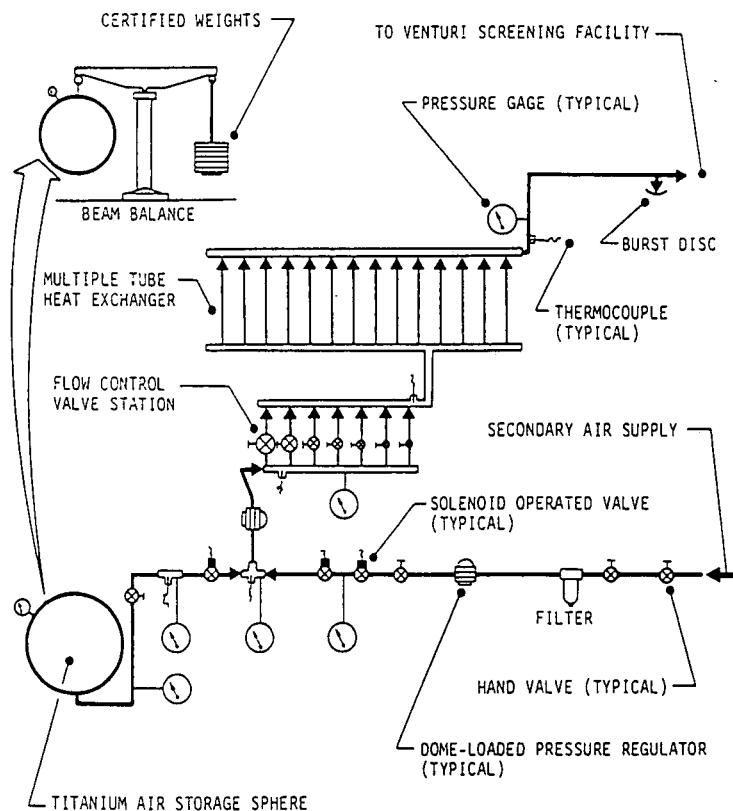
Figure 6 - Mass-Time Calibration System
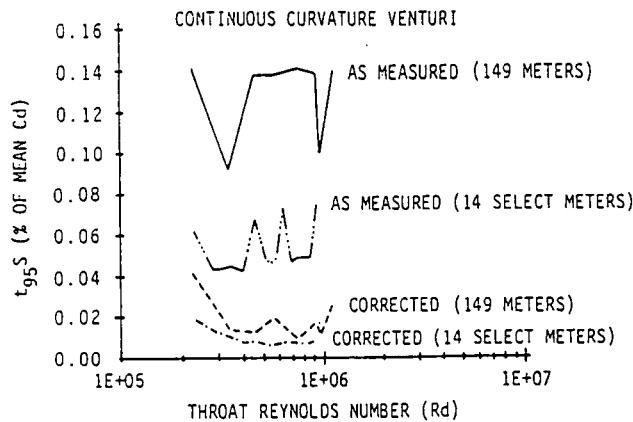
Figure 5 - Throat Diameter Correction Results
(163 Venturi Meters)

$$Cd = (-5.03815E-03)(LOG_{10}Rd)^2 + (6.39382E-02)(LOG_{10}Rd) + (0.79127)$$

NOTE: 3 POINTS OUT OF 121
REMOVED AS OUTLIERS
BY THE "GRUBBS"
METHOD

95% CONFIDENCE BAND (±0.026%)
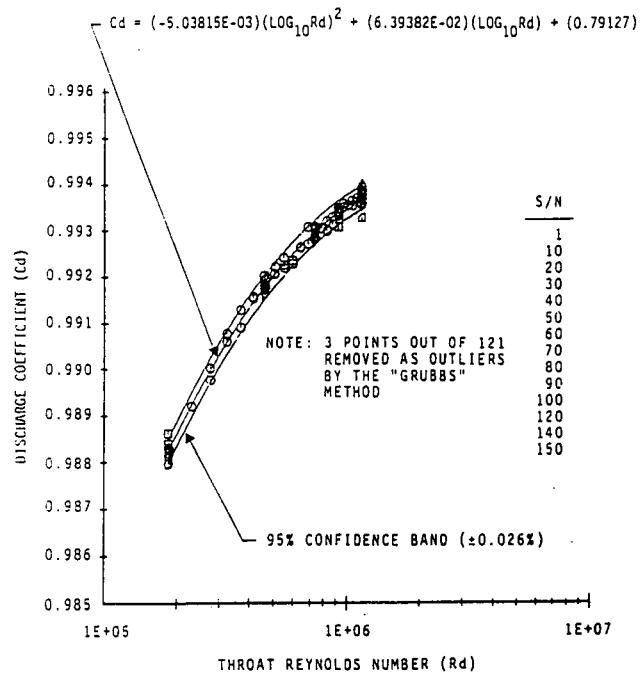
Figure 7 - Mass-Time System Calibration Results for 14
Transfer Standard Venturi Meters
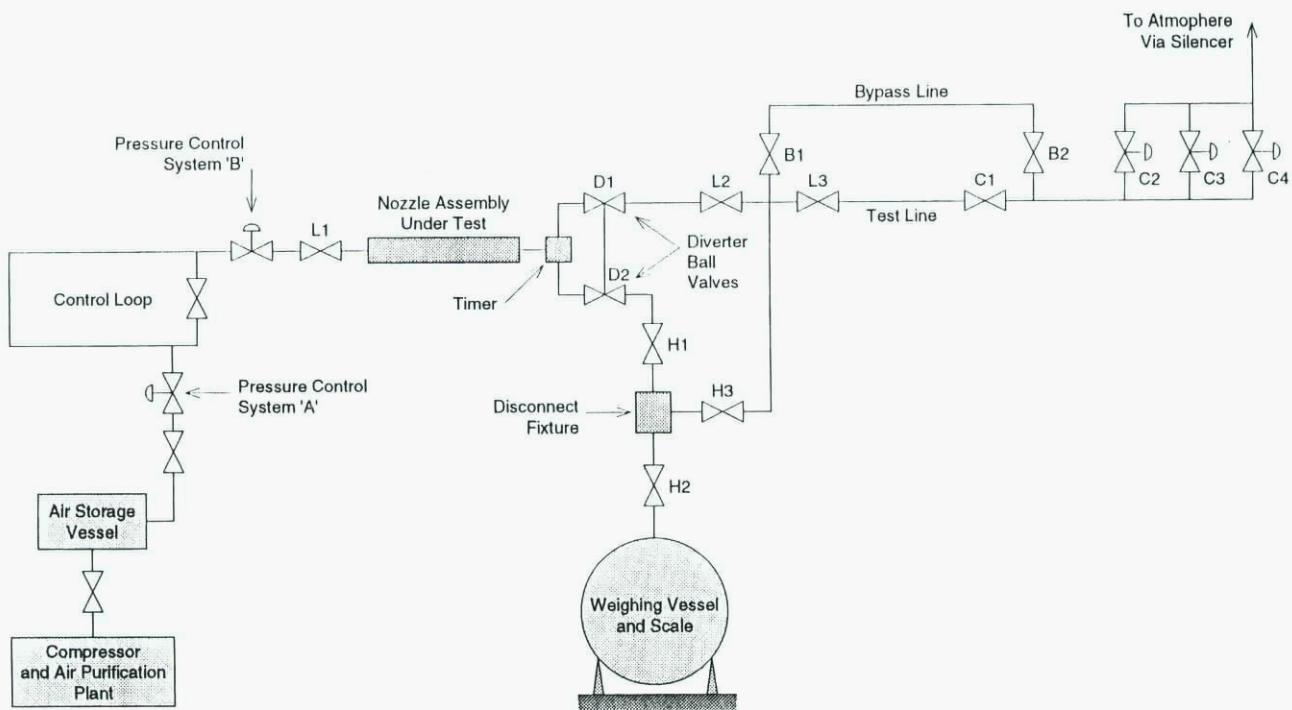
Fig. 8 - *Line diagram of NEL primary gravimetric air flow standard.*

MCV Code	Throat Dia. (inche)
1	0.1870
2	0.2645
4	0.3740
8	0.5289
16.1	0.7480
16.2	0.7480
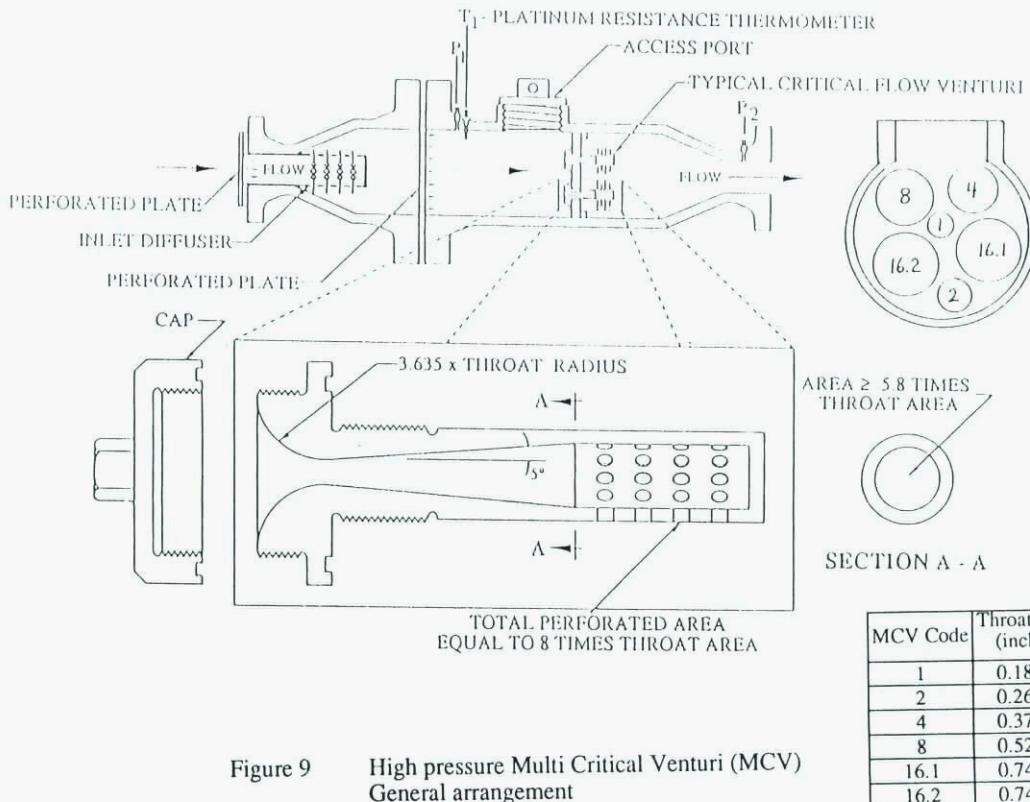
Figure 9   High pressure Multi Critical Venturi (MCV)
             General arrangement

48
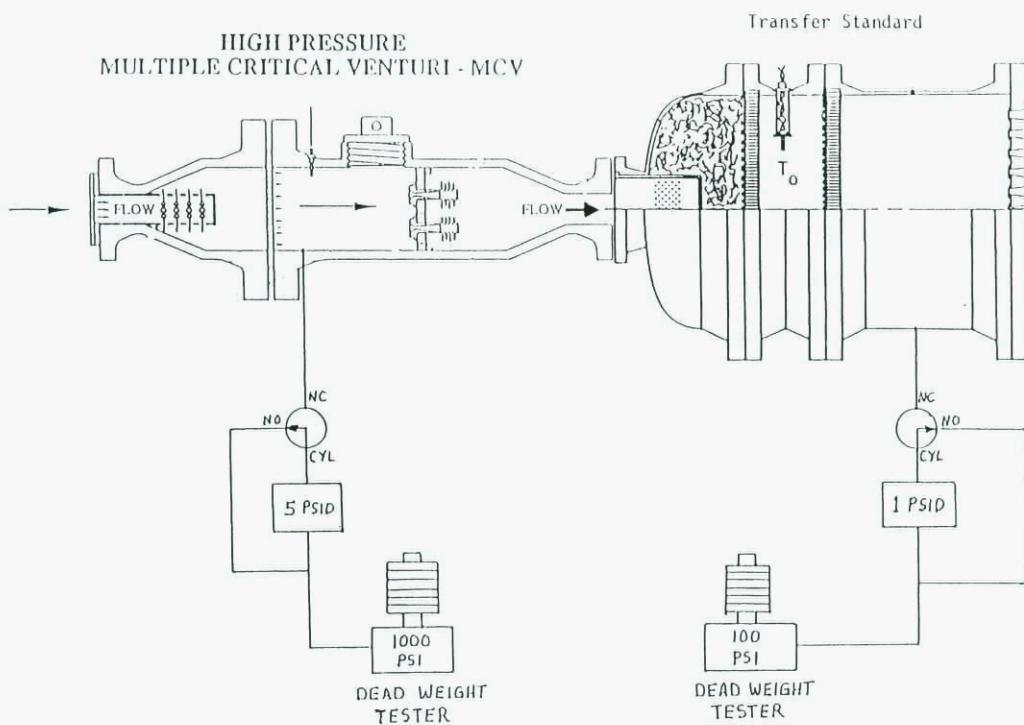
Figure 10   MCV airflow calibration
Instrumentation schematic

MASS FLOW TARE CALIBRATION :

$$F_{CORR} = F_{BAL} - K_p \, (P_Z - P_A) - K_w \left(\frac{W_a^2 \times T_Z}{P_Z} \right)$$

where :

F_{CORR} = Balance measurements corrected for mass flow and pressure tares

F_{BAL} = Balance measurements corrected for interactions

K_p = Pressure tare constant

K_w = Mass flow tare constant

P_Z = Pressure in zero thrust body

P_A = Ambient pressure

T_Z = Air temperature in zero thrust body

W_a = Air mass flow
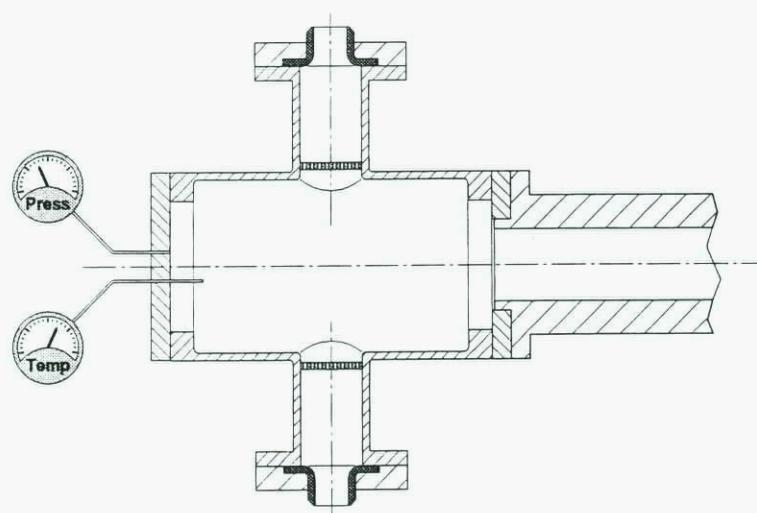
Fig. 11 - *Zero thrust body for momentum tare evaluation.*
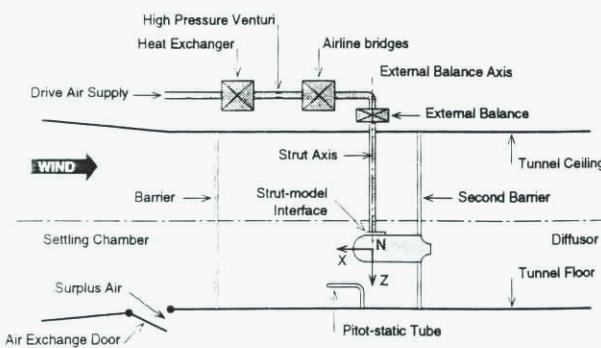
Fig. 12 A - *Sketch of 3" cubic nozzle in LST, down-wind blowing.*
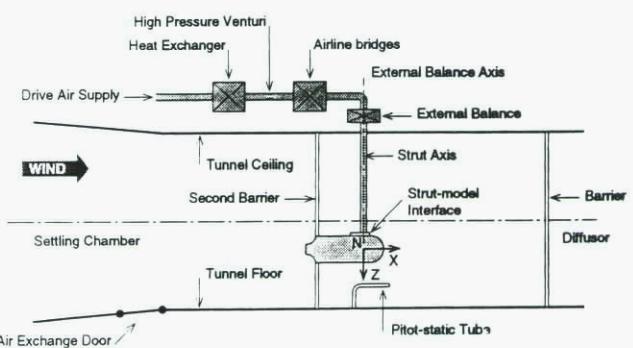
Fig. 12 B - *Sketch of 3" cubic nozzle in LST, up-wind blowing.*
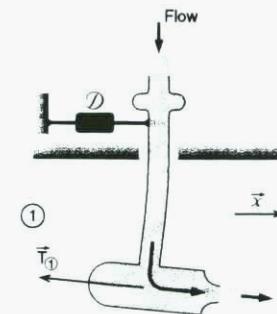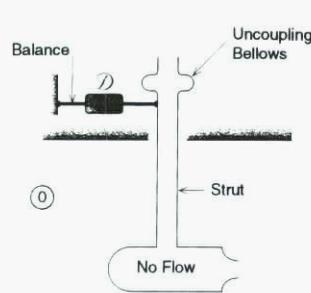
Down-wind blowing nozzle
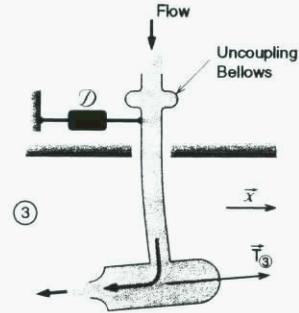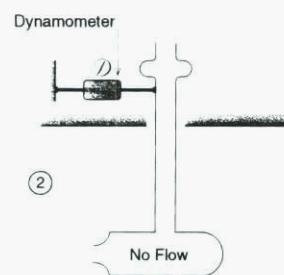
Up-wind blowing nozzle

Notations : $\vec{x}$: unit vector oriented down-wind

$\vec{T}$: net thrust of the nozzle

$\mathcal{D}$: horizontal force measured by the dynamometer (and exerted on the metric part)

ε : momentum correction due to momentum effect at the uncoupling belows.

Case ① : $\vec{T}_① \cdot \vec{x} + \varepsilon_① + \mathcal{D}_① = 0$

Case ③ : $\vec{T}_③ \cdot \vec{x} + \varepsilon_③ + \mathcal{D}_③ = 0$

If mass flow rates are the same in cases ① and ③, then $|\vec{T}_①| = |\vec{T}_③|$, strut deflections are opposite, so $\vec{T}_① \cdot \vec{x} = -\vec{T}_③ \cdot \vec{x}$; $\varepsilon_① = \varepsilon_③ = \varepsilon$.

Adding the two equalities gives : $2\varepsilon + \mathcal{D}_① + \mathcal{D}_③ = 0$

The momentum correction ε can in that way be evaluated.

Fig. 13 - *Momentum tare evaluation using down-wind and up-wind blowing nozzles.*

50
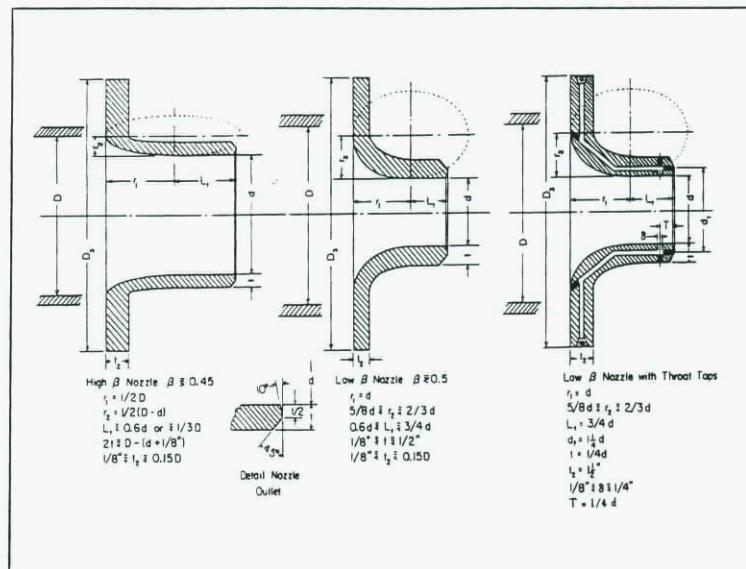
Figure 14   ASME Long Radius Nozzle (LRN)

Euler calculation (non viscous)

- Air, $\gamma = 1.4$
- 2D grid model
- 1515 grid points
- 2D axisymmetric calculation

Navier-Stokes calculation (viscous)

- Air, $\gamma = 1.4$
- 2D grid model
- 6161 grid points
- 2D axisymmetric calculation
- Turbulent calculation
- $Re_d = 8 \; 10^6$
- Baldwin Lomax turbulence model
- Sutherland's formula for viscosity

$$\mu = \mu_0 (T_0 + S)/(T + S) (T/T_0)^{3/2}$$
$$S = 110 \; K \; (air)$$

Boundary conditions

- Total pressure, $p_0 = 45$ bar
- Total temperature, $T_0 = 293$ K

Euler mesh
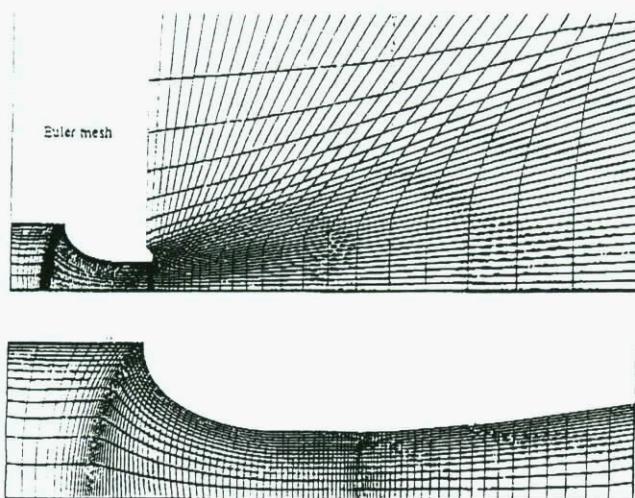
FIGURE 15 · Reference condition for reference ASME nozzle
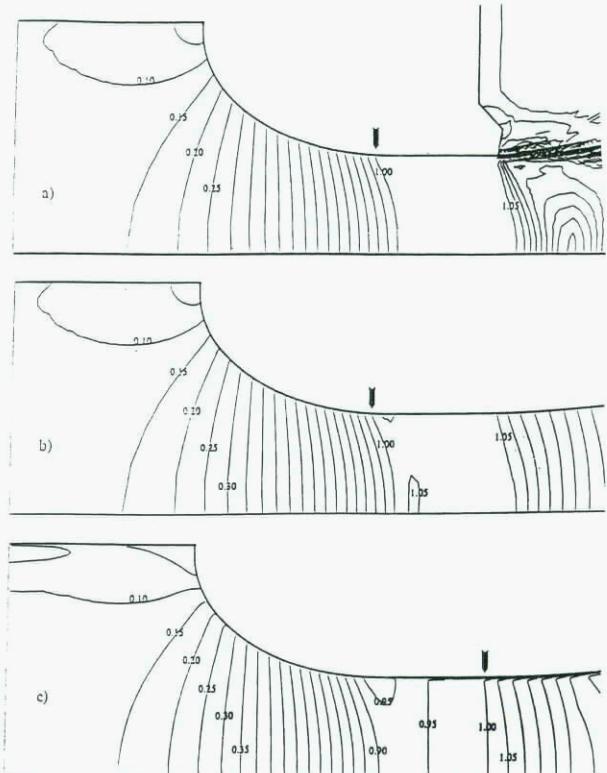
Numerical flow solutions for ASME nozzle
a) Euler (nonviscous), reference nozzle
b) Euler (nonviscous), with divergent exit
c) Navier-Stokes (viscous), with divergent exit

Figure 16

CIRCULAR ARC NOZZLE

SMITH-MATZ NOZZLE   ONERA R_c/d_c NOZZLE
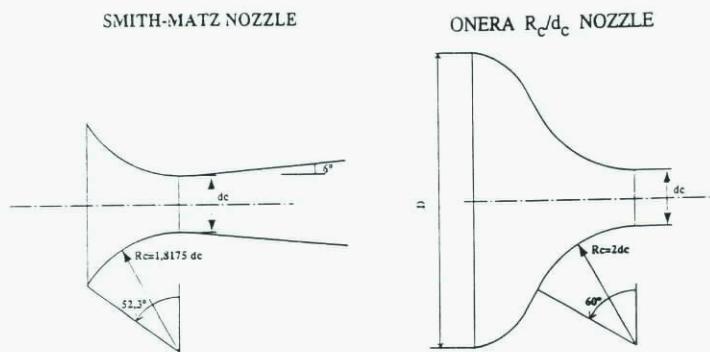
CONTINUOUS CURVATURE ENTRANCE SHAPE
(Boeing Transfer Standard Nozzle)
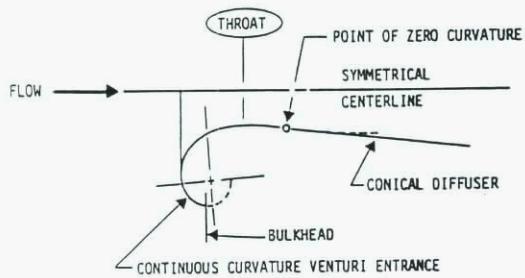
figure 17 Short radius nozzles
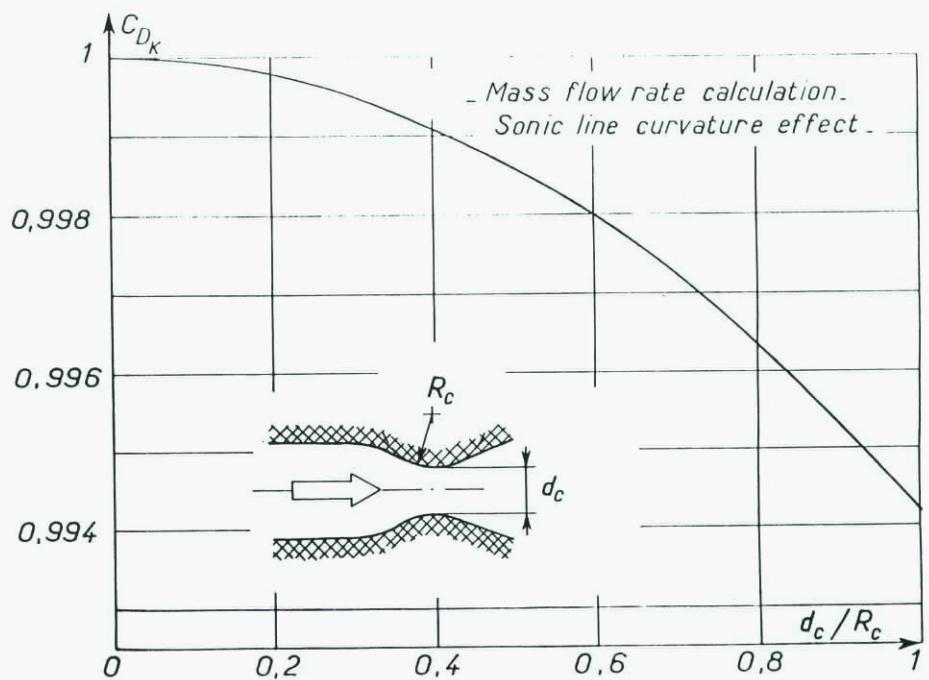
Figure 17 bis - a   Mass-flow rate calculation
Sonic line curvature effect (Masure [30])

$(1-C_{D_\delta}) \mathscr{R}e_{o,h}^{1/6}$

Mass flow rate calculation.
Turbulent boundary-layer effect.

$\mathscr{R}e_{o,h}= \dfrac{a_0 \cdot h}{\nu_0}$

$d_c = 2h$

d_c/R_c
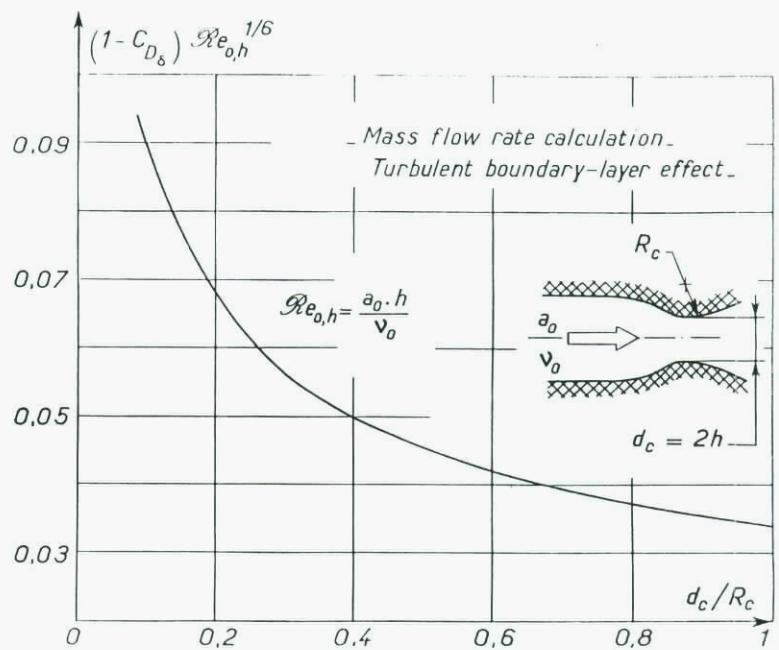
Figure 17 bis - b   Mass-flow rate calculation
Turbulent boundary layer effect (Masure [30])

$\left[\dfrac{q_{real\ air}}{\bar{q}_{(\gamma=1,4)}} - 1\right] \times 10^3 = \left[C_{D_{Virial}} - 1\right] \times 10^3$

$T_0 = 0°C$
$T_0 = 25°C$
$T_0 = 50°C$
$T_0 = 75°C$

Mass flow rate calculation.
Virial effect.

p_0 (atm)
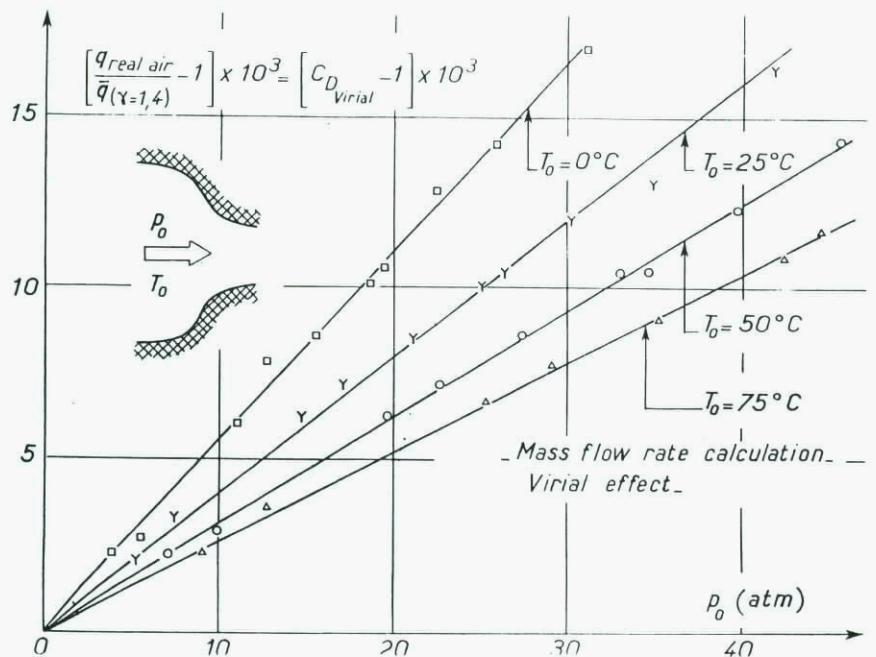
Figure 17 bis - c   Mass-flow rate calculation
Virial effect (Masure [30])

Virial effect on thrust.

$T_0(°C)$

$\dfrac{A_\varepsilon}{A_c}$
1
1,7
3
∞

$\left[\dfrac{F_{real\ air}/q_{real\ air}}{F_{(\gamma=1,4)}/\bar{q}_{(\gamma=1,4)}} - 1\right]\dfrac{10^4}{P_0\ (atm)}$
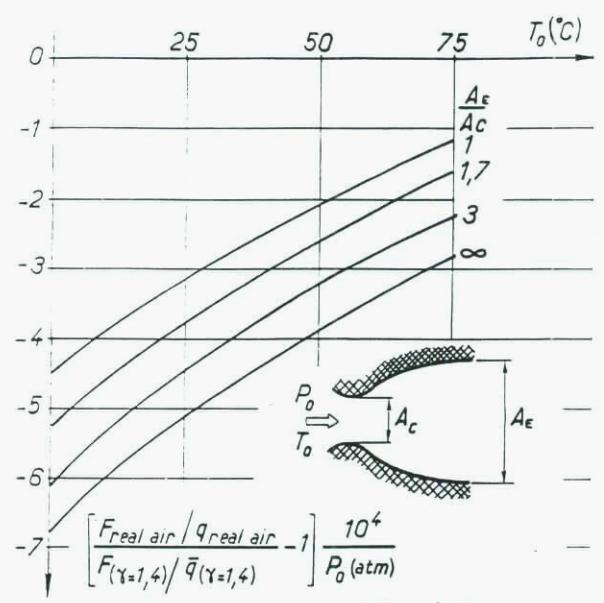
Figure 17 bis - d   Virial effect on thrust
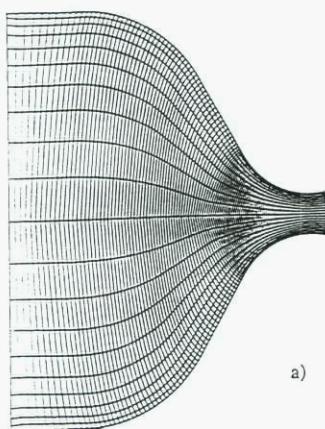
a)
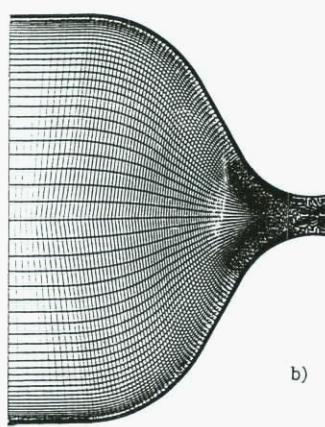
b)

Numerical grid for ONERA short nozzle
a) Euler grid
b) Navier-Stokes grid

Figure 18

Mach-contours

0.05
0.10
0.15
0.20
0.25
0.30
0.35
0.40

Velocity-vectors

0.05
0.10
0.15
0.20
0.25
0.30
0.35

SONIC LINE
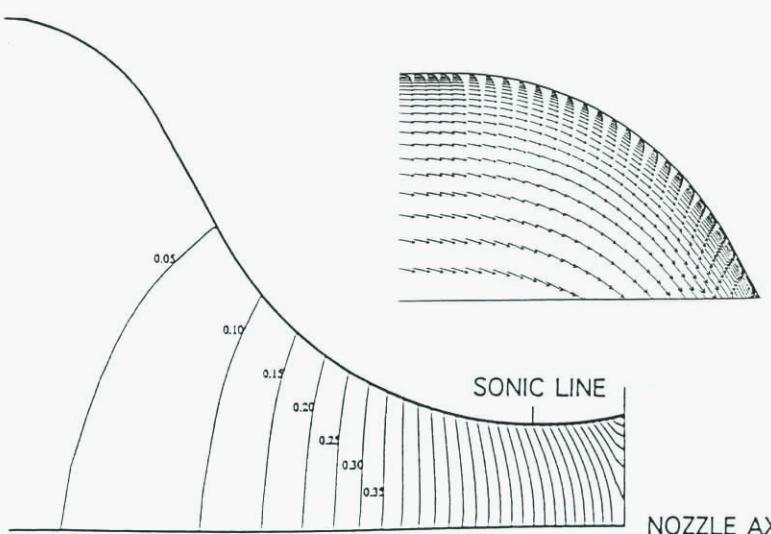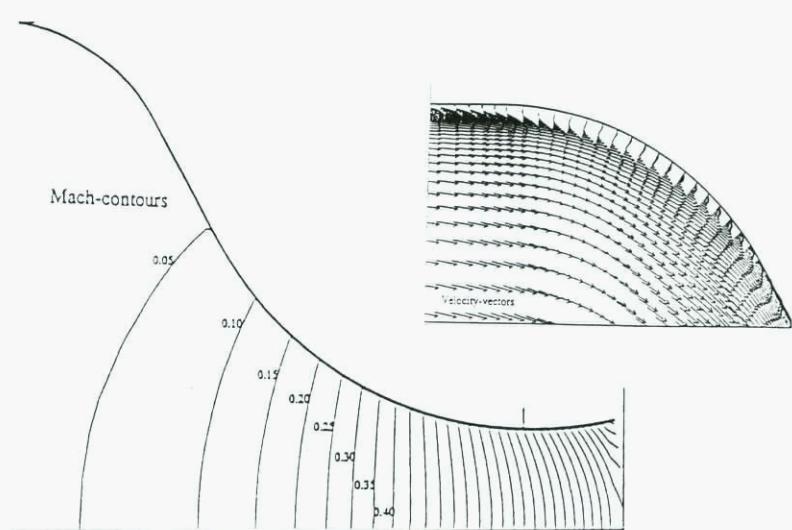
NOZZLE AXIS
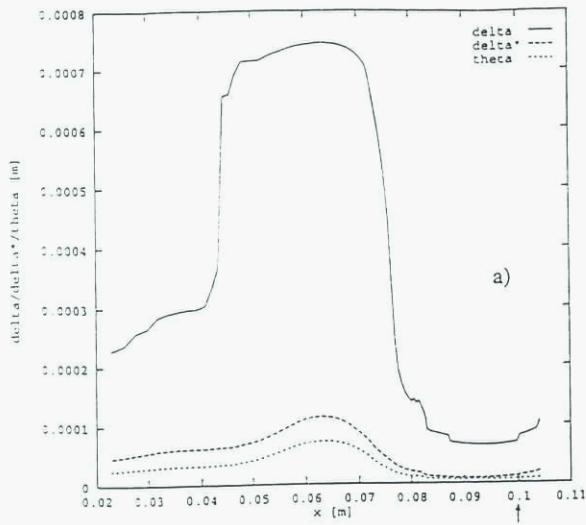
Figure 19

a)
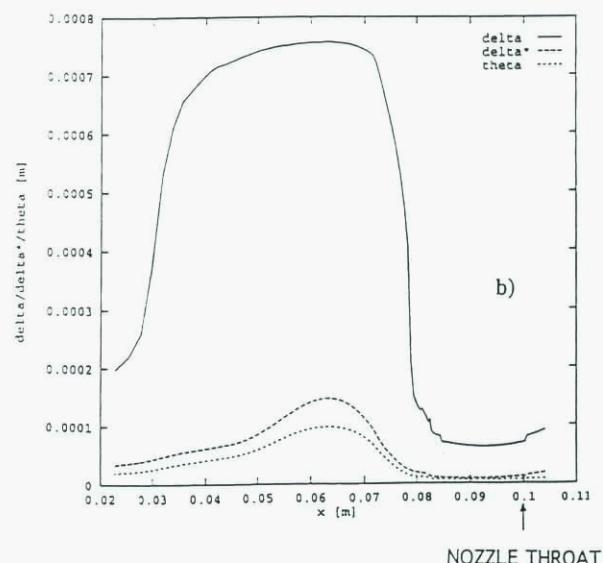
b)

NOZZLE THROAT

Figure 20   Axial distribution of boundary layer quantities
(thickness ; displacement thickness ; momentum thickness)
a) Case 1 : $Re_d = 3.8 \ 10^6$
b) Case 2 : $Re_d = 6.8 \ 10^6$

54

NOZZLE THROAT

NOZZLE THROAT
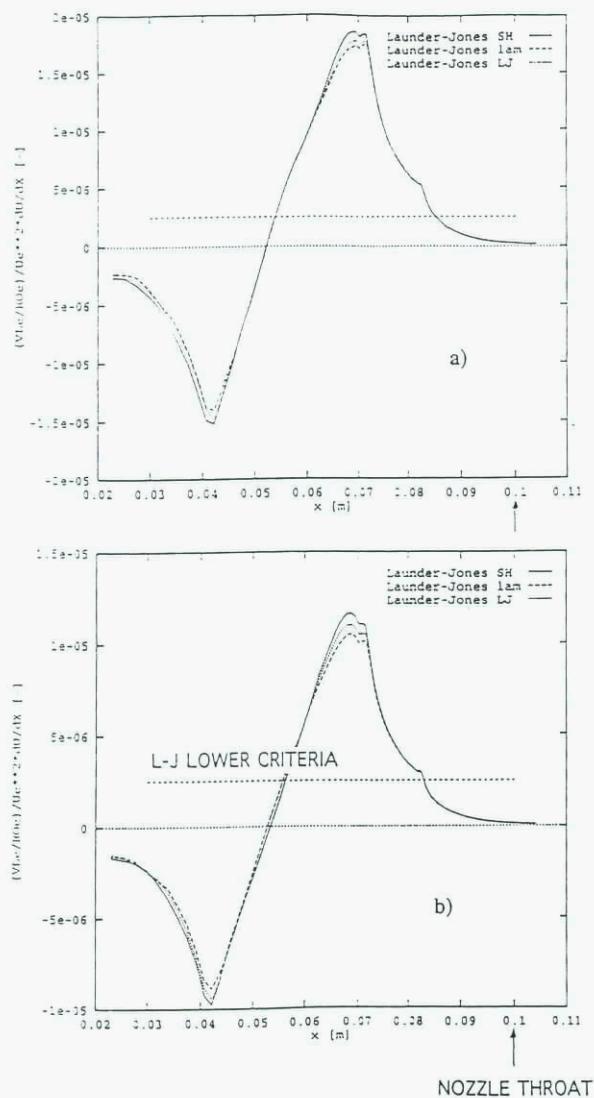
Figure 21   Axial distribution of Launder and Jones parameter
a) Case 1 : $Re_d = 3.8 \ 10^6$
b) Case 2 : $Re_d = 6.8 \ 10^6$
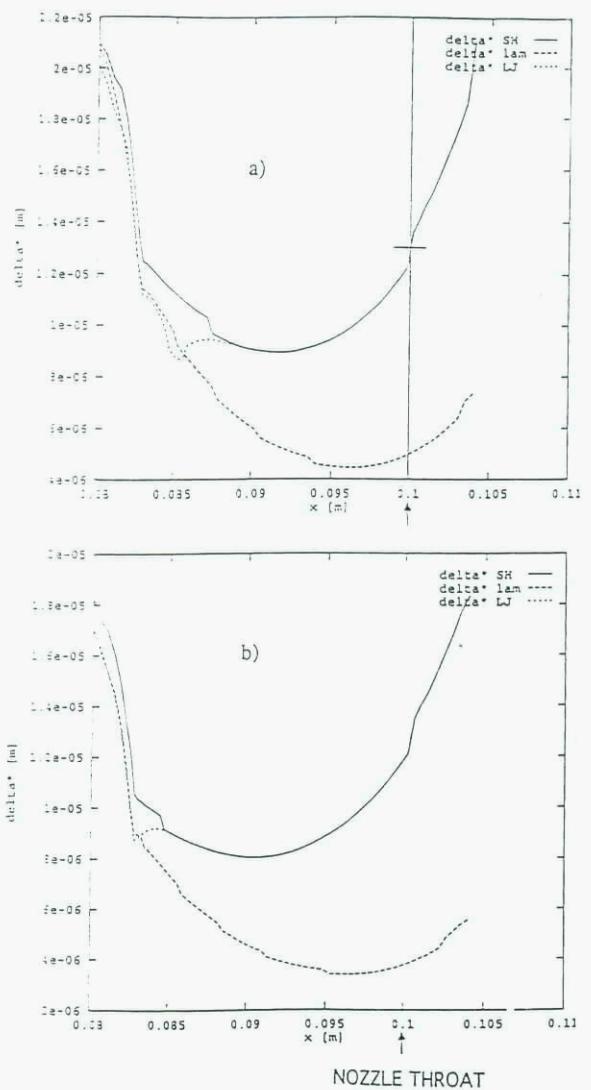
Figure 22   Axial distribution of the displacement thickness [delta*]
a) Case 1 : $Re_d = 3.8 \ 10^6$
b) Case 2 : $Re_d = 6.8 \ 10^6$
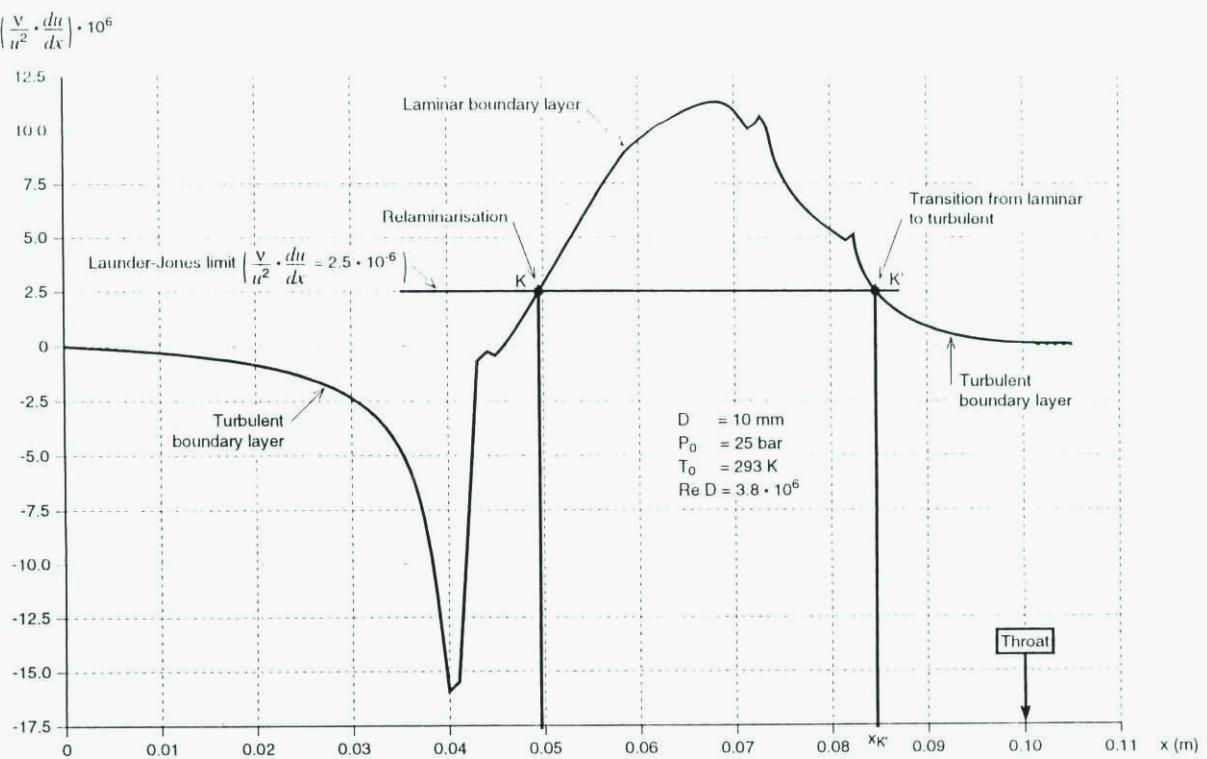
Fig. 23 - *Relaminarisation criteria (Launder-Jones) applied to ONERA short radius nozzle ($\frac{d_c}{R_c} = 2$).*

M960312
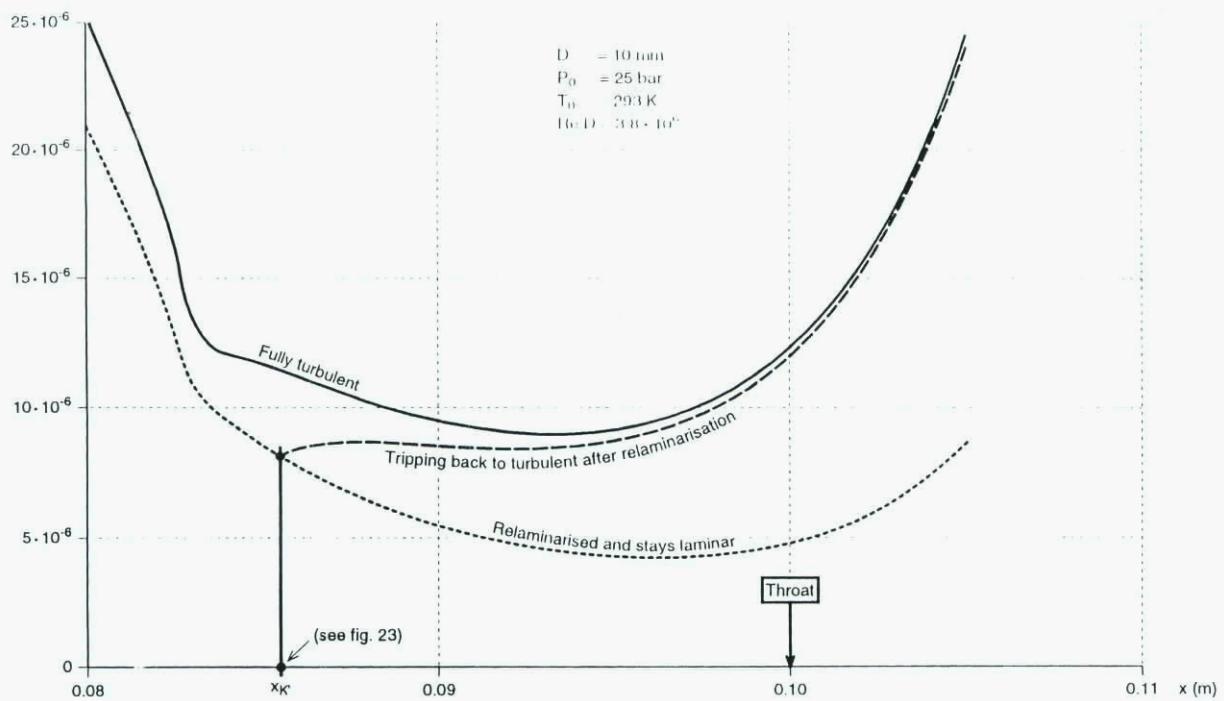
Fig. 24 - *Boundary layer computations close to the throat of the ONERA short radius nozzle ($\frac{d_c}{R_c} = 2$).*

M960313

56

$$C_{Dv} = 1 + 0,03454 . 10^{-5} \frac{P_0 (Pa)}{T_0(K) - 210}$$

$$P_0 < 60 \text{ bar}$$

$$270 \text{ K} < T_0 < 320 \text{ K}$$
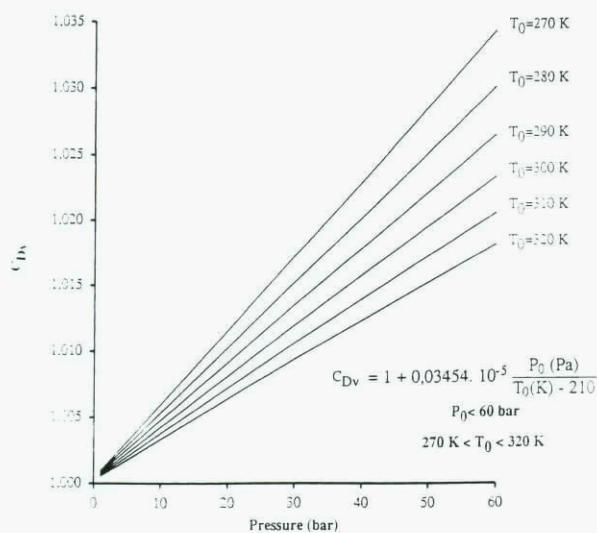
Figure 25   Real gas effect on mass flow rate (Virial effect) for a sonic venturi

Masure's results for C_{Dv}
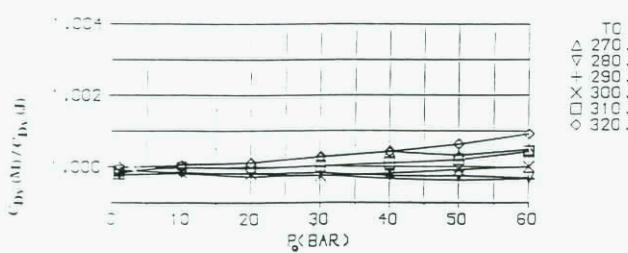
Figure 26   Real gas effect on mass flow rate for a sonic venturi

Ratio of C_{Dv} coefficients from Masure (M) and Johnson (J)

$$C_{Tv} = \frac{\dfrac{F_v \text{ real gas}}{Q \text{ real gas}}}{\dfrac{F_v (\gamma = 1.4)}{Q (\gamma = 1.4)}}$$
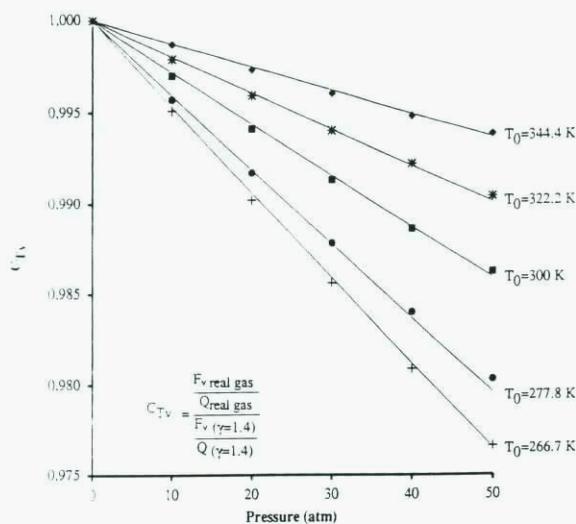
Figure 27   Real gas effect on thrust (Virial effect) for a sonic nozzle

Johnson's results for C_{Tv}

$$y = ax^3 + b$$

Exit diameter – inch	A	B	x_{max}
2	0.058309	1.0	3.5
3	0.046648	1.5	3.5
4	0.023438	2.0	4.0

Fig. 29 - Boeing's "cubic" nozzle.

Figure 28   Real gas effect on thrust for a sonic nozzle

Ratio of C_{Tv} coefficients from Masure (M) and Johnson (J)

2.0029" AND 3.0004" DIA. CUBIC NOZZLES

THRUST STAND - BLOWING NOZZLE DATA

F.S.C. BLOWING AND FLOW-THRU NOZZLE DATA

CVN MEAN LINE

2",3" & 4" DIA. CUBIC NOZZLES

1978 THRU JULY 1985

CVN

CDN

CDN MEAN LINE

2" & 3" DIA. CUBIC NOZZLES

PTN / P

Figure 30

3.9976" DIA. CUBIC NOZZLE

THRUST STAND - BLOWING NOZZLE DATA

F.S.C. BLOWING AND FLOW-THRU NOZZLE DATA

CVN MEAN LINE

2",3" & 4" DIA. CUBIC NOZZLES

1978 THRU JULY 1985

CVN

CDN

CDN MEAN LINE

4" DIA. CUBIC NOZZLE

PTN / P

Figure 31

58

Figure 32

Figure 33

3.9989" DIA. ASME NOZZLE

THRUST STAND - BLOWING NOZZLE DATA

F.S.C. BLOWING AND FLOW-THRU NOZZLE DATA

CVN

G.E.-FLUIDYNE EQUATION

BACK-TO-BACK DATA
WITH CUBIC NOZZLES

CDN

G.E.-FLUIDYNE EQUATION

PTN / P

Figure 34

SECTION A-A

o Total pressure hole
+ Total temperature
   (thermocouple)
▮ Total temperature
   (pt 100 element)

Figure 35   DNW 3" cubic nozzle (identical to Boeing's 3" cubic nozzle)
Instrumentation of the nozzle

60

DNW 3" STARBOARD CUBIC NOZZLE

Figure 36   DNW 3" starboard cubic nozzle
             Flow coefficient

Figure 37   DNW 3" starboard cubic nozzle
             Velocity coefficient

Figure 38   3" cubic nozzle
             Flow coefficient

Figure 39   3" cubic nozzle
             Velocity coefficient
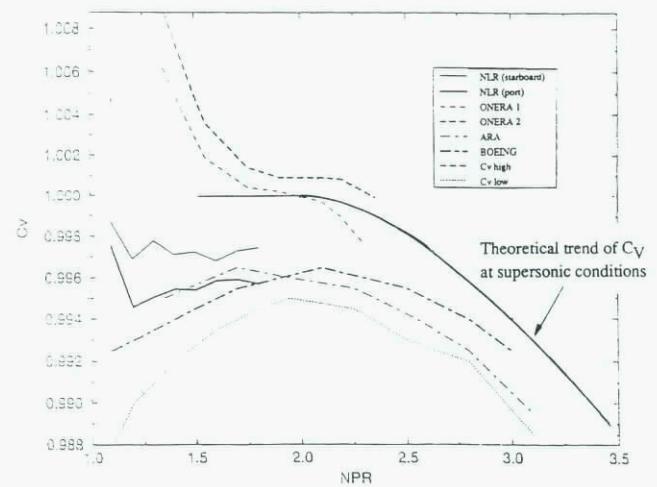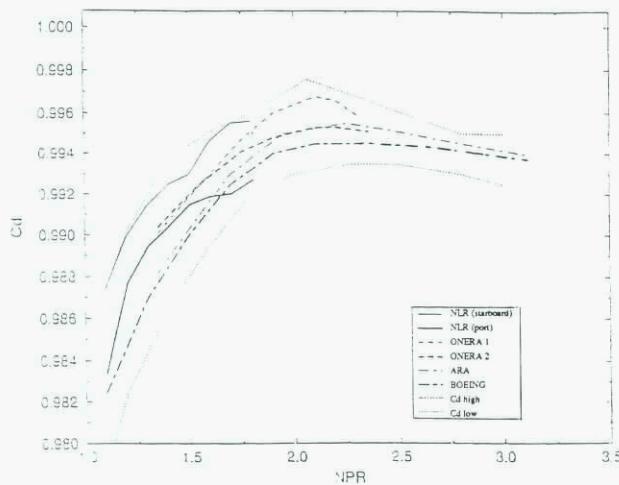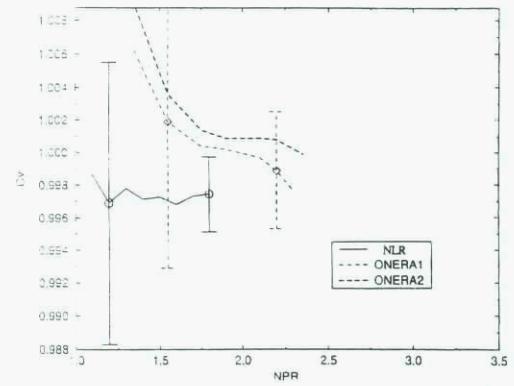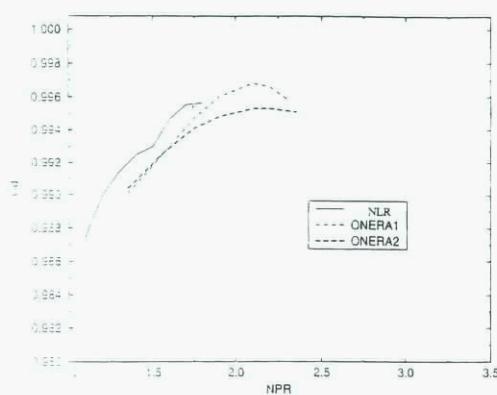
APPENDIX A

ONERA static thrust benches

ONERA operates in the Modane-Avrieux Center three facilities devoted to measure nozzles thrust and mass flow.

Two of them, located in a vacuum tank named S4B, operate only with air at ambient temperature. The third one, named dynalpy bench BD2, can provide hot gas (up to 1100K) and works only at atmospheric exhaust pressure.

1. ONERA test benches located in S4B

The two benches located in S4B are based on the same principle ; only components sizes are different (balance, massflowmeters, plenum chamber).

1.1 A sketch of the facility which can operate with a mass flow up to 3,5 kg/s is shown figure A_1 ($A_{1.1}$ & $A_{1.2}$)

The flow feeding the nozzle is provided from a high pressure storage (270 bar) of very dry air (dew point : below -60°C). The flow, after heating (up to 80°C) and filtering (12μm), is controlled by a regulation valve : the mass flow is measured upstream by the way of sonic throats massflowmeters. The maximum pressure upstream the massflowmeters is 9 bar.

The air flow crosses the balance through an uncoupling system having a very low stiffness compared to the balance stiffness, giving low and repeatable pressure tares (< 0,4% of loads capacities), and cancelling the momentum tares. The 6-components balance capacities are the following :

X : 3300N   Y : 25000N   Z : 20000N
L : 3700 Nm M : 4000 Nm N : 4000 Nm

The air flow then feeds a metric plenum chamber on which the tested nozzle is connected. The 6-component balance directly measures the jet thrust vector. The pressure in the plenum chamber is limited at a value of 1.5 bar above the external pressure.

The facility is installed in a sealed tank connected to vacuum by the way of an adjustable nozzle, controlling the exhaust pressure in the sealed tank between vacuum and atmospheric pressure.

Nozzles with inlet at high pressure (blown nacelle) (fig. A.1.2) can be tested using the primary pipe on the balance. The maximum pressure at the inlet of the nozzle is 50 bar for a maximum mass flow of 1.6 kg/s.

1.2 A larger thrust bench is used to test nozzles with a maximum mass flow of 10 kg/s. It operates on the same principle as the previous one. The main difference consists in the use of a static ejector to get the pressure level at the nozzle exhaust. The side forces cannot be achieved because the large pressure tares in these axis distort the accuracy. For this larger thrust bench, the capacities are the following:

Pressure in the plenum chamber : 1.5 bar above external pressure.
Thrust capacity : - 1000 N to + 5000 N.
Nozzles with inlet at high pressure (blown nacelle) can be tested using the primary pipe on the balance. The maximum pressure at the inlet of the nozzle is 50 bar for a maximum mass flow of 4 kg/s.
The configuration of the bench for turbofan simulator calibration is shown fig.A_2.

62

2. Dynalpy bench BD2

The dynalpy bench BD2 (fig.A.3) is made up with two frames (a fixed one and a metric one)
connected by a dynamometer measuring the axis thrust and by springy blades allowing to get the side
forces. It can operate with two airflows measured upstream by sonic throats mass flow-meters : a
combustion chamber on the primary flow can heat a maximum mass flow of 3,3 kg/s up to 1100 K.
The characteristics of this rig are the following :
- thrust dynamometer capacity : 13500 N ;
- secondary flow : 14 kg/s at a maximum pressure of 25 bar ;
- primary flow : see operating map.
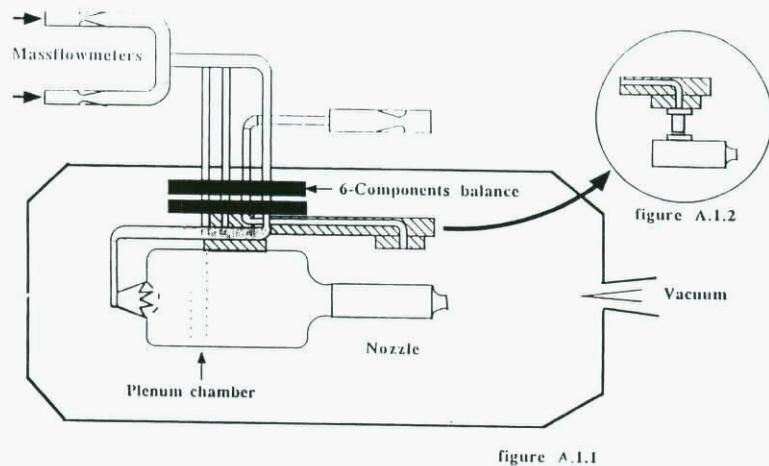
Figure A.1   Sketch of one of the ONERA test benches located in S4B
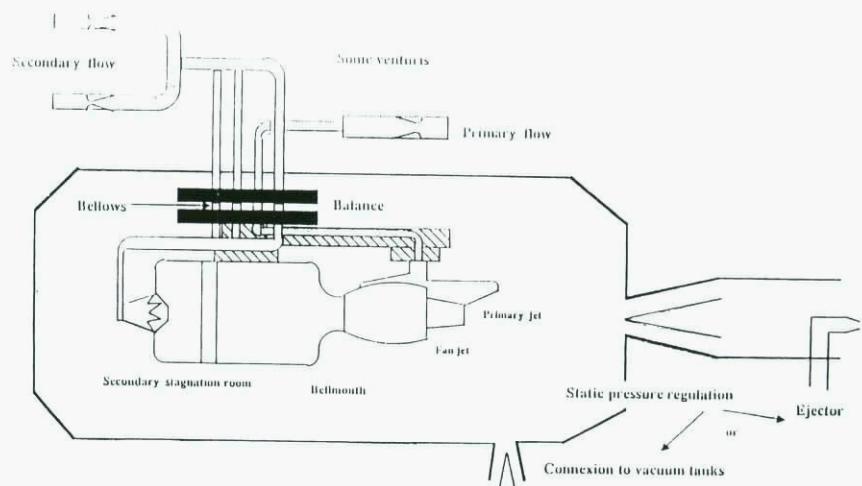
Figure A.2   Configuration of one of the ONERA test benches located in S4B
for turbofan simulator calibration
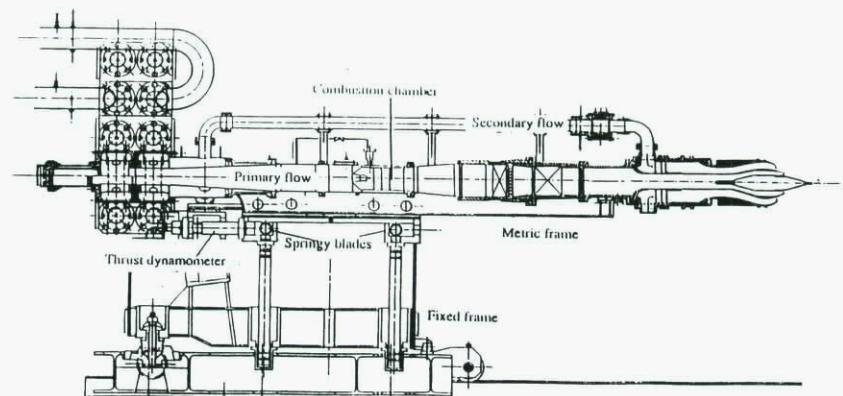
Figure A.3   ONERA dynalpy bench BD2

APPENDIX B

DLR static thrust bench

The ETG is used for calibration of Turbine Powered Simulators (TPS) under simulated wind-tunnel conditions without external flow. By evacuating the tank, a Mach number equivalent pressure ratio is simulated which is required for determination of nozzle and thrust coefficients.
This facility is also able to measure nozzle mass flow and thrust coefficients.
A sketch of the tank is shown fig.B1; the installation of a cubic nozzle is presented fig.B2.
Tank size : length 4.2 m ; diameter 1.6 m
Max. nacelle diameter : 300 mm
Tank pressure : .2 x 10^5 Pa up to 1.5 x 10^5 Pa
Max. mass flow : up to 24 kg/s at tank pressure 1.0 x 10^5 Pa
Vacuum storage : 10.000 m^3 at .2 x 10^5Pa
Drive air supply : up to 4.5 kg/s at 40 x 10^5 Pa
Drive air temperature : up to 415 K.

Instrumentation

Six-component balance integrated in the front plate for a maximum thrust force of 6000 N in axial direction (accuracy 0.03%).
9 calibrated sonic nozzles for high-precision mass flow determination (accuracy 0.3%).
Scanivalves, pressure transducers and PSI systems for a pressure range from .01 x 10^5 up to 50 x 10^5 Pa.
Statically and dynamically calibrated thermocouples and PT-100 sensors.
Computer controlled 4-axis traversing mechanism for probes to measure the flow field behind a simulator.
Pressure and temperature rake for measurements upstream and downstream of a TPS.

Data Acquisition
Real-time data acquisition and reduction with local computer for numerical and graphical quick look.
On-line data transfer to DLR network and on request to customers.

Measuring Techniques
Measurement of thrust, mass flow rate, pressure and temperature distribution behind fan and turbine for determination of calibration coefficients. Laser measurements and Schlieren photography of the jet.

[1] Binder, B. ; Melzer, E. ; Wulf, R.
Der Eichtank für Triebwerksimulation in der DFVLR Göttingen.
DFVLR-IB 29112-84A01 (1984).

[2] Binder, B. ; Melzer, E. ; Wulf, R.
The new calibration tank for engine simulation at DFVLR Göttingen.
AGARD-CP-348 (1983).

64
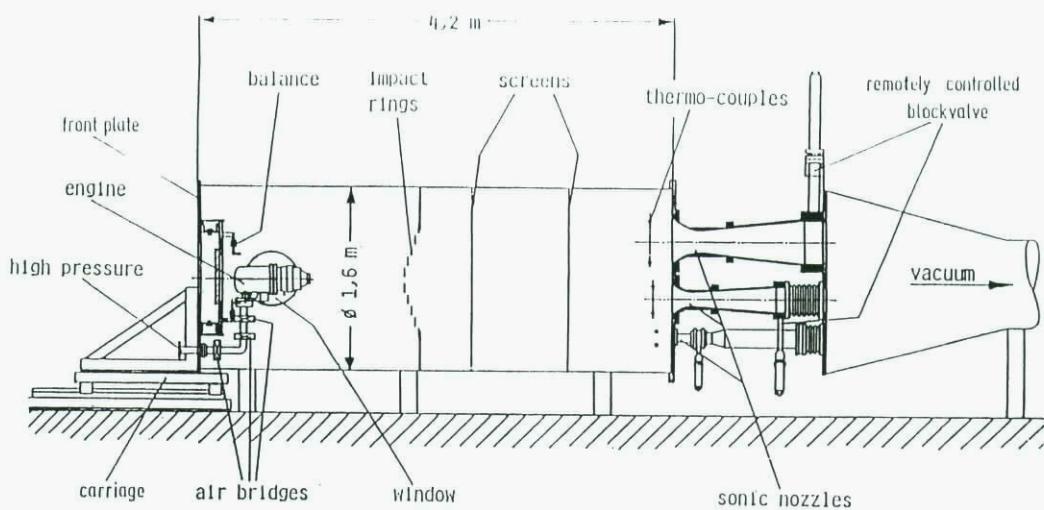


Figure B.1   DLR Calibration tank
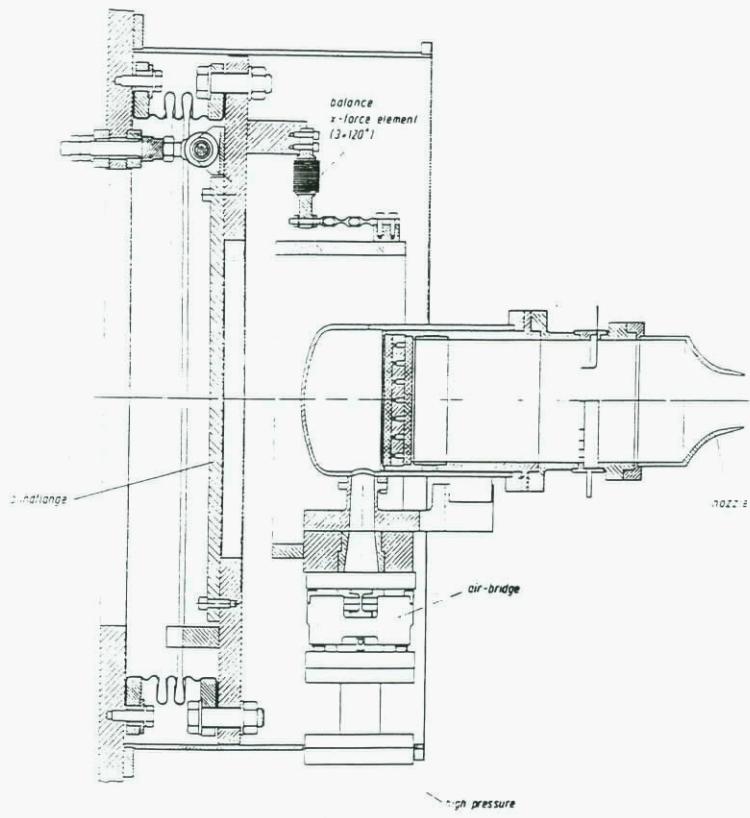
Figure B.2   Cubic nozzle mounted on DLR Calibration tank

APPENDIX C

ARA static thrust benches

1. The ARA Large Scale Thrust Measuring Rig LSTMR

The LSTMR facility (fig.C1) provides a means of assessing the performance of either single or twin stream nozzle configurations both in terms of nozzle discharge and thrust characteristics. A cylindrical pressure vessel with a central bulkhead forms two plenum chambers. These two chambers, ultimately feeding the core and fan flows, are connected through to the rig/model interface by means of a pair of concentric ducts. Simultaneous flows of up to 12 kg/s and 4 kg/s can be provided for the fan and core respectively. The air supply to the LSTMR comes from two separate air systems. The majority of the flow is provided from a series of storage tanks initially pressurised to 10 bar with clean dry air. Air is fed to each chamber via a single 0.250 m diameter air feed which bifurcates downstream of a master control valve into individual 0.25 m and 0.203 m lines for the fan and core streams respectively. Other than a pair of butterfly valves which govern the pressure drop into each plenum chamber, the 10 bar supply is uncontrolled. Constant nozzle pressure ratios (NPRs) are achieved by augmenting the flow in each stream with that from a separate 250 bar high quality air supply. The amount of augmentation is controlled by a closed loop servo system which responds to changes in mass flow. The airflow in each stream is carefully metered using critical venturi meters. The venturi diameters in the Fan and Core streams are fixed at .0089m and 0.051m respectively whereas those for the 250 bar augmentation lines are selectable from a minimum of 0.003m to a maximum of 0.015m diameter depending on the flow requirements.
A hydrogen burner installed in the core duct can be used to provide heated air up to 600°C to the nozzle system under test.
The plenum chamber assembly is floated on a pair of air bearings which constrain all loads with the exception of those in the axial and torsional directions. The bearings lift the rig by 0.1 mm and provide a near friction free support enabling the thrust to be measured by a single load cell mounted on the thrust axis. The two air bearings are mounted below the plenum chamber thus enabling lateral forces to be measured by load cells mounted perpendicular to the thrust axis at each end of the plenum chamber available with capacities ranging from 2200N to 8900N.

2. The ARA Mach Simulation Tank MST1

MST1 was commissioned in 1979-80 and has subsequently been developed into a highly productive and repeatable nozzle system calibration facility.

MST1, (fig.C2), consists of a plenum chamber (or tank) connected to an external suction device, providing tank pressures in the range atmospheric (M=0) to 0.35 bar (M = 1.3). This variation (for a fixed set of model internal conditions) is achieved by variation of tank exit area. A binary set of sonic venturi meters (MCV's) are used to set up an exit area (AMCV from 3.23×10^{-4} m^2 to a maximum of 0.051 m^2 in steps of 3.23×10^{-4} or larger). The venturis are also used to measure the tank exit mass flow rate.

The nozzle system under test is mounted at the forward end of the tank supported on a live (metric) frame. The forces acting on the live frame and model are measured by a pair of six component strain gauged balances. The balances are each capable of measuring up to 1300N axial force with a measurement resolution of between 0.22 and 0.44N. The large pressure area term experienced by the live frame due to the differential pressure acting across it is counteracted by a series of annular pressure chambers which provide the reacting force. Rolling diaphragm seals are used to maintain pressure/mass flow integrity combined with a low axial stiffness.

High pressure air for TPS, ejector or blown models is supplied from the ARA 250 bar system capable of providing air to the model at operating pressures up to 69 bar. The air is transferred across the balances by means of three caged bellows arrangements mounted in a plane perpendicular to the MST1 thrust axis. A closed loop servo system and high pressure sonic venturi meter are used to control and measure the mass flow to a high degree of accuracy.

Calibrations using a dedicated system of reference nozzles are routinely performed to ensure the long term repeatability of the facility.

66
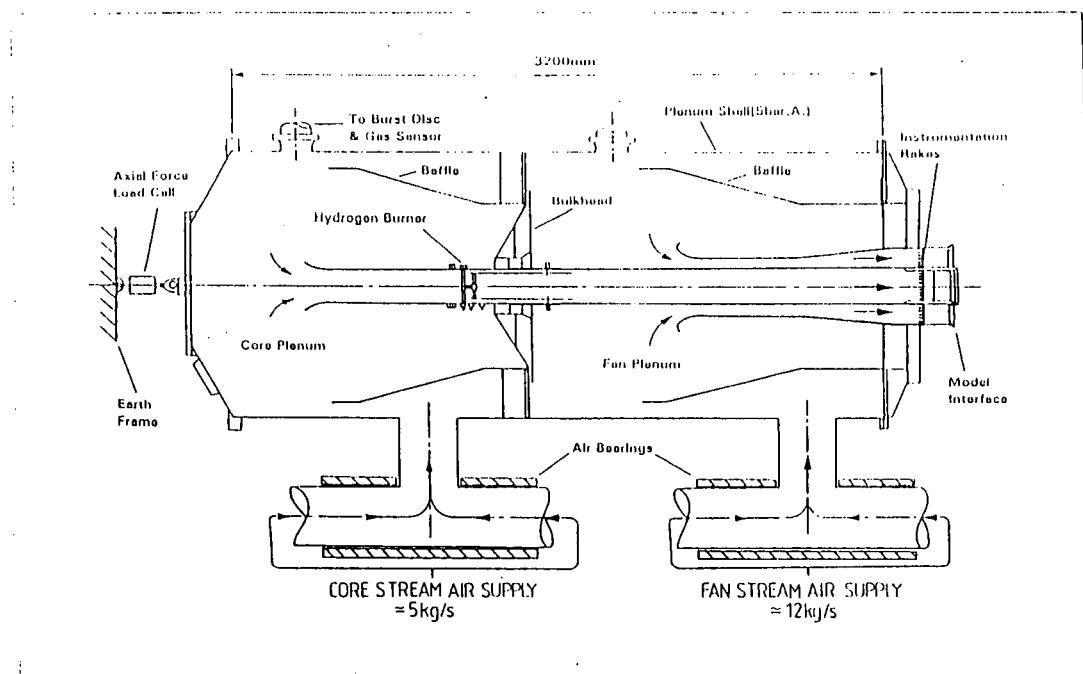
Figure C.1   Large Scale Thrust Measuring Rig (LSTMR) at ARA
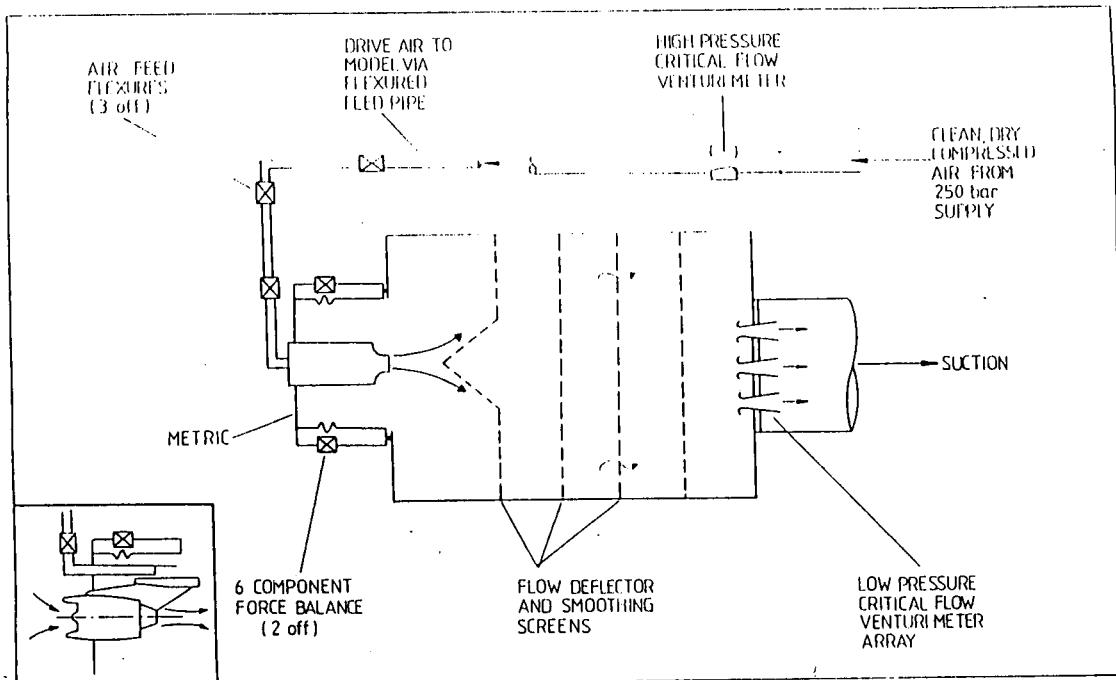
Figure C.2   General arrangement of the ARA Mach Simulation Tank (MST)

APPENDIX D

NLR static thrust bench

NLR Model Engine Calibration Facility (ECF)

The NLR Model Engine Calibration Facility (ECF) is designed for calibration of nacelles equipped with turbo powered model engines such as Turbofan Propulsion Simulators. However, blown nacelle and through flow nacelle configurations can be calibrated as well. In the facility the model engine thrust and mass flows are determined under simulated wind tunnel conditions without external flow.

A schematical drawing of the 3" cubic nozzle mounted in the facility is given in fig.D.1. The nozzle is mounted in the front end of the tank. The tank inlet is closed by the nozzle and the nozzle exhausts into the tank. Air suction from the tank is established by three centrifugal compressors in series, with a total drive power of 720 kW.

A pipeline brings 110 bar compressed dry air (dew point temperature is about 218 K at the air storage pressure of 260 bar) to the ECF. In the so-called "skid", the pressure can be reduced to 80 bar and below. The maximum mass flow is 6 kg/s. After passing a heat exchanger (heating-up the drive air to a temperature of 293-343 K), the compressed air has to be supplied to the model through an air duct which has to cross the balance with only minor interaction. Three flexible air couplings are mounted, each with two degrees of freedom, so that balance forces exerted by the through-flowing high pressure air in all six possible degrees of freedom are minimized. The high pressure air mass flow is measured in the supply line by a sonic venturi.

The mass flow can also be measured at the downstream end of the tank via a set of 9 sonic venturis. When they are choked their mass flow can be determined very accurately. At steady state conditions the high pressure mass flow should be equal to the tank venturis mass flow. Because steady state is approached asymptotically, the tank venturis mass flow is used for check only. During a test sufficient tank venturis are opened to run them unchoked during most of the test datapoints. The tank pressure can then be controlled independently by the suction compressors rpm. Only at the highest mass flows sonic conditions are attained for a mass flow check.

For measurement of the model engine thrust the facility is equipped with an external balance system. The balance consists of bars which connect the metric part to earth. Three bars are connected through high accuracy load cells so that three components are measured (side force, axial force and yaw moment).

A central bellows forms a flexible air-tight connection between the metric part of the balance and the non-metric tank. In this central bellows the engine model is mounted 60 mm below the centre line (see fig.D1). To minimize the parasitic force due to the pressure differences over the central bellows two compensating bellows are installed at the upper and lower side of the central bellows.

The main characteristics are the following :
- internal diameter of the nacelle housing: 0.5m
- maximum engine weight (incl.support): 150kg at 0.8m from balance center
- maximum axial thrust force: ±3,000N
- maximum side force: ±900N
- fan inlet air: atmospheric
- drive air: maximum 6 kg/s at 80 bar
- drive air control: incremental steps of 0.0005 kg/s
- drive air temperature: 243 K to 343 K
- maximum tank suction capacity: 0.58 bar (M=0.92)
- tank size: L=6M   D=3M
- data processing and data plotting: on line
- fan exhaust mass flow: see map

68
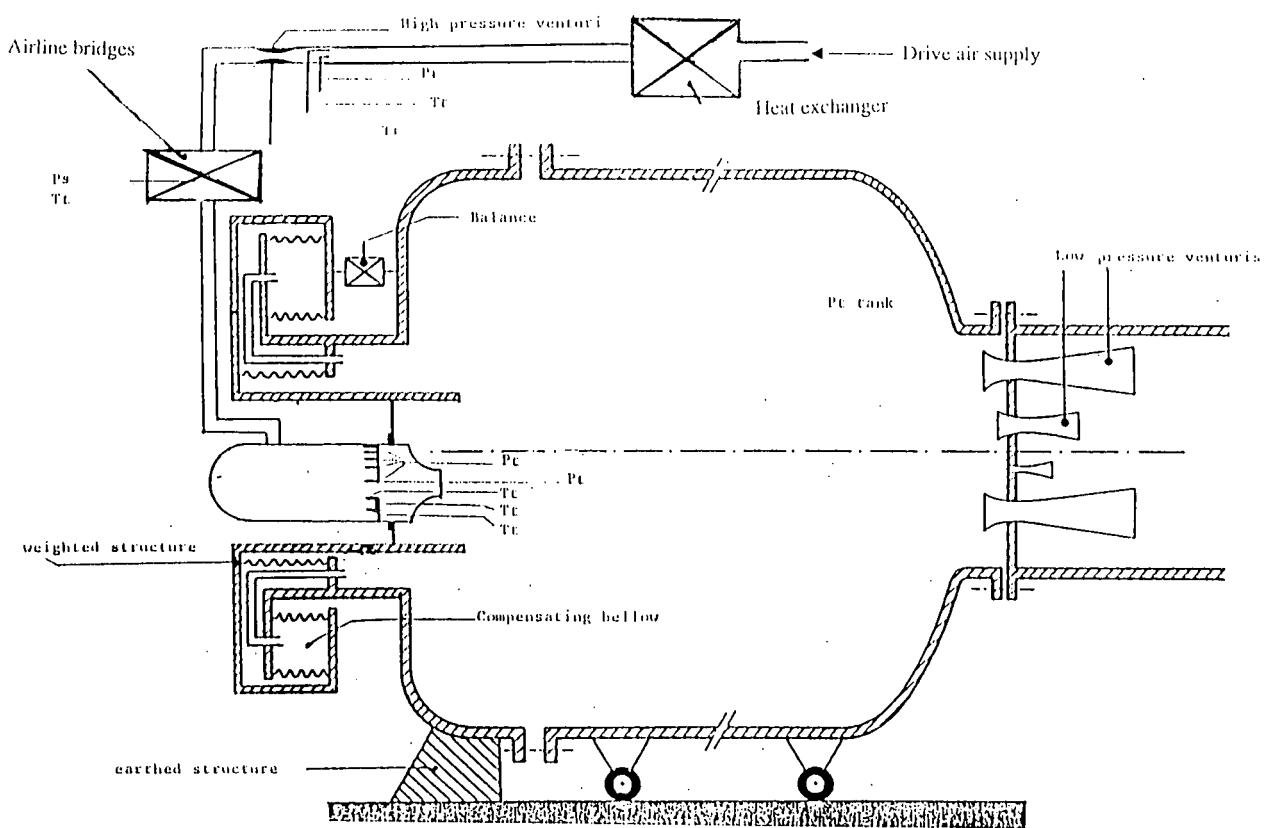
Figure D.1   NLR model Engine Calibration Facility (ECF)

APPENDIX E

Boeing Thrust Stands or Benches

Four static thrust stands are provided at Boeing's Seattle, Washington plant for thrust and airflow measurements. Two thrust stands are at the Wind Tunnel Facilities and two thrust stands are at the Propulsion Laboratories. Each thrust stand has a unique capability and purpose.

Two continuous air supplies are shared by the Wind Tunnel Facilities and the Propulsion Laboratories. A high pressure system supplies 9 kg/s at 69 bar. A low pressure system supplies 20.4 kg/s at 21 bar. The air is filtered and dried to a dew point below - 46°C. Both systems have storage so the above continuous flow rates can be exceeded for limited time periods.

2-Balance Thrust Stand

The first of the Wind Tunnel thrust benches is the 2-Balance Thrust Stand shown in figure E.1. Loads are measured by two 6-component balances mounted 1.829 meters apart. The main load carrying member is located 0.457 meters below the balance centerlines, so that the thrust vector can be located at or near the plane of the balance axial force centerlines as shown. A complete wind tunnel model with engine nozzles on both wings can be calibrated with the thrust vectors on or close to the plane of axial force. The nozzles can be calibrated separately or together. The type of air flexure shown here has no momentum tare and only a small repeatable pressure tare. The balances are thermally isolated from temperature gradients by insulators at both ends of each balance. Load induced and thermally induced dimensional changes of the structures between the balances, produce equal and opposite loads in the balances which cancel. The twelve components measured by the two balances are resolved into 6-component data midway between the two balances. Thrust loads up to 2900 N can be measured, accurately defining the magnitude, angularity, and position of the thrust vector. Alternate balances can increase thrust capacity up to 5300 N. Air mass flow can be measured upstream of the thrust stand with a Multiple Critical Venturi (MCV) shown in Figure 9, or with sonic venturis mounted inside the wind tunnel model. Total model weight can be up to 550 kg.

Flight Simulation Chamber (FSC)

The second Wind Tunnel thrust facility is the Flight Simulation Chamber (FSC) which was designed primarily for calibrating Turbo-Powered-Simulators (TPS). This facility is shown in Figure E.2 and described in more detail in Reference 12. In addition to TPS calibrations, it is used to calibrate blowing nacelles and define the internal drag of flow-through nacelles. Like the 2-Balance Thrust Stand, loads are measured by two 6-component balances, and the same type of air bridge is used for high pressure air. Thrust can be measured up to 1550 N.

High pressure air flow can be measured upstream of the air bridge by a sonic venturi or high pressure MCV. The total flow through the chamber is measured by the Low Pressure MCV at the downstream end of the chamber. Air mass flow ranges for High Pressure and Low Pressure MCV's are shown in Figure E.3. Two air ejectors provide suction to maintain sonic flow in the Low Pressure MCV. Model weights up to 180 kg can be accommodated.

A 7 year history of standard "cubic" thrust nozzle data from the 2-Balance Thrust Stand and the FSC are shown in figures 30 and 31.

70

Large Dual Flow Rig (LDFR)

The Propulsion Laboratory Large Dual Flow Rig (LDFR) is designed for static nozzle thrust and thrust reverser testing. Loads are measured by a 3-component balance in a horizontal plane, with thrust capacity from - 2225 to 8900 N. Two major air bridges bring primary and secondary airflow from the low pressure system on to the balance. The primary airflow can be heated on balance by a Propane burner system to temperatures up to 922°K with flow rates up to 9 kg/s and pressure up to 9.3 bar. The secondary flow system is ambient temperature at flow rates up to 15.9 kg/s and pressure up to 9.3 bar. The primary and secondary flow systems are independently controlled, and flow rates are measured by large MCV's upstream of the balance. A tertiary flow system has been added to provide air flow up to 2.7 kg/s and pressure up to 48 bar for complete simulation of some nozzle systems. A third pressure control, MCV, and air bridge is provided for this system. Model weight up to 725 kg can be accommodated.

High Pressure Ratio Rig (HPR)

The second Propulsion Laboratory thrust bench is the High Pressure Ratio Rig (HPR) which can provide a single flow at nozzle pressure ratios from 2 to 40. Loads are measured by a 6-component balance with thrust capacity up to ± 4450 N. The single flow system can provide air mass flow up to 11.3 kg/s at pressures up to 48 bar. Air mass flow is measured by a high pressure MCV. Model weight up to 725 kg can be accommodated.

Each of the Propulsion Laboratory thrust rigs is housed in a 6 by 6 meter cross section by 19 meter long test cell vented at the far end to maintain atmospheric pressure in the cell, and isolate noise from the surrounding areas.

2 - BALANCE THRUST STAND

Figure E.1

FLIGHT SIMULATION CHAMBER

Figure E.2

MCV MASS FLOW RANGES

Figure E.3

HIGH PRESSURE MCV
$$\dot{\omega}_{nom} = \frac{MCV - CODE}{1600} \times P$$

LOW PRESSURE MCV
$$\dot{\omega}_{nom} = \frac{MCV - CODE}{205} \times P$$

72
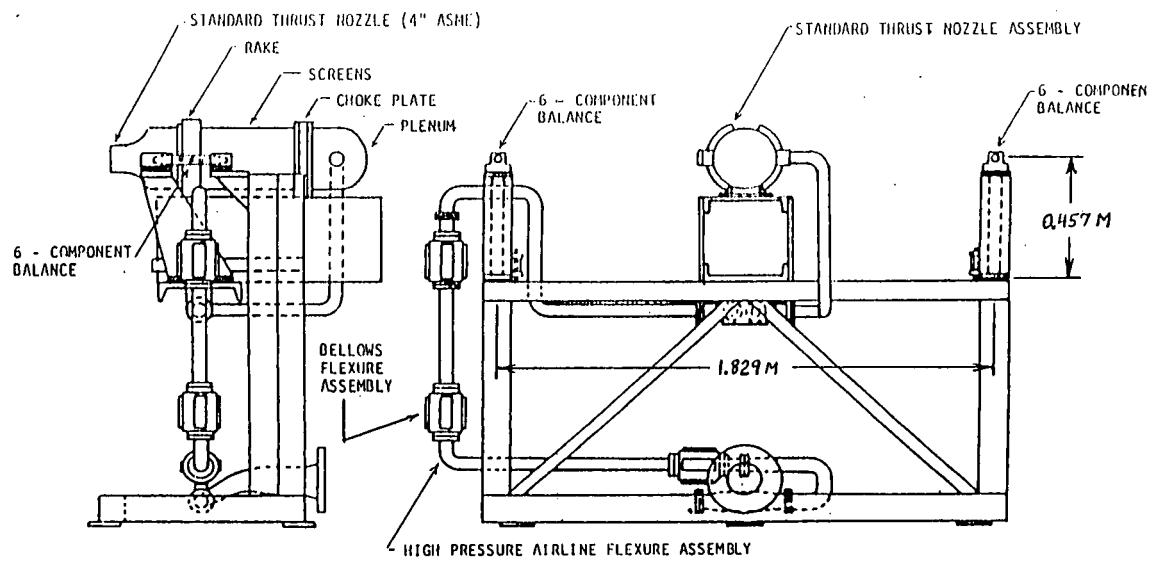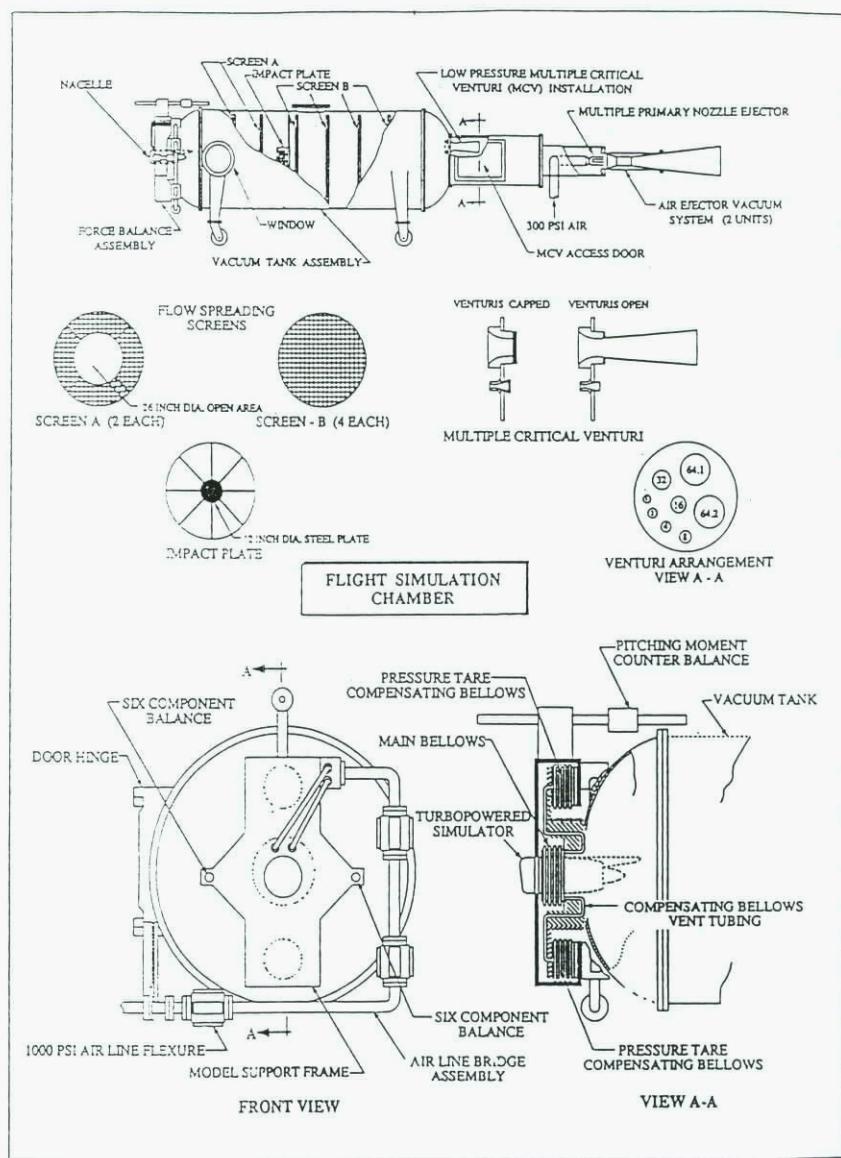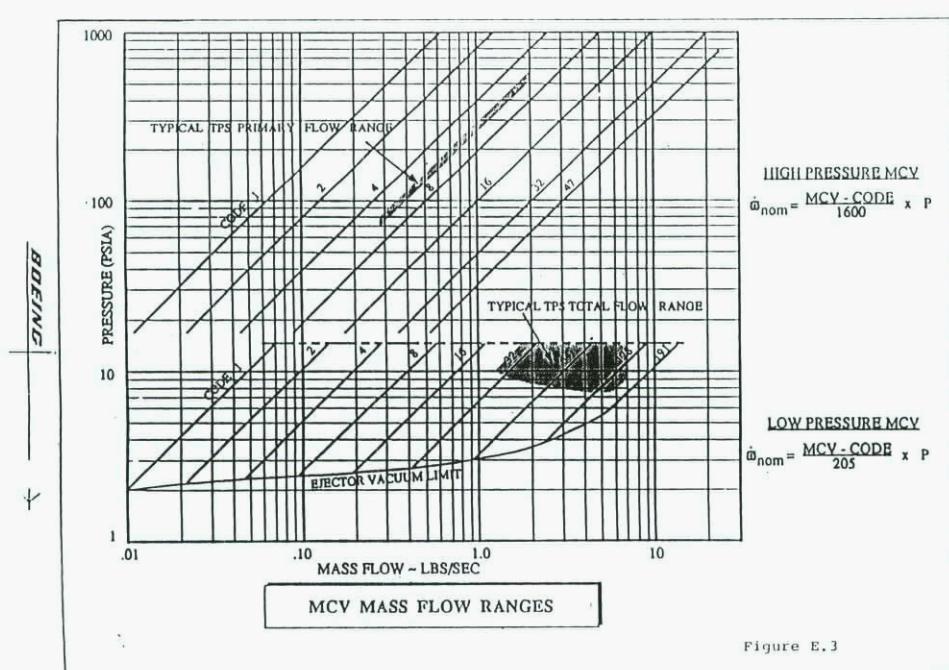
APPENDIX F

ONERA SHORT RADIUS NOZZLE ($R_c/d_c = 2$)

1- Notations and conventions

1-1 Axis system

The selected axis system is Oxy; the point O is the geometrical center of the throat; Ox axis is the throat axis, positive from upstream to downstream; Oy is orthogonal to Ox, positive to the top.

1-2 Throat definition

The throat shape is broken up in three parts : from downstream to upstream:

    - a circular shape; the center is the point P, and the radius R_c is equal to two times the throat diameter dc. $R_c = 2d_c$

This part stops at the point M, at an angle of 60°. The coordinates of P and M are the following:

$$P \begin{vmatrix} x_P = 0 \\ y_P = -\frac{5}{2}d_c \end{vmatrix} \qquad M \begin{vmatrix} x_M = -\sqrt{3}\,d_c \\ y_M = -\frac{3}{2}d_c \end{vmatrix}$$

- a linear part, from M to B, which is a part of the tangent in M to the circle (P, Rc); the tangent equation is:

$$y = \sqrt{3}\,x + \frac{3}{2}d_c$$

    - a second circular curvature; the center is the point T; the radius is r. C and B are on the circle; BM is the tangent in B to the circle (T, r).

the coordinates of C are given values:

$$C \begin{vmatrix} x_C = -58,5 \ \ mm \\ y_C = -51,2 \ mm \end{vmatrix}$$

2- Coordinates of points T and B and value of radius r

2-1 Ideal case

The ideal case is to get an horizontal tangent in C. In this case, the coordinates of the different points would be:

$$T \begin{vmatrix} x_T = x_C = -58,5 \ mm \\ y_T = -\sqrt{3}\,x_C + 2y_C -1,5\,d_c \end{vmatrix} \qquad B \begin{vmatrix} x_B = -\frac{1}{2}x_C + \frac{\sqrt{3}}{2}y_C - \frac{3\sqrt{3}}{4}d_c \\ y_B = -\frac{\sqrt{3}}{2}x_C + \frac{3}{2}y_C - \frac{3}{4}d_c \end{vmatrix} \qquad r = y_C - \sqrt{3}\,x_C - 1,5\,d_c$$

2-2 Real case

In fact, for machining problems, it is difficult to get an horizontal tangent in C. So, we give for radius r, a value slightly greater than the one defined in 2-1. Once the value of r is selected, the coordinates of T et B can be calculated.

74
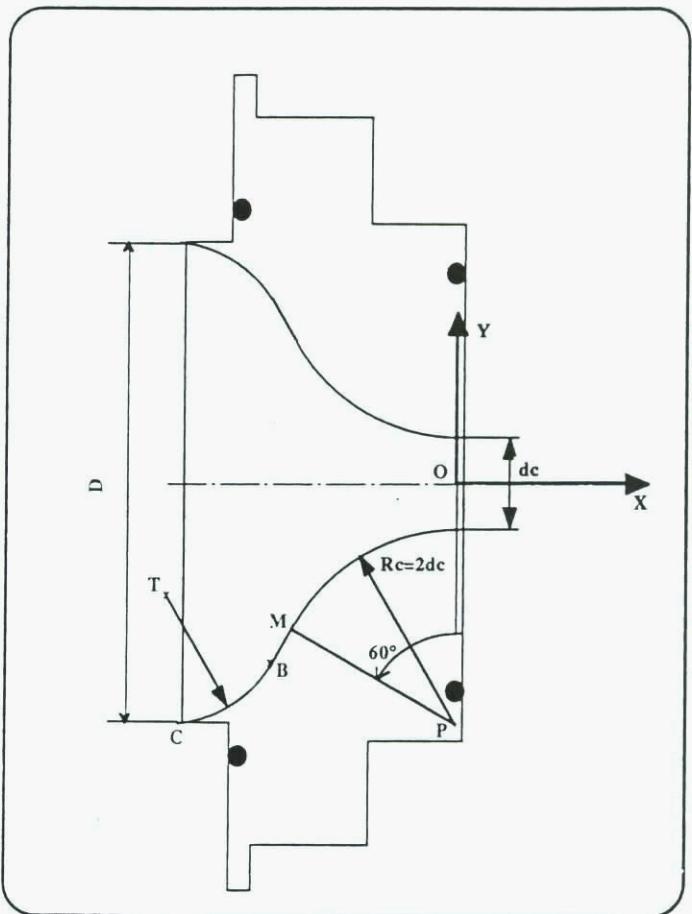
With:

$$U = 4$$

$$V = -2\left[x_C + \sqrt{3}\left(y_C - 2r - \frac{3}{2}d_c\right)\right]$$

$$W = x_C^2 - r^2 + \left[y_C - 2r - \frac{3}{2}d_c\right]^2$$

$$\Delta = V^2 - 4\ U\ W$$

$$T \left|\begin{array}{l} x_T = \dfrac{-V + \sqrt{\Delta}}{2\ U} \\[2mm] y_T = \sqrt{3}\ x_T + 2r + \dfrac{3}{2}\ d_c \end{array}\right. \qquad B \left|\begin{array}{l} x_B = x_C + \dfrac{\sqrt{3}}{2}\ r \\[2mm] y_B = y_C - \dfrac{1}{2}\ r \end{array}\right. \qquad \text{r selected}$$

2-3 Value of r

The following figure shows the selected values of r with the throat diameter d_c.

Second curvature radius
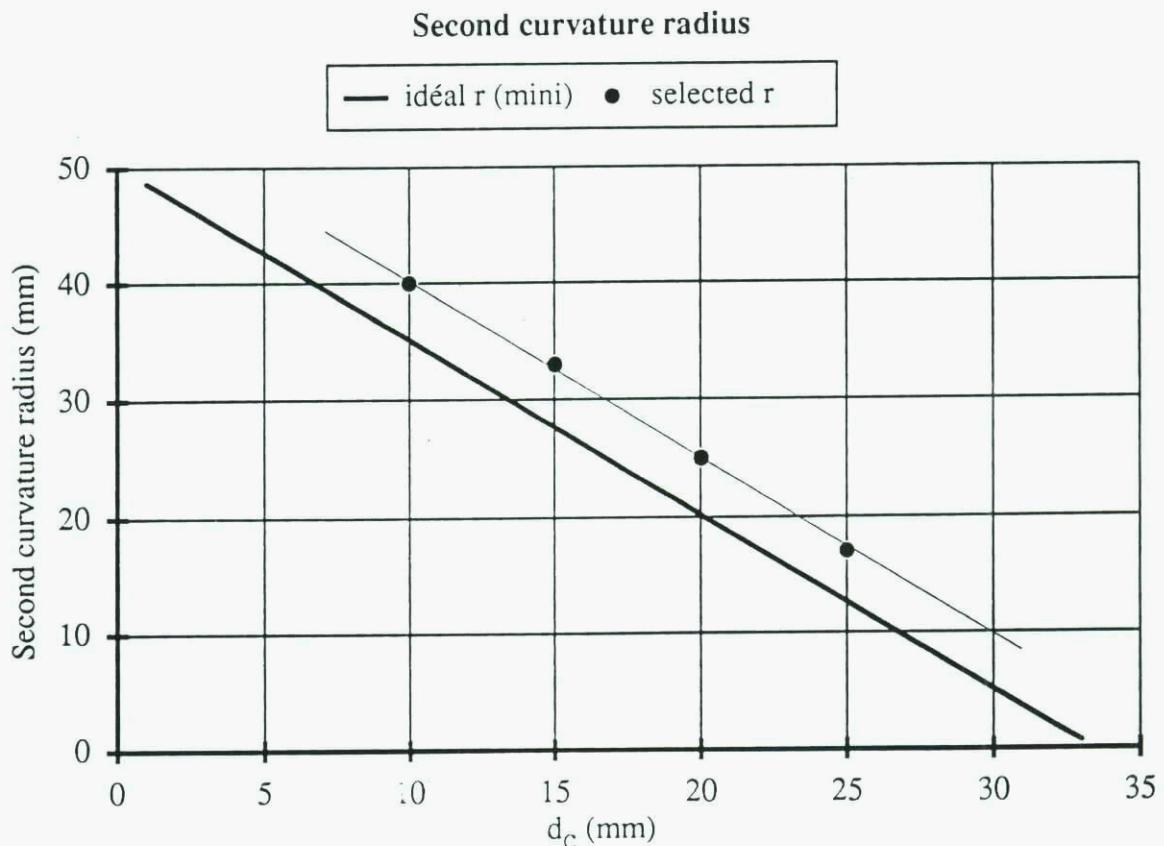
Those values are:

$d_c = 10mm \Rightarrow$ **r=40mm**

$d_c = 15mm \Rightarrow$ **r=33mm**

$d_c = 20mm \Rightarrow$ **r=27mm**

$d_c = 25mm \Rightarrow$ **r=17mm**

REPORT DOCUMENTATION PAGE

1. Recipient's Reference	2. Originator's Reference	3. Further Reference	4. Security Classification of Document
	AGARD-AR-321	ISBN 92-836-1056-3	UNCLASSIFIED/ UNLIMITED

5. Originator	Advisory Group for Aerospace Research and Development North Atlantic Treaty Organization 7 rue Ancelle, 92200 Neuilly-sur-Seine, France

6. Title	Sonic Nozzles for Mass Flow Measurement and Reference Nozzles for Thrust Verification

7. Presented at/sponsored by	

8. Author(s)/Editor(s)	9. Date
	June 1997

10. Author's/Editor's Address	11. Pages
	84

12. Distribution Statement	There are no restrictions on the distribution of this document. Information about the availability of this and other AGARD unclassified publications is given on the back cover.

13. Keywords/Descriptors

Aerodynamic characteristics	Thrust meters
Wind tunnels	Convergent divergent nozzles
Mass flowmeters	Viscosity
Flow measurement	Experimental data
Drag	Tests
Calibrating	Nozzles
Transferring	Aircraft engines
Standards	Integrated systems

14. Abstract

This report presents the results of a multinational effort to reflect the state-of-the-art for the accurate measurement of massflow and thrust. The accurate measurements of these quantities is essential to the success of windtunnel tests supporting engine-airframe aerodynamic integration studies. It is concluded that the measurement of gaseous mass flows with ±0.1% or better is still very difficult. For most test cases, however, with reasonable care, bias and random errors can be kept within ±0.1% respectively. For thrust measurements, these values must typically be doubled.

This report present the results of work conducted by Working Group 19 of the AGARD Fluid Dynamics Panel.

AGARD

NATO ⊕ OTAN

7 RUE ANCELLE ● 92200 NEUILLY-SUR-SEINE

FRANCE

Télécopie 0(1)55.61.22.99 ● Télex 610 176

DIFFUSION DES PUBLICATIONS

AGARD NON CLASSIFIEES

Aucun stock de publications n'a existé à AGARD. A partir de 1993, AGARD détiendra un stock limité des publications associées aux cycles de conférences et cours spéciaux ainsi que les AGARDographies et les rapports des groupes de travail, organisés et publiés à partir de 1993 inclus. Les demandes de renseignements doivent être adressées à AGARD par lettre ou par fax à l'adresse indiquée ci-dessus. *Veuillez ne pas téléphoner*. La diffusion initiale de toutes les publications de l'AGARD est effectuée auprès des pays membres de l'OTAN par l'intermédiaire des centres de distribution nationaux indiqués ci-dessous. Des exemplaires supplémentaires peuvent parfois être obtenus auprès de ces centres (à l'exception des Etats-Unis). Si vous souhaitez recevoir toutes les publications de l'AGARD, ou simplement celles qui concernent certains Panels, vous pouvez demander à être inclu sur la liste d'envoi de l'un de ces centres. Les publications de l'AGARD sont en vente auprès des agences indiquées ci-dessous, sous forme de photocopie ou de microfiche.

CENTRES DE DIFFUSION NATIONAUX

ALLEMAGNE
Fachinformationszentrum Karlsruhe
D-76344 Eggenstein-Leopoldshafen 2

BELGIQUE
Coordonnateur AGARD-VSL
Etat-major de la Force aérienne
Quartier Reine Elisabeth
Rue d'Evere, 1140 Bruxelles

CANADA
Directeur - Gestion de l'information
  (Recherche et développement) - DRDGI 3
Ministère de la Défense nationale
Ottawa, Ontario K1A 0K2

DANEMARK
Danish Defence Research Establishment
Ryvangs Allé 1
P.O. Box 2715
DK-2100 Copenhagen Ø

ESPAGNE
INTA (AGARD Publications)
Carretera de Torrejón a Ajalvir, Pk.4
28850 Torrejón de Ardoz - Madrid

ETATS-UNIS
NASA Center for AeroSpace Information (CASI)
800 Elkridge Landing Road
Linthicum Heights, MD 21090-2934

FRANCE
O.N.E.R.A. (Direction)
29, Avenue de la Division Leclerc
92322 Châtillon Cedex

GRECE
Hellenic Air Force
Air War College
Scientific and Technical Library
Dekelia Air Force Base
Dekelia, Athens TGA 1010

ISLANDE
Director of Aviation
c/o Flugrad
Reykjavik

ITALIE
Aeronautica Militare
Ufficio del Delegato Nazionale all'AGARD
Aeroporto Pratica di Mare
00040 Pomezia (Roma)

LUXEMBOURG
Voir Belgique

NORVEGE
Norwegian Defence Research Establishment
Attn: Biblioteket
P.O. Box 25
N-2007 Kjeller

PAYS-BAS
Netherlands Delegation to AGARD
National Aerospace Laboratory NLR
P.O. Box 90502
1006 BM Amsterdam

PORTUGAL
Estado Maior da Força Aérea
SDFA - Centro de Documentação
Alfragide
2700 Amadora

ROYAUME-UNI
Defence Research Information Centre
Kentigern House
65 Brown Street
Glasgow G2 8EX

TURQUIE
Millî Savunma Başkanliği (MSB)
ARGE Dairesi Başkanliği (MSB)
06650 Bakanliklar-Ankara

Le centre de distribution national des Etats-Unis ne détient PAS de stocks des publications de l'AGARD.

D'éventuelles demandes de photocopies doivent être formulées directement auprès du NASA Center for AeroSpace Information (CASI) à l'adresse ci-dessous. Toute notification de changement d'adresse doit être fait également auprès de CASI.

AGENCES DE VENTE

NASA Center for AeroSpace Information
  (CASI)
800 Elkridge Landing Road
Linthicum Heights, MD 21090-2934
Etats-Unis

The British Library
Document Supply Division
Boston Spa, Wetherby
West Yorkshire LS23 7BQ
Royaume-Uni

Les demandes de microfiches ou de photocopies de documents AGARD (y compris les demandes faites auprès du CASI) doivent comporter la dénomination AGARD, ainsi que le numéro de série d'AGARD (par exemple AGARD-AG-315). Des informations analogues, telles que le titre et la date de publication sont souhaitables. Veuiller noter qu'il y a lieu de spécifier AGARD-R-nnn et AGARD-AR-nnn lors de la commande des rapports AGARD et des rapports consultatifs AGARD respectivement. Des références bibliographiques complètes ainsi que des résumés des publications AGARD figurent dans les journaux suivants:

Scientific and Technical Aerospace Reports (STAR)
publié par la NASA Scientific and Technical
Information Division
NASA Langley Research Center
Hampton, Virginia 23681-0001
Etats-Unis

Government Reports Announcements and Index (GRA&I)
publié par le National Technical Information Service
Springfield
Virginia 22161
Etats-Unis
(accessible également en mode interactif dans la base de données bibliographiques en ligne du NTIS, et sur CD-ROM)
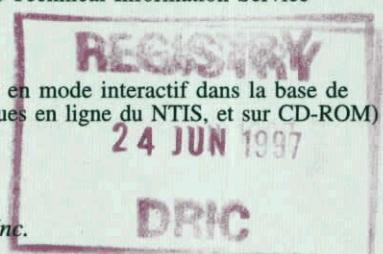
AGARD

NATO ⊕ OTAN

7 RUE ANCELLE • 92200 NEUILLY-SUR-SEINE

FRANCE

Telefax 0(1)55.61.22.99 • Telex 610 176

UNLIMITED

DISTRIBUTION OF UNCLASSIFIED
AGARD PUBLICATIONS

AGARD holds limited quantities of the publications that accompanied Lecture Series and Special Courses held in 1993 or later, and of AGARDographs and Working Group reports published from 1993 onward. For details, write or send a telefax to the address given above. *Please do not telephone.*

AGARD does not hold stocks of publications that accompanied earlier Lecture Series or Courses or of any other publications. Initial distribution of all AGARD publications is made to NATO nations through the National Distribution Centres listed below. Further copies are sometimes available from these centres (except in the United States). If you have a need to receive all AGARD publications, or just those relating to one or more specific AGARD Panels, they may be willing to include you (or your organisation) on their distribution list. AGARD publications may be purchased from the Sales Agencies listed below, in photocopy or microfiche form.

NATIONAL DISTRIBUTION CENTRES

BELGIUM
Coordonnateur AGARD — VSL
Etat-major de la Force aérienne
Quartier Reine Elisabeth
Rue d'Evere, 1140 Bruxelles

CANADA
Director Research & Development
 Information Management - DRDIM 3
Dept of National Defence
Ottawa, Ontario K1A 0K2

DENMARK
Danish Defence Research Establishment
Ryvangs Allé 1
P.O. Box 2715
DK-2100 Copenhagen Ø

FRANCE
O.N.E.R.A. (Direction)
29 Avenue de la Division Leclerc
92322 Châtillon Cedex

GERMANY
Fachinformationszentrum Karlsruhe
D-76344 Eggenstein-Leopoldshafen 2

GREECE
Hellenic Air Force
Air War College
Scientific and Technical Library
Dekelia Air Force Base
Dekelia, Athens TGA 1010

ICELAND
Director of Aviation
c/o Flugrad
Reykjavik

ITALY
Aeronautica Militare
Ufficio del Delegato Nazionale all'AGARD
Aeroporto Pratica di Mare
00040 Pomezia (Roma)

LUXEMBOURG
See Belgium

NETHERLANDS
Netherlands Delegation to AGARD
National Aerospace Laboratory, NLR
P.O. Box 90502
1006 BM Amsterdam

NORWAY
Norwegian Defence Research Establishment
Attn: Biblioteket
P.O. Box 25
N-2007 Kjeller

PORTUGAL
Estado Maior da Força Aérea
SDFA - Centro de Documentação
Alfragide
2700 Amadora

SPAIN
INTA (AGARD Publications)
Carretera de Torrejón a Ajalvir, Pk.4
28850 Torrejón de Ardoz - Madrid

TURKEY
Millî Savunma Başkanliği (MSB)
ARGE Dairesi Başkanliği (MSB)
06650 Bakanliklar-Ankara

UNITED KINGDOM
Defence Research Information Centre
Kentigern House
65 Brown Street
Glasgow G2 8EX

UNITED STATES
NASA Center for AeroSpace Information (CASI)
800 Elkridge Landing Road
Linthicum Heights, MD 21090-2934

The United States National Distribution Centre does NOT hold stocks of AGARD publications.

Applications for copies should be made direct to the NASA Center for AeroSpace Information (CASI) at the address below. Change of address requests should also go to CASI.

SALES AGENCIES

NASA Center for AeroSpace Information
 (CASI)
800 Elkridge Landing Road
Linthicum Heights, MD 21090-2934
United States

The British Library
Document Supply Centre
Boston Spa, Wetherby
West Yorkshire LS23 7BQ
United Kingdom

Requests for microfiche⁀ include the word 'AGARD' and the AGARD seria⁀ title and publication date is desirable. Note that A⁀-nnn and AGARD-AR-nnn, respectively. Full biblic⁀ollowing journals:

Scientific and Tec⁀ments and Index (GRA&I)
published by NAS⁀nical Information Service
Information Divisi⁀
NASA Langley R⁀
Hampton, Virginia⁀
United States

⁀IS Bibliographic

UNLIMITED

ISBN 92-836-1056-3